Ultrafast Optical Probing of Carrier Dynamics in Semiconductor Heterostructures in Magnetic Field

Thesis for the Ph.D. Degree

by

Shimshon Bar-Ad

Department of Physics
The Weizmann Institute of Science

Submitted to the Scientific Council
of the Weizmann Institute of Science
Israel

November 1993

This work was carried out under the supervision of Dr. I. Bar-Joseph in the Department of Physics at the Weizmann Institute of Science, Rehovot.

Acknowledgements

I wish to thank all the people who helped me accomplish this research work. Special thanks are due to Israel, who always provided help, encouragement and advice, and the ever necessary criticism and balancing. Obviously, without his contribution this work wouldn't have been possible. I am also very grateful to Proffesor Yehoshua Levinson, for his support in almost every theoretical aspect of this work. His genuine interest in experimental work I will always remember, as well as the successful colaboration with Gleb Finkelstein, which he initiated. Special thanks are also due to Dr. Michael Rappaport, who taught me everything I know about cryogenics and leak-testing (and unfortunately I know a lot about *that*). Thanks to all the students in the optical lab, who were always there to help save a dying cryostat, discuss physics, drink coffee and gossip, and in particular Yoram, 2 × Guy, Гleb, Amit, David and Omer. I wish to thank Nathalie for her help with the Polaron (as well as other duties nobody else was willing to volunteer for). I am particularly indebted to Gleb for his contribution to the modelling of the biexcitonic effects. Hadas Shtrikman deserves thanks for the awesome samples which she grew, as are Amit and Yaniv, for the assistance with writing this thesis. Special thanks to all the people who provided the day to day support: Janet, He-rmann and Yossi... And last but not least - all the other students, technicians, secretaries, staff members and other friends, who made their respective lairs friendly places to stay, or at least friendly retreats.

Abstract

Advanced semiconductor growth techniques have in recent years stimulated a tremendous progress in the exciting research field of low-dimensionality systems such as quantum wells. One of the most important tools being applied to the study of these structures are short-pulse lasers, allowing the investigation of dynamical processes which the charge carriers undergo. This thesis describes a research work on GaAs quantum wells, in which sub-picosecond laser techniques, such as differential absorption and four-wave mixing, have been applied. The time-dependent nonlinear optical response of intrinsic and doped structures were studied in the high magnetic field regime.

Starting with the investigation of the spin relaxation of excitons in intrinsic samples, we present data which supports theoretical calculations, predicting a suppressed hole spin relaxation in quantum wells. We were the first to unambiguously resolve this slow process, and take advantage of the spin orientation which it implies in a demonstration of Zeeman absorption quantum beats. We use the beating in a measurement of the exciton g-factor, and extract the exciton dephasing time from their decay. Next the biexcitonic coupling between the excitons is discussed in detail. This coupling is manifested in a novel type of oscillations, which persist only as long as there is a temporal overlap between the two exciting laser pulses. Comprehensive modelling of the time-dependent nonlinear interaction yields an excellent agreement with experiment. Beyond unveiling the nature of the coupling between spin-polarized excitons, these oscillations give the opportunity to measure the biexciton binding energy and its dephasing time.

The final part of this work is devoted to an investigation of modifications to the nonlinear response in the presence of a two-dimensional electron gas in doped samples. Our measurements show a decrease of electron-electron scattering rates at the high magnetic field regime, and a strong footprint of the Fermi edge singularity. We discuss the effect of the magnetic field on electron-electron scattering in detail.

Contents

1. Introduction

1.1. Scientific and technological background

In recent years there has been a great progress in the field of epitaxial growth of ultrathin semiconductor layers.[1] Growth techniques such as MBE (Molecular Beam Epitaxy) allow the preparation of samples made up of layers of different semiconductor materials (such as GaAs, AlAs and AlGaAs alloys), each layer having a typical width on the order of tens of angstroms. These heterostructures have discontinuous potential profiles of the valence and conduction bands, due to the different energy gaps in the different materials. The confinement by the potential profile along the growth axis results in the energy spectrum in these structures being characterized by discrete levels, and the electrons and hole exhibiting a two dimensional behavior.

Basic examples of such heterostructures are heterojunctions, quantum wells and superlattices. In the simplest heterojunction, a layer of low-gap material is grown on a high-gap material. A quantum well is formed by growing a layer of low-gap material between two layers of high-gap material. Several quantum wells may be grown in succession, and if the barriers between them are wide enough, a multiple-quantum-well structure is formed, in which the wells are uncoupled. A superlattice is a multiple-quantum-well structure with narrow barriers, in which the coupling between the energy levels of the separate wells results in the formation of minibands.

Modulation-doping of multiple quantum wells, i.e. doping the potential barriers while leaving the potential wells undoped, allows the formation of a high-mobility two-dimensional electron (hole) gas, free of scattering dopants, in the wells. Alternatively, such a 2DEG (two-dimensional electron gas) may be formed at the interface plane of a heterojunction, by doping the high-gap material. Due to the reduced impurity scattering, the low-density Fermi sea which is formed in these semiconductor systems has many metal-like properties.

The advancement of growth techniques led to extensive research of the transport and optical properties of the two-dimensional systems, and of systems of lower dimensionality

which are produced from them by lithographic techniques.[1] The rich transport phenomena which are exhibited by the 2DEG include quantum mechanical interference effects in the electric conductivity of the layers and tunneling across potential barriers. The 2DEG under combined electric and magnetic fields gives rise to the celebrated Integer and Fractional Quantum Hall Effect in the high magnetic field regime.[2]

The formation of bound states and the confinement of carriers to two dimensions by the heterostructure potential are clearly evident in their optical spectra, so a large part of the research in the field of GaAs heterostructures concerned their optical properties. These have been extensively studied by various cw (continuous wave) optical techniques,[1] primarily photo-luminescence and absorption. In recent years, an increasing interest in dynamical processes in these quasi-two-dimentional structures, coupled with technical developments in the field of tunable short pulse ("ultrafast") lasers, stimulated the study of fast phenomena in two dimentions.[3]

In this work we used sub-picosecond short pulse laser spectroscopy in a study of the time-dependent nonlinear optical response of GaAs heterostructures in high magnetic fields. The rest of this chapter is devoted to a brief review of the basic physical aspects of optical experiments in heterostructures. We describe the band structure and the selection rules for optical transitions in GaAs heterostructures, and discuss their modification in the presence of a magnetic field. In chapter 2, previous works on related subjects are surveyed, with emphasis on time-resolved optical experiments. Some of the questions which were left open by these early studies are cited, leading to the formulation of the research objectives.

1.2. Band structure and optical selection rules in GaAs

GaAs is a well known direct bandgap semiconductor of the III-V group, in which the bottom of the conduction band and the top of the valence band are located at the center of the Brillouin zone (Γ point).[4] The band structure of bulk GaAs in the vicinity of the Γ point is schematically shown in Fig. 1.1. The conduction band is *S*-like, and the *P*-like valence band consists of three subbands: the heavy-hole and the light-hole subbands, which are degenerate at $k = 0$, and the split-off subband, which has a lower energy. Without taking into account small terms caused by the absence of an inversion center, all these bands have spin degeneracy. They are all approximately spherically-symmetric, with

parabolic dispersions. Both the large splitting of the valence subbbands, and the different effective masses which are associated with them, result from the large spin-orbit coupling, which is characteristic of most III-V compounds.

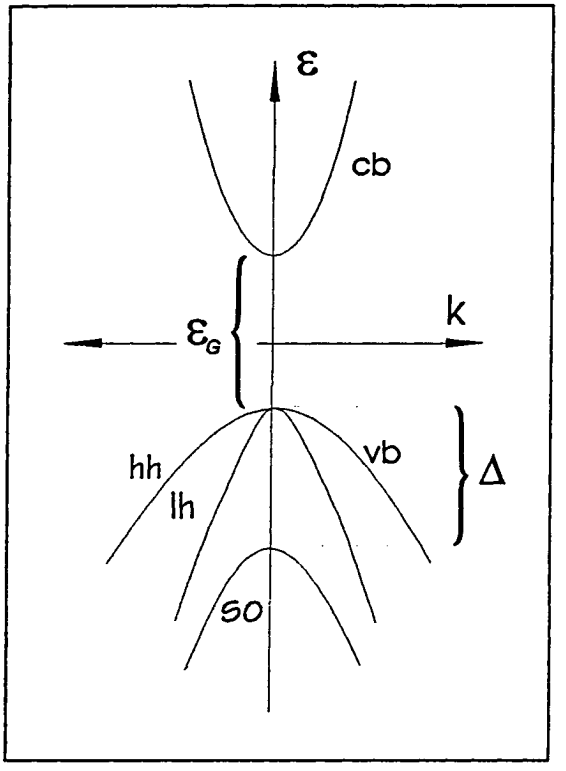

FIG. 1.1: The band structure of bulk GaAs near the Γ symmetry point. .

There are several deviations from spherical symmetry, parabolicity and degeneracy. The absence of an inversion center gives rise to a small spin splitting of the bands and a small displacement of the band edges from the point $k = 0$. The interaction with remote bands results in nonparabolicity of all the bands. This mechanism is particularly important for holes with excess energy close the the spin-orbit splitting Δ (Fig. 1.1). Finally, the fact that GaAs has cubic rather than spherical symmetry causes warping of the energy surfaces (i.e. the effective mass is dependent on the direction of k). These deviations play an important role in spin relaxation processes, as will be detailed in the following chapters.

If nonparabolicity of the conduction band is ignored, the electron spin can be considered as a good quantum number, $s = 1/2$. Similarly, the angular momentum of the hole (or hole "spin") is also a good quantum number, as long as the energy of the hole is low compared to the spin-orbit splitting Δ. Close to the Γ point the heavy-hole and light-

hole subbands correspond to the angular momentum quadruplet $J = 3/2$. The projection of the angular momentum along the z axis is $J_z = \pm 3/2$ for heavy-holes and $J_z = \pm 1/2$ for the light-holes. The split-off band corresponds to the angular momentum doublet $J = 1/2$, with eigenvalues $J_z = \pm 1/2$ for its projection along the z axis.

The allowed interband dipole transitions in bulk GaAs are presented in Fig. 1.2. They reflect the selection rule for optical transitions, which states that angular momentum must be conserved in the absorption or emission of a photon: $\Delta m = \pm 1, 0$. If the quantization axis (z axis) is directed along the wave vector k, then the allowed transitions from the heavy-hole subband to the conduction band correspond to circularly-polarized light, with the dipoles rotating clockwise and counterclockwise in the plane perpendicular to k. The allowed transitions from the light-hole and split-off subbands to the conduction band correspond to circularly-polarized light, with the dipoles rotating in the plane perpendicular to k, or to linearly-polarized light, with the dipoles oscillating along the direction of k.

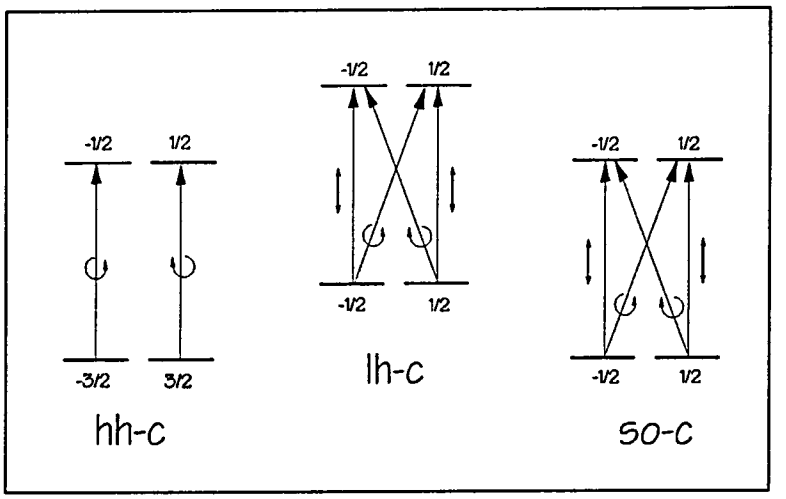

FIG. 1.2: The allowed interband dipole transitions in bulk GaAs. The numbers near the levels correspond to the projection of the total angular momentum on the quantization axis directed along the quasimomentum. The small arrows indicate the corresponding light polarizations.

The above picture is fundamentally changed in heterostructures like quantum wells. This is the result of the energy quantization introduced by the potential discontinuities along the sample growth axis. First, the degeneracy between the heavy-hole and light-hole subbands at the Brillouin zone center is removed. This removal of degeneracy is

accompanied by changes to the effective masses of the subbands. The higher energy band turns out to have the lower effective mass at the Γ point, and away from the zone center the subbands anti-cross each other.[5] In the anti-crossing wave-vector range the two subbands mix and become nonparabolic. These effects are shown in Fig. 1.3, which is reproduced from the calculations of Bastard. Furthermore, the potential discontinuities introduce a prefered quantization axis for the angular momentum, which is reflected in changes of the optical selection rules. Close to the zone center the hole subbands become approximate eigenstates of J_z, where z is now the heterostructure growth axis.[6] The higher-energy subband, with the lower effective mass at the zone center, has angular momentum $J_z = 3/2$, and is still being referred to as the "heavy-hole". The wave-vector range in which angular momentum is a good quantum number increases as the separation between the two subbands increases, as the quantum well is being narrowed. The modified selection rules near the zone center are shown in Fig. 1.4 for light propagating perpendicular to the heterostructure layers. It can be seen in the figure that the allowed transitions from the heavy-hole and light-hole subbands to the conduction band correspond to circularly-polarized light (for the above experimental geometry).

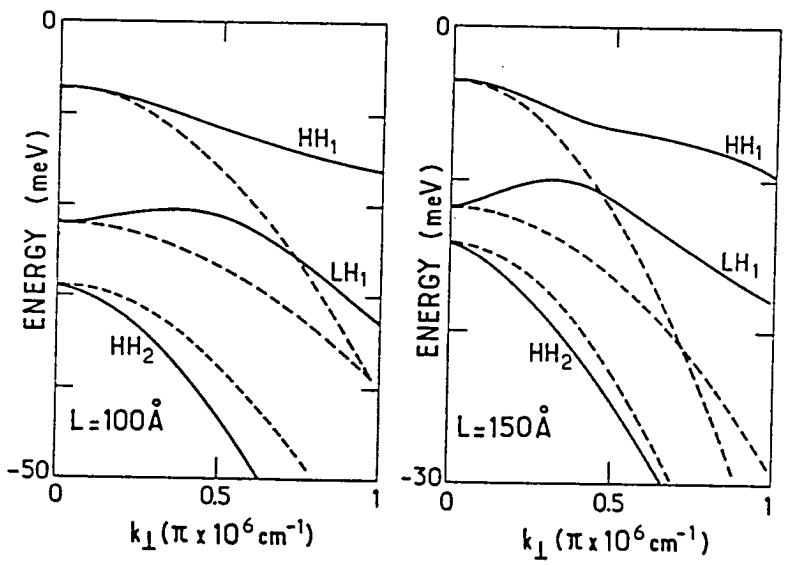

FIG. 1.3: In-plane dispersion relations of the valence subbands of GaAs-$Ga_{0.7}Al_{0.3}As$ quantum wells, of widths L = 100 Å and L= 150 Å. The dashed lines are the subband dispersion obtained without mixing.[5]

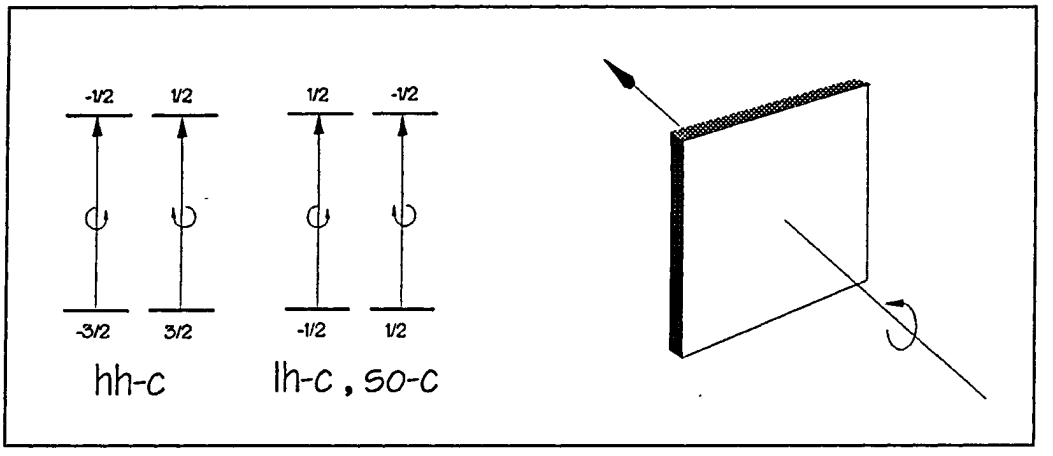

FIG. 1.4: The allowed dipole transitions from the heavy-hole subband to the conduction band in GaAs quantum wells. The numbers near the levels correspond to the projection of the total angular momentum on the quantization axis directed along the quasimomentum. The small arrows indicate the corresponding light polarizations.

An important aspect of optical experiments in semiconductors is the excitonic phenomenon.[7] An exciton is an optical excitation in which a bound state of a conduction electron and a valence hole is formed below the semiconductor bandgap. The excitonic phenomenon is particularly significant in heterostructures, since the confinement of the electron and the hole in a quantum well increases the exciton binding energy appreciably (in GaAs the binding energy increases from ~ 5 meV in the bulk to ~ 10 meV in quantum wells). The selection rules for the creation and annihilation of excitons are a direct consequence of the selection rules for the respective electron and hole which form the exciton (an exciton may be simply described as a wave packet which is constructed from the free electron and hole states at the band edges, so the angular momentum of the exciton is well-defined). Thus an optically-active exciton, that is, an exciton which can be optically excited, has angular momentum ±1 (fot light perpendicular to the heterostructure plane). Excitons are the lowest energy excitations in intrinsic samples, and their large oscillator strength and comparatively slow relaxation encouraged many experimentalists to study them, as will be discussed in the following.

In MD samples the 2DEG excludes absorption into states below the Fermi energy. The excitonic interaction is screened, but a logarithmic divergence of the absorption develops for optical transitions to the vicinity of the Fermi energy.[8] This effect, which results from

the scattering of the electrons in the Fermi sea by the photo-excited holes, is the well-known Fermi-edge singularity (or "Mahan exciton").

1.3. Heterostructures in a magnetic field

The spin degeneracy of the electronic band structure in GaAs quantum wells is removed by the application of a magnetic field. This Zeeman splitting is characterized by the Lande g-factor. The deviation of the g-factors in semiconductors from the g = 2 of the free electron can be quite remarkable, and its sign may be either positive or negative: while in the conduction band of GaAs it is as low as -0.41, in InSb it reaches a high value of -50. This considerable variation is a result of the spin-orbit interaction,[9] the strength of which varies between various materials and the different bands in each material. In quantum wells, the g-factor of the valence subbands is dependent on the well width and the magnetic field orientation. Although spin-orbit effects are less important in the conduction band, there is still well-width dependence of the g-factor of conduction electrons. The spill-out of the electron's wave function into the AlGaAs barriers, which have a different g-factor, makes a strong contribution.[10]

The effect of a magnetic field on a heterostructure is however not limited to their Zeeman splitting. When the magnetic field is applied normal to the layers of the heterostructure, the electronic density of states and wave functions of the semiconductor material radically change.[11] The zero field continuous density of states of the quasi-two-dimensional structures changes into a discrete spectrum of degenerate Landau levels, while the electronic wave functions change from plane waves to localized (gauge dependent) functions. In intrinsic samples the combined magnetic and Coulomb correlations between optically excited electron and holes results in the appearance of multiple magneto-excitonic lines in the optical absorption spectrum at the high magnetic field regime. Each of these lines is associated with an allowed optical transition, from a Landau level in the valence band to one in the conduction band.[12] The selection rule for the transition is $\Delta n = 1$, where n is the magnetic quantum number. The spacing between the magneto-excitonic lines is given by the sum of the cyclotron frequencies for the two bands. In GaAs this spacing is approximately 10 meV in a magnetic field of 5 Tesla. In such a field the magnetic length (classical cyclotron radius) becomes comparable with the excitonic Bohr radius, defining the transition between the low and high magnetic field regimes. The above simple picture is complicated by mixing and anti-crossing of Landau

levels in the valence band.[13] This band mixing also affects the g-factor, making it magnetic-field dependent.

The optical properties of doped samples in a magnetic field is strongly affected by the 2DEG. Similarly to the situation in zero magnetic field, the 2DEG excludes absorption into Landau levels below the Fermi energy, and screens the excitonic interaction. The optical absorption spectrum of MD samples in a magnetic field is characterized by peaks which correspond to excitations of electrons from filled Landau levels in the valence bands to empty Landau levels in the conduction band. These levels are significantly broadened due to various scattering mechanisms which are present in any real sample (including electron-electron scattering).[14] As the magnetic field is increased the higher Landau levels are emptied of electrons, and the Fermi energy gradually shifts to the lower levels. Absorption into the emptied Landau levels becomes possible, and one observes a new peak at the absorption edge each time the Fermi level shifts to a lower Landau level.[15] A well known consequence of this is the afforementioned Integer Quantum Hall Effect in magneto-transport experiments on similar samples.[16]

2. The research objectives

In the last decade there has been an increasing interest in the dynamical aspects of optical excitations in quasi-two-dimentional structures. This interest was stimulated by technological breakthroughs in the field of mode-locked short-pulse lasers. Most of the time-resolved studies on heterostructures focussed on the energy relaxation and thermalization of optically excited carriers, in both intrinsic and doped samples.[17] Many studies on intrinsic quantum well samples concerned the dynamics of the two-dimensional excitons.[18] During the last few years there is a growing interest in the application of coherenct techniques to the study of fast processes. These techniques allowed the determination of scattering rates by measuring the dephasing of the coherent signal.[19] Relatively slow dephasing rates were demonstrated in the case of excitons which are localized due to the interface roughness in narrow quantum well samples.[20,21] Another interesting aspect of the use of coherent techniques is the ability to resolve small energy splittings, otherwise hidden by the inhomogeneous broadening of spectral lines (the splitting leads to the appearance of beating in the coherent signal).[22]

Time-resolved optical experiments on heterostructures in high magnetic fields have not been published before the start of the current research work, but the interest in this field was growing rapidly. The modifications to the density of states and phase space for scattering, and alterations of the electronic wave functions and scattering matrix elements, were expected to lead to substantial changes of the relaxation rates which are measured by time-resolved optical spectroscopy. Such experiments were expected to reveal clear differences between the relaxation of high Landau levels and magneto-excitons, and the fast relaxation of above-band-gap free-carrier excitations in zero magnetic field.[17] The main objective of the research was to study these modifications in both intrinsic and MD samples.

In parallel to the start of our research work, other laboratories had also embarked on short-pulse experiments on GaAs heterostructures in high magnetic fields. Among these were groups at Bell labs., UC Berkeley and the University of Michigan, Ann Arbor. Within this developing field we defined two main goals for our experiments: the

investigation of spin dynamics of magneto-excitons in intrinsic samples, and electron-electron scattering in MD samples in the high field regime.

Unlike energy relaxation, the spin relaxation of photo-excited carriers in heterostructures has recieved relatively little attention until very recently. In the case of GaAs heterostructures a slow-down of the hole spin relaxation was predicted, due to the changes to the expectation values of angular momenta of the hole states away from the zone center, and a suppression of the scattering between them.[6,23] The polarization degree of freedom in optical experiments provides a convenient way for studying this spin relaxation. Indeed, spin relaxation is frequently studied in cw experiments, by measuring the depolarizations of the emitted luminescence, following excitation with polarized light.[4] Time-resolved experiments with circularly polarized pulses have the advantage of providing a *direct* measurement of spin relaxation rates, and a few such experiments have been done previously in zero magnetic field.[24,25,26] The spin relaxation in high magnetic fields was previously studied *exclusively* by the cw photo-luminescence depolarization technique.[27] Yet, there was still no clear experimental evidence of the predicted slow hole spin relaxation in quantum wells. It was also unknown how the excitonic interaction would affect the spin relaxation, although the slow dephasing of localized excitons hinted that the spin relaxation could be slow. These open questions had motivated us to start our research with a study of exciton spin relaxation in intrinsic quantum well samples, its effects on the dephasing of the excitons, and its dependence on the magnetic field strength.

Our interest in MD samples in high magnetic fields was stimulated by the unique transport phenomena which are exhibited by them in this regime. Several workers have addressed the complicated many-body interactions of the optically excited carriers with the 2DEG in the magnetic quantum limit, using various cw optical techniques such as inelastic light scattering[28] and photo-luminescence.[29] The clear footprint of the interacting 2DEG in the cw optical spectrum of MD samples in a magnetic field, motivated us to study this case in the time domain. We had realized that many-body effects will most certainly modify the simple two-level system picture, which is generally used in the interpretation of time-resolved optical experiments in intrinsic samples. It was also obvious that electron-electron scattering would play an important role in the behavior of MD samples, and that this behavior in a magnetic field would be different from that which was observed in earlier experiments in zero field.[17] Our motivation for using time-resolved optical spectroscopy in the study of MD structures was thus two-fold: to study the effect of the magnetic field on

electron-electron scattering, and to examine the modifications to the simpler excitonic non-linear response, which was to be studied first in detail.

Other questions which came up as the research work proceeded concerned the interaction of light with the spin-degenerate exciton and the binding of excitons in biexcitonic molecules. Numerous studies of exciton dynamics have shown that the coherent nonlinear optical interaction in intrinsic quantum wells could be described in most cases using a simple two-level atom model. However, the spin degeneracy of the exciton means that it actually should be described by two sets of two-level systems. A substantial part of the work was dedicated to the study of the coupling between these two systems, and to the effect of the coupling on exciton dephasing. This study culminated in a thorough investigation of the biexciton phenomenon. The application of a magnetic field removed the degeneracy of the pair of two-level systems. In this case, the coherent nature of the nonlinear optical interaction allowed us to observe quantum beats between the Zeeman-split levels.

The structure of the work is as follows: In chapter 3 we describe the experimental method and setup. In chapter 4 we present a study of spin relaxation in quantum wells. We first review the mechanisms for the spin relaxation of electrons, holes and excitons, and review earlier works on the subject. We then present our experimental data, which are the first to unambiguously resolve the slow hole spin relaxation in quantum wells. Chapter 5 is dedicated to the demonstration of the Zeeman quantum beats, and to a discussion of appropriate level diagrams for the heavy-hole exciton system. In chapter 6 the biexcitonic coupling is introduced. This coupling is manifested in remarkable oscillations, which appear during the overlap of the pump and probe pulses. Comprehensive modelling of the time-dependent nonlinear interaction yields an excellent agreement with experiment. In chapter 7 we investigate modifications to the nonlinear response due to the presence of a two-dimensional electron gas. Our measurements show a decrease of electron-electron scattering rates at the high magnetic field regime, and a strong footprint of the Fermi edge singularity.

3. The experimental method

3.1. Time-resolved differential absorption and four-wave mixing

Time-resolved differential absorption (DA, also known as "pump-probe") and four-wave mixing (FWM) are two nonlinear experimental techniques which are often used in investigating the nonlinear response of quantum wells.[85] In these techniques two pulses, delayed by t_D with respect to each other, are incident on a sample. In a DA experiment (Fig. 3.1) one of the pulses (the "pump" pulse) excites the sample, and the change of absorption of the second pulse ("probe") is measured as a function of t_D. To measure the change of absorption due to the pump, the latter is modulated by a low-frequency chopper, and the changes in the output probe intensity are detected by a slow detector and a lockin amplifier. In a FWM experiment (Fig. 3.2) the two laser pulses coherently excite the sample, and the signal which is emitted following the excitation is measured as function of the delay. In this experiment the two pulses have wave vectors $\boldsymbol{k}_1$ and $\boldsymbol{k}_2$ with a small angle between them, and the integrated light intensity in direction $2\boldsymbol{k}_2$-$\boldsymbol{k}_1$ or $2\boldsymbol{k}_1$-$\boldsymbol{k}_2$ is measured by a slow detector. A chopper is used in this experiment as well, to reduce backgound signals.

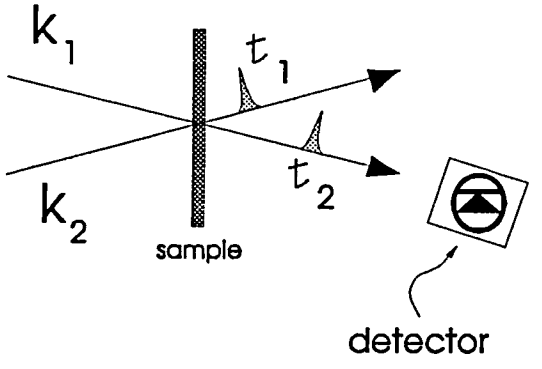

FIG. 3.1: A differential absorption (DA) experiment.

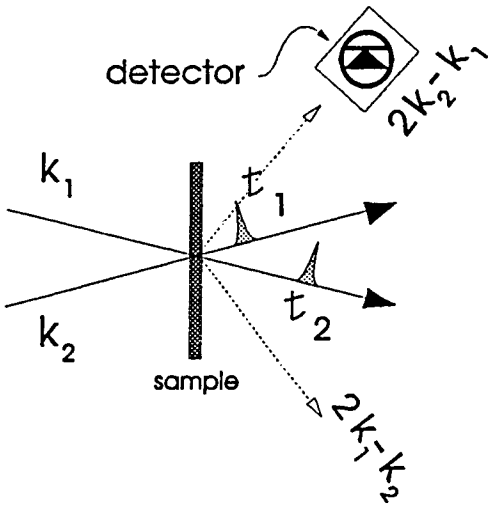

FIG. 3.2: A Four-Wave Mixing (FWM) experiment.

In ultrafast nonlinear optical experiments the measured signal is proportional to the third order dipole moment.[30] It can be shown that this is the case in the DA and FWM experiments. In DA experiments the signal which is measured by the detector contains first order contributions as well, but the differential measurement at the chopping frequency filters out only third order terms. In the FWM signal the "diffracted" signal in the directions $2\boldsymbol{k}_2$-$\boldsymbol{k}_1$ and $2\boldsymbol{k}_1$-$\boldsymbol{k}_2$ by definition contains only third order terms, as can be realized from momentum conservation arguments. The change of absorption $Q^{(3)}$ in a DA experiment is given in terms of the third order dipole moment by:

$$Q^{(3)} = \int_{-\infty}^{\infty} dt\, E_\beta(t) \frac{\partial}{\partial t} d_\beta^{(3)}(t) \,, \tag{3.1}$$

where $d_\beta^{(3)}$ is the β polarization component of the third order dipole moment, proportional to $E_\beta E_\alpha^2$, and E_α and E_β are the pump and probe fields, respectively. Similarly, the signal

in a FWM experiment is proportional to:

$$P \sim \int_{-\infty}^{\infty} dt \left| d^{(3)}(t) \right|^2 , \tag{3.2}$$

and $d^{(3)}(t)$is the relevant contribution to the third order dipole moment proportional to $E_1^2 E_2$ (direction $2\boldsymbol{k}_1$-$\boldsymbol{k}_2$) or $E_2^2 E_1$ (direction $2\boldsymbol{k}_2$-$\boldsymbol{k}_1$).

In Appendix A we use the density matrix formalism to give a general expression to the third order dipole moment in a time-resolved experiment.[31]

The DA experiment is commonly regarded as a measurement of the *population*. The rate of decay (as function of the delay time) in a time-resolved DA experiment can be related to the lifetime of the photoexcited population, which is usually denoted by T_1. This is clear if one considers only the phase space filling effect of the pump pulse. In most cases, however, the excitation by the pump also leads to a shift of the absorption spectrum (due to a change of the self-consistent energy spectrum of the crystal), as well as to its broadening (due to scattering by the optically excited carriers). Each of these effects is reflected differently in the spectral variation of the DA signal, but the rate of decay in a temporal measurement at any fixed spectral position will always be related to T_1.

The FWM signal is a measure of the induced polarization in the sample, and the rate of decay of this signal as function of the time delay is a measure of the *phase relaxation rate* of the coherent excitation. It should be emphasized that the phase relaxation rate in FWM experiments is generally different from the phase relaxation rate of electrons in transport experiments. Assuming a phase relaxation time T_2, the decay rate of the FWM signal is $2/T_2$ and $4/T_2$ for homogeneous and inhomogeneous broadening, respectively.[32] For homogeneous broadening the FWM signal is a "free polarization decay", emitted coincidently with the second pulse.[32] For inhomogeneous broadening it is a "photon-echo", which is emitted at a delay of t_D relative to the second pulse.[32]

DA and FWM are thus complementary techniques, which give information on different relaxation processes.

3.2. The experimental system

Figure 3.3 illustrates the experimental setup for the DA and FWM experiments. The figure depicts the mode-locked Nd-YAG laser, which emits approximately 20 Watts of IR radiation (1.06 μm) in 90 ps pulses, at a PRF (Pulse Repetition Frequency) of 80 MHz. The IR beam is focussed on a KTP nonlinear crystal, in which part of it is up-converted to 1-2 Watts of visible light by second-harmonic generation. The output pulses of 532 nm radiation are synchronously pumping a two-jet dye laser - either Pyridine 2 (700-780 nm) or Styryl 8 (760-840 nm). The autocorrelation time of the pulse is approximately 1 ps in both dye lasers, which sets the temporal resolution of the experiment. To stabilise the pumping of the dye lasers we used a closed-loop stability augmentation system, with feedback to the Nd-YAG cavity.

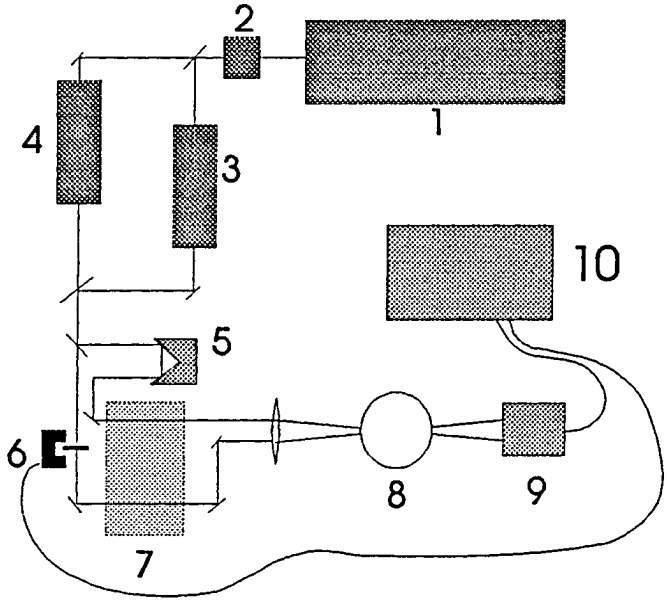

FIG. 3.3: The experimental setup: (1) Mode-locked Nd-YAG laser with frequency doubling; (2) Beam stabilization; (3) and (4) Dye lasers; (5) Variable delay step-motor; (6) Chopper; (7) Polarization and beam-width control; (8) Magneto-optical cryostat; (9) Detector; (10) Lock-in amplifier.

The laser beam is split to a pump and probe beams with an intensity ratio of 10:1. The probe beam is then passed through a variable delay, consisting of a retroreflector mounted on a linear step-motor. The step-motor has an accuracy of 1 μm, translating to a temporal resolution of 6.7 fs. The two beams are then brought, through the chopper slits, to the optical aperture of the cryostat. The polarizations of the two beams are independently controlled by means of half-wave and quarter-wave plates, or Fresnel rhombs. In most of our experiments the probe beam was expanded

by a factor of three, to give a smaller spot size and reduce the sensitivity to misalignment of the delay line (this was particularly important in our spin relaxation measurements, in which the full 14-cm travel of the step-motor was used). The beams are focussed on the sample by a single 250-mm lens, and a CCD imaging system is used for fine adjustment of the beams overlap. The beams exiting the cryostat are analysed by a polarizer, and focussed on a silicon photodetector. The detector is aligned either to the probe (in DA experiments) or to the direction of the emitted FWM signal ($2\boldsymbol{k}_2-\boldsymbol{k}_1$).

In the experiments we use one of two split-coil magneto-optical cryostat with variable-temperature inserts. One has a 5 Tesla magnet, while the other has a 7 Tesla magnet which can be operated at 8 Tesla when pumping on its Lambda-plate. Most experiments were performed at liquid-helium temperature. An important feature of the cryostats are their low-birefringence antireflection-coated windows, which are mounted on strain-relief leak-proof mounts. This arrangement is critical for controlling the polarizations of the exciting laser beams.

4. A study of spin relaxation

4.1. Spin relaxation in bulk GaAs

In an ideal parabolic, spherically symmetric band structure the two degenerate spin states are orthogonal, and one wouldn't expect spin-flip processes to occur. Deviations from this ideal structure, which were outlined in the introduction, may give rise such processes. Optical experiments, which allow selection of the spin states by varying the polarization of the light, make it possible to investigate these processes. The subject of optical orientation in bulk semiconductors of the III-V group was extensively studied both theoretically and experimentally. It was found that the mechanisms which dominate the spin relaxation of electrons in the conduction band are quite different from those which affect the holes in the valence bands.[33]

A valence hole in bulk GaAs can relax its spin through scattering between the different hole subbands. The large spin-orbit coupling in the valence band, which is characteristic of most III-V compounds, implies that the hole spin is a good quantum number as long as the energy of the hole is low compared to the split-off band (see section 1.2). In other words, the heavy-hole and light-hole subbands are eigenstates of the angular momentum operator J_z close to the subbands' edges. At the instant of photoexcitation the holes are oriented. However, because of the strong coupling between the hole's angular momentum and quasimomentum $\boldsymbol{k}$, which is the result of the spin-orbit coupling, the orientation of the holes is quickly destroyed. For holes with high excess energy this occurs in parallel to the fast energy and momentum relaxation to the bottom of the band. The thermalization of holes with low excess energy to states with a finite momentum also brings about spin relaxation within a period which is on the order of the momentum relaxation time. This relaxation is fast even at low temperatures, since the two subbands are degenerate at the subbands' edges, where $\boldsymbol{k}$ vanishes.

The degeneracy of the two valence subbands at the zone center is easily removed by mechanisms which break symmetry, such as deformations[4] (externally-applied or phonon-induced) and inhomogeneities. This leads to the destruction of the coupling between the angular momentum and quasi-momentum, but may also bring about spin relaxation by

phonon scattering.[34] In any case, a valence hole in bulk GaAs typically relaxes its spin within less than a picosecond. Indeed, instant depolarization of the holes was assumed in optical experiments on bulk GaAs, as well as in some works on GaAs quantum wells.[35]

The spin relaxation of electrons in the conduction band of bulk GaAs is more subtle. These electrons can relax their spin by the Elliott-Yafet[34,36] or D'yakonov-Perel[37] mechanisms, both of which are the result of deviations from the spherical-parabolic band approximation near the Γ point of the conduction band. The Elliott-Yafet mechanism is due to the weak spin-orbit mixing of the valence band states into the conduction band for $k \neq 0$. This mixing produces a non-zero matrix element for scattering between spin-up and spin-down electron states. The D'yakonov-Perel mechanism also originates from the spin-orbit interaction, and is unique to semiconductors which lack inversion symmetry, such as the III-V group. When this lack of inversion symmetry is taken into account in the spin-orbit interaction, a splitting of the conduction band results, which is equivalent to a pseudo magnetic field acting on the electrons. This pseudo magnetic field leads to a precession of the electron spin, which depends on the direction and magnitude of the electron's momentum. Collisions, which change the momentum of the electron, rotate the precession axis, and if the time interval between collisions is much smaller than the precession period a spin relaxation process ensues.

There is a fundamental difference between the Elliot-Yafet and D'yakonov-Perel mechanisms: while the Elliott-Yafet mechanism causes a conduction electron spin to flip *in a momentum scattering event*, in the D'yakonov-Perel mechanism spin reorientation actually takes place *in the intervals between spin-preserving collisions*. The collisions are essential to the D'yakonov-Perel mechanism in that they randomise the direction of the precession. As the rate of these collisions (the momentum relaxation rate) increases, the mean angle of precession between collisions is decreased, and so does the spin relaxation rate. This leads to a characteristic inverse proportionality of the spin relaxation time and the momentum scattering time: $\tau_s \approx 1/(\Omega^2 \tau_p)$, where Ω is the precession frequency. (Such an inverse proportionality is known as "motional narrowing": since in the absence of collisions the precession is momentum-dependent, the momentum distribution of the electrons leads to an inhomogeneous broadening of the spin resonance line, in analogy to the effect of a random local magnetic field; collisions result in the spin resonance line being narrowed back). It is believed that the D'yakonov-Perel mechanism is dominant in GaAs,[38] in which Ω^{-1} is estimated to be on the order of 10^{-10} sec for thermalized electrons at low

temperatures (4°K). A characteristic momentum scattering time of 10 ps therefore translates to a spin relaxation time of ~ 1 ns in bulk GaAs.

The spin relaxation processes discussed so far are relevant for non-correlated free carriers. When excitons are considered, it is obvious that their spin can be changed by flipping the spin of either the electron or the hole, or by *simultaneously flipping the spins of both constituents*. Bir *et al.* have shown[39] that the exchange interaction can lead to an efficient spin-flip scattering of electrons by holes. There are two different contributions to this mechanism, one of them related to the exchange-induced splitting of heavy holes excitons (optically active and inactive states). The other contribution is related to a long-range annihilation interaction, the exchange counterpart of the long-range direct Coulomb interaction which binds the exciton. It had been shown in cw photo-luminescence experiments on p-type GaAs that at low temperatures (T<100°K) this Bir-Aronov-Pikus (BAP) mechanism dominates.[40]

4.2. Spin relaxation in quantum wells

While the confinement in a quantum well does not result in any substantial modification of the spin relaxation of the conduction band electrons, beyond its $\boldsymbol{k}$ dependence (due to the two-dimensional dispersion), it does modify the spin relaxation of holes in a pronounced way. As outlined in the introduction, the energy quantization which is introduced by the potential discontinuities along the sample growth axis results in a removal of degeneracy, at the Brilouin zone center, between the heavy-hole and light-hole subbands, accompanied by mixing of the two subbands, changes of their effective masses, nonparabolicity and changes of the expectation values of the hole angular momenta. There exists an in-plane wave-vector range where the valence subbbands are approximate eigenstates of J_z, and this wave-vector range increases as the separation between the two subbands increases. The removal of degeneracy and the well-defined J_z eigenstates at the band edge result in a suppression of the heavy-hole spin relaxation,[6,23] and gives rise to spin-flip times which are much longer than in the bulk semiconductor. This suppression of the hole spin-flip is increasingly effective as the quantum well is narrowed.

Since excitons are made up of linear combinations of free electron and hole states, the slowing down of the hole spin relaxation in quantum wells would result in a corresponding slow down of the single-particle spin flip in excitons. However, the enforced close

proximity of the electron-hole pair leading to the strong exciton binding in a quantum well is also expected to lead to a strong spin relaxation due to exciton exchange. At the start of this research work there was no experimental study of these effects. It was not clear weather single-particle spin-flip would lead to a sequential relaxation of the hole and the electron spins, or strong exchange-induced spin-flip will dominate. The assumption of a slow down of the hole spin relaxation indeed led to a different and more satisfactory explanation of cw luminescence polarization in quantum wells,[23] but there was still no *direct* experimental evidence of this effect. It was also unclear to us how the slow dephasing of localized excitons in narrow quantum wells[20] is related to the spin relaxation process.

4.3. Optical probing of spin relaxation - experimental considerations

Let us now consider an optical experiment, with circularly polarized light incident along the growth axis of the quantum well, tuned to the lowest-energy heavy-hole exciton. The $m_h = \pm 3/2$ components of the angular momentum dominate the valence hole of that exciton, so that the total spin of a photo-excited heavy-hole exciton is ± 1. For these optically active heavy-hole excitons, spin flip of either constituent would transform the exciton to a spin ± 2 optically inactive state, while simultaneous flipping of the spins of both the electron and hole will transform one optically active exciton to the other.

From the above discussion it can be understood how spin dynamics would be reflcted in optical experiments. Consider as an example a cw luminescence experiment in which the sample is excited by σ^+ light, and the polarization of the emitted photons is analysed. The probability to emit a σ^- photon would equal the probability to emit a σ^+ photon only after a complete depolarization of the excitons had occured, so a measurement of the luminescence polarization, plus the knowledge of the exciton recombination time, can be used to derive an estimate for the spin relaxation time. However, this method of extracting the spin relaxation time is reliable only in simple cases. Such is the case of bulk GaAs, where instant spin relaxation of the holes can be assumed, and consequently the only relevant dynamics are those of the conduction electrons.

Time-resolve optical spectroscopy allows better understanding of the spin dynamics. The two techniques which can be used in this case are time-resolved photo-luminescence and time-resolved DA ("pump-probe"). Consider an optical excitation by a σ^+ circularly

polarized laser pulse. A spin-flip event of a single constituent (electron or hole) into an optically inactive state produces a decay of the σ^+ photo-luminescence emission, but no corresponding increase of the σ^- photo-luminescence emission. Only when both constituents flip their spins does a σ^- photo-luminescence signal show up. A comparison of the initial decrease of the σ^+ signal to the rise of the σ^- signal can thus give information about the spin-flip rates of the different excitonic constituents. To allow the observation of a single-particle fast hole spin relaxation in a photo-luminescence experiment, it is possible to provide an equilibrium population of unpolarized electrons in the conduction band by means of doping.[41] This inevitably modifies the well potential, introduces scattering centers, and does not allow a study of *exciton* spin relaxation. Another disadvantage of the time-resolved photo-luminescence technique is its basic signal-to-noise limitation in resonant excitation.

Contrary to time-resolved photo-luminescence, time-resolved DA allows resonant excitation and probing of the excitonic transition. Another advantage of a DA experiment is that following a spin-polarized (σ^+ or σ^-) excitation, one may expect to observe changes in the absorption of *both circular polarizations* as a result of a single-particle spin-flip event. This is easily understood if free carriers are considered. In this case the probability of absorbing a photon is dependent on $(f_c - f_v)$, the difference between the occupation of the conduction band f_c and that of the valence band f_v. A hole spin-flip following a σ^+ excitation, for example, involves the destruction of a valence band state which could otherwise be excited by a σ^- photon, and the creation of a valence band state which may be excited by a σ^+ photon. In other words, a hole spin-flip changes f_v for the transition associated with both circular polarization. In the excitonic representation one must take into account the fact that the phase space for the creation of optically active and inactive excitons is coupled, i.e., the same valence band states are required to build one optically active exciton and one optically inactive exciton (note that in a DA experiment an additional exciton must be created by the probe, while in a photo-luminescence experiment the phase space for the *creation* of excitons does not matter).

Before the start of the current research work, most studies of spin relaxation in GaAs quantum wells were by the cw luminescence polarization technique. The electron spin relaxation time, deduced with the assumption of an instantaneous hole spin relaxation, was found to be ~200 ps at 4K.[35] This is not very different from the electron spin relaxation times which were reported for bulk GaAs and AlGaAs. Freeman *et al.* combined cw and time-resolved photo-luminescence measurements and showd that spin lifetimes cannot be

reliably extracted from cw measurements.[24] Their work had also indicated that the depolarization rate is sample dependent. Damen *et al.* also used time-resolved photoluminescence spectroscopy in the study of spin relaxation.[26] These early works, which were performed on relatively wide quantum wells (~100Å), failed to resolve the spin relaxation of the holes. Time-resolved DA measurements had been reported for narrow quantum wells at room temperatures only,[25] in which case an instantaneous depolarization of the holes was found. With these early results in mind we had started our own investigation of exciton spin relaxation.

4.4. Exciton spin dynamics - experimental results in zero magnetic field

In order to study the spin relaxation process of excitons in quantum wells we performed a time-resolved differential-absorption experiment on several GaAs quantum well samples at liquid helium temperature. Using circularly polarized pump and probe tuned to the heavy-hole exciton, we were able to confirm the theoretical prediction of a slow hole spin-flip in narrow quantum wells.

We used our mode-locked pyridine 2 and styryl 8 lasers in this experiment, both with sub-picosecond resolution. The polarization of the pump (σ^+) was fixed, while the mounting of a quarter-wave plate in the probe beam allowed reversing of the probe handedness (from σ^+ to σ^-) without affecting the zero time of our setup. Special care was taken to eliminate possible birefringent elements in the setup.

We studied three different GaAs/AlGaAs samples: a square multiple quantum well (MQW) sample, a stepped MQW sample, and a superlattice. Spectral transmission curves of the three samples are shown in Fig. 4.1. The square MQW sample has 20 periods of 80-Å GaAs wells separated by 300-Å $Al_{0.3}Ga_{0.7}As$ barriers, with a strong heavy-hole excitonic absorption line at 1.570 eV. The stepped MQW sample has 100 stepped wells, with adjacent layers of 30-Å GaAs and 100-Å $Al_{0.1}Ga_{0.9}As$, separated by 100-Å $Al_{0.3}Ga_{0.7}As$ barriers. The structure is embedded in the intrinsic region of a *p-i-n* structure. The wave functions associated with the first energy levels of the electron and holes are confined mainly in the 30-Å GaAs layer. The first electron energy level in this structure coincides with the potential step of the well, which makes the structure prone to large potential disorder due to well width and alloy fluctuations. Indeed, the absorption spectrum of that sample shows a wide (≈6 meV), inhomogeneously broadened, heavy-hole

excitonic peak at 1.617 eV. The superlattice sample consists of 100 periods of alternating 30-Å layers of GaAs and $Al_{0.3}Ga_{0.7}As$, with the heavy-hole excitonic absorption line at 1.683 eV. This structure is also embedded in the intrinsic region of a *p-i-n* junction.

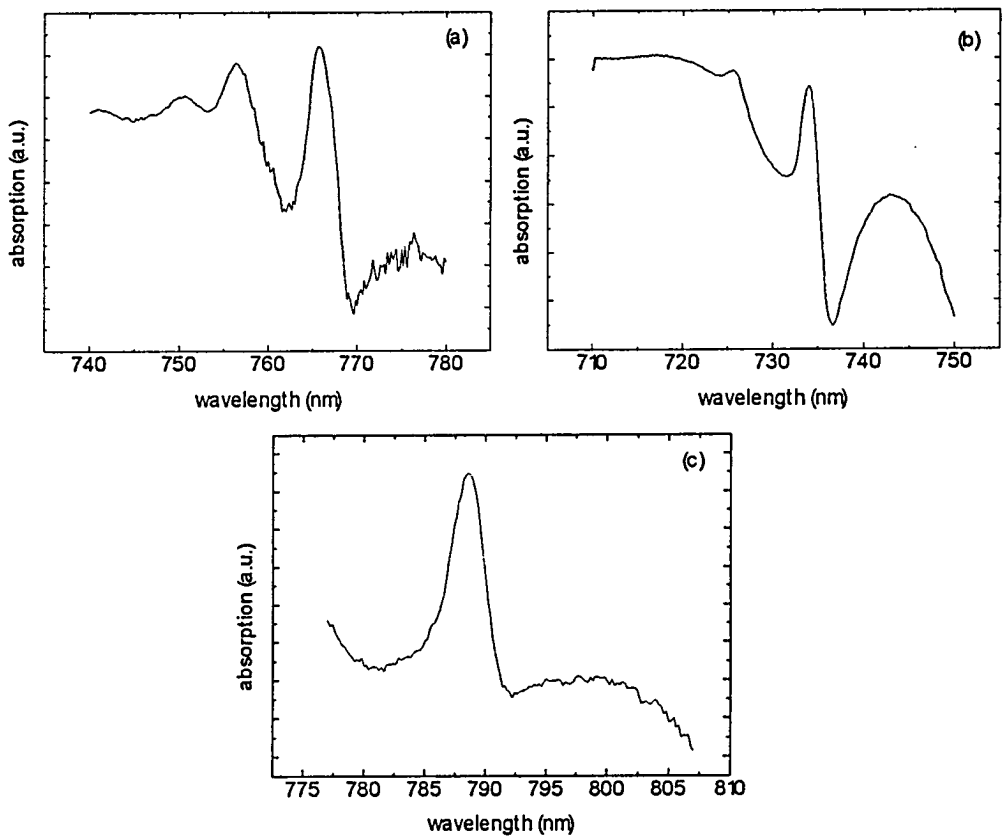

FIG. 4.1: Spectral absorption curves for the three samples used in the study of exciton spin relaxation: (a) the stepped MQW sample; (b) the superlattice; (c) the square MQW sample. The feature at the long wavelength end of each spectrum is a Fabri-Perot fringe.

Figure 4.2 shows the temporal evolution of the signal when the stepped MQW sample is degenerately pumped and probed just below the heavy-hole exciton absorption peak (1.613 eV). Figure 4.2(a) shows the change of absorption of a σ^+ probe and that of a σ^- probe, following excitation by a σ^+ pump. In Fig. 4.2(b) the σ^- signal is plotted with better definition. The data shown in the figure were taken with a pump intensity of approximately 30 W/cm^2 (corresponding to an exciton density of 1.5×10^{10} cm^{-2}). The first few tens of picoseconds after the excitations are characterized by a sharp decrease of the σ^+ signal and a sharp rise of the σ^- signal. The two curves then converge gradually and coincide approximately 350 ps after the excitation, indicating that complete spin relaxation

has been reached by then. This behavior suggests the existence of two sequential processes. In Fig. 4.2(c) the logarithm of the difference between the two signals of Fig. 4.2(a) is plotted, as a measure of the net relaxation rate of the difference between the σ^+ and σ^- exciton populations. Two time constants, approximately 50 ps and 120 ps, are clearly observed. We associated the fast decay with the spin relaxation of the heavy-hole, and the slow one, following which the two spin populations are equalized, with the electron spin relaxation. Note that the σ^- signal is decaying at long delays rather than increasing with the spin relaxation of the electrons (this point will be adressed in section 6.5). The same general behavior, of two time constants and a decrease of the σ^- signal when spin relaxation is not complete, was observed when the pump intensity was lowered over two decades. This is demonstrated in Fig. 4.3, which shows the σ^- signal measured with a pump intensity of 3 W/cm^2 (exciton density of 1.5×10^9 cm^{-2}).

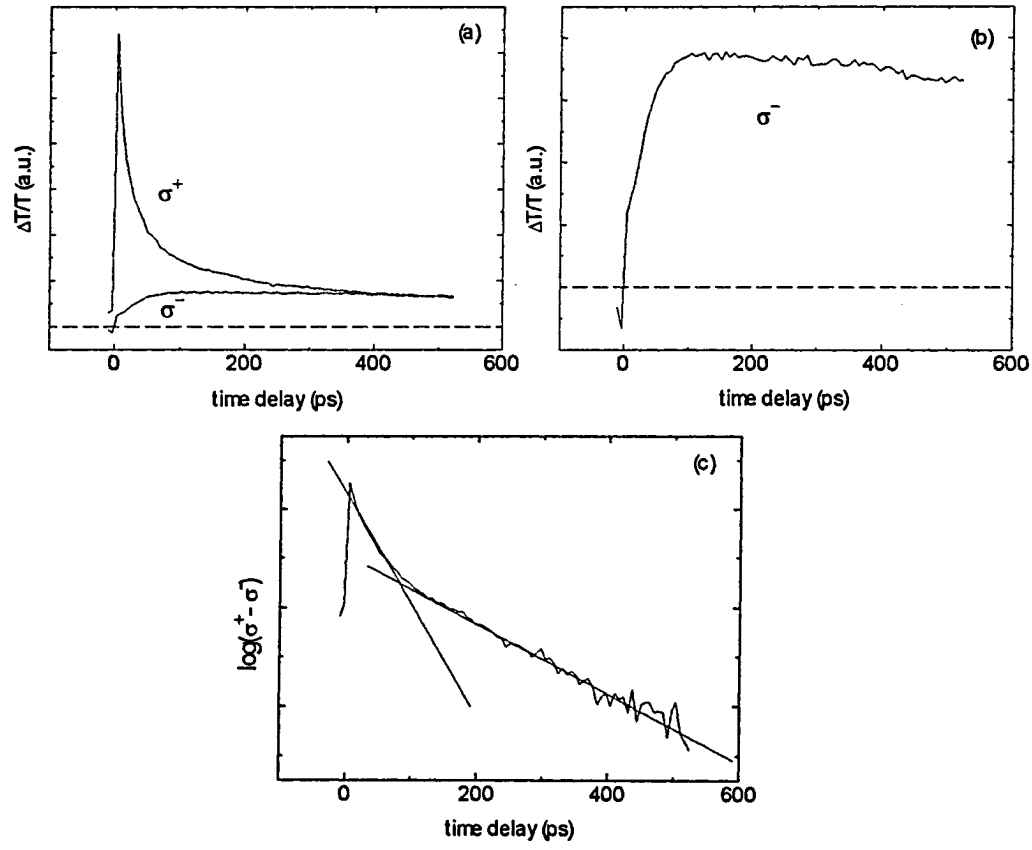

FIG. 4.2: The differential absorption signal ΔT/T slightly below the heavy-hole exciton of the stepped MQW sample, with σ^+ pump polarization and intensity of 30 W/cm^2. (a) The signal for σ^+ and σ^- probe at B=0. (b) The σ^- signal with better definition. (c) The logarithm of the difference between the σ^+ and σ^- signals.

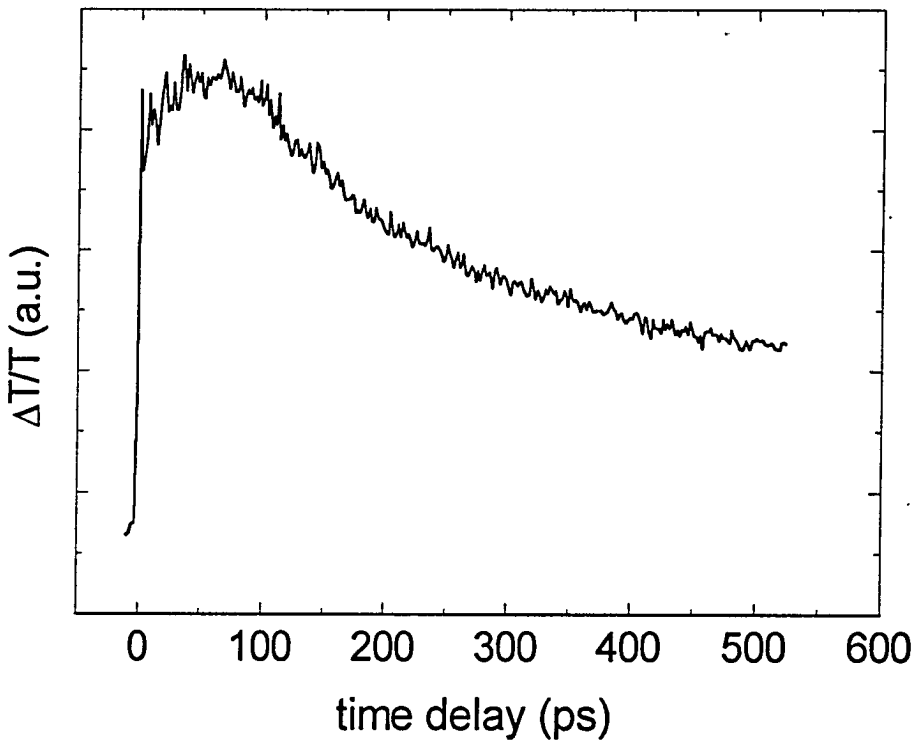

FIG. 4.3: The differential absorption signal in the stepped MQW sample, with σ^+ pump polarization, σ^- probe polarization, and intensities of 3 W/cm^2 (B=0).

The superlattice sample also shows a clear double-exponent behavior, with somewhat different time constants (35 ps and 250 ps for the holes and electrons, respectively), as shown in Fig. 4.4(a,b). In the square MQW sample, on the other hand, the rise of the σ^- signal is very fast and the hole spin relaxation cannot be reliably resolved. This is seen in Fig. 4.4(c), in which the the σ^- signal and the σ^+ signal approach the same level after 400 ps. This behavior is similar to that which was observed by Damen *et al.* in a time-resolved photo-luminescence experiment on a high-quality sample with 80-Å wells. The difference between the square MQW sample and the two other samples shows up in another form: The pump-probe signal in that sample does not show any Stokes shift relative to the absorption spectrum, contrary to the case of the two other samples. The existence of such a shift between the linear and the nonlinear responses is an indication of the existence of localized excitons in the sample.[42] The role of exciton localization will be discussed in more detail in the following chapters.

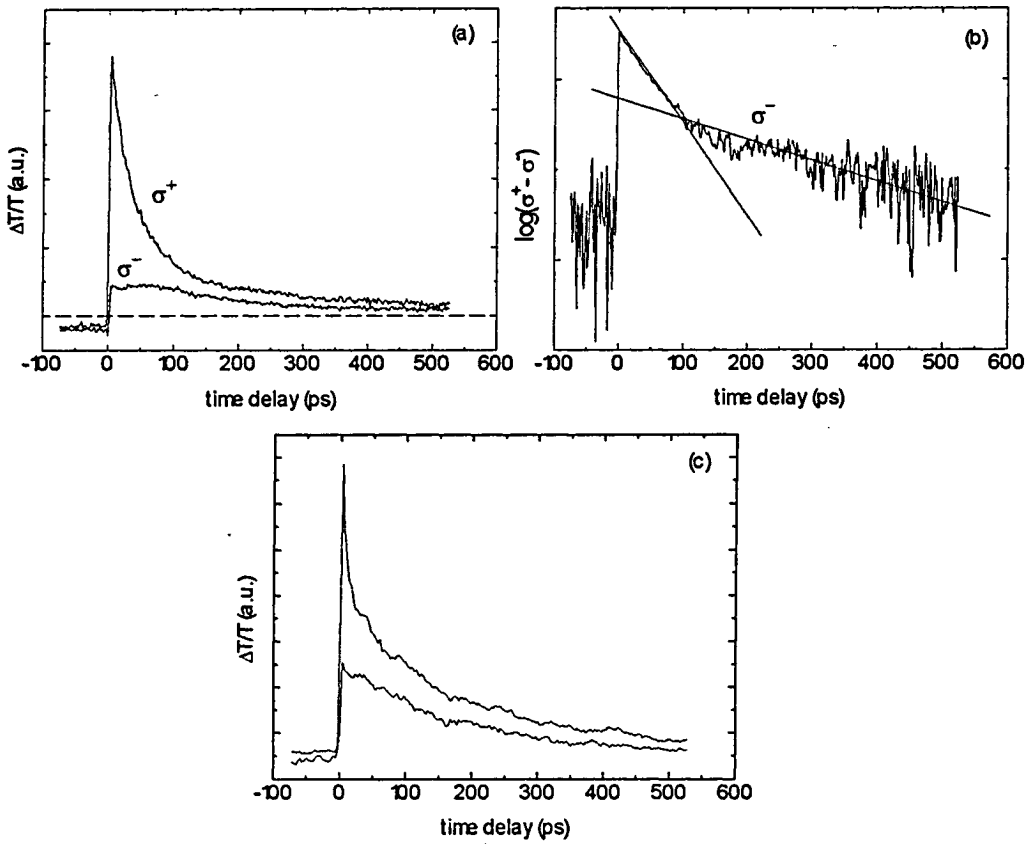

FIG. 4.4: (a) The differential absorption signal in the superlattice, with σ^+ and σ^- probes and intensities of 3 W/cm^2. (b) The logarithm of the difference between the σ^+ and σ^- signals in the superlattice. (c) The differential absorption signal in the square MQW sample, with σ^+ and σ^- probes and intensities of 20 W/cm^2. All signals measured at B=0.

Our experimental results were the first to unambiguously demonstrate the slow spin relaxation of excitons in intrinsic samples. Concurrently with our work, a group at Bell labs measured a hole spin relaxation time of ≈4 ps in a time-resolved photo-luminescence experiment on a slightly n-doped 80-Å quantum well sample.[41]

4.5. The evolving picture of exciton spin relaxation

Following the publication of the experimental data, the subject of spin relaxation in GaAs heterostructures has generated a lot of interest. Quivy-da Silva *et al.* studied the degree of the polarization of the cw luminescence as function of energy in undoped and modulation-doped samples, and confirmed that the hole spin relaxation time must be taken into account in the explanation of their findings.[43] This group also studied the effect of magnetic field, both perpendicular and parallel to the heterostructure layers. They found that in undoped samples a very high field (10 Tesla) parallel to the layers and perpendicular to the light propagation (Hanle configuration[4]) was needed to depolarize the luminescence, which is a further indication of very long spin relaxation times. Roussignol *et al.* investigated the dependence of the hole spin relaxation on the electron density in an n-modulation-doped 75-Å quantum well, in a time-resolved photo-luminescence experiment.[44] Their rate-equation fit to the data gives a density-independent hole spin relaxation time on the order of 1 ps. Wang *et al.* have estimated an "effective" exciton spin relaxation time of 100 ps from cw FWM spectral hole-burning measurements on a 100-Å quantum well.[45] Brener *et al.* have found an extremely fast hole spin relaxation (~400 fs) in shallow GaAs / $Al_xGa_{1-x}As$ quantum wells, with a transition from a two-dimensional to a bulk-like hole spin relaxation at $x \sim 5\%$.[46] These measurements again show that the spin relaxation is strongly sample dependent.

Very recently a comprehensive theory for exciton spin dynamics in quantum wells was proposed,[47] which calculates the spin relaxation of heavy-hole excitons due to the exchange Coulomb interaction between the electron and the hole. It is found that the exchange-induced exciton spin relaxation belongs to the "motional narrowing" class, with its characteristic inverse proportionality to the momentum scattering time of the exciton center of mass. The dependence on momentum scatterings means that exciton spin relaxation should indeed be sample-dependent. The authors then use a rate equation to describe recombination and the scattering between the exciton states, also taking into account single-particle spin-flip into optically-inactive states. This procedure was shown to give a very good fit to the experimental data from our stepped MQW sample. The authors attribute that the initial rise of the σ^- signal in our data is due to the exchange-induced spin-flip rather than due to a slow hole spin-flip (which they claim is undetectable in the σ^- signal since it produces an optically inactive exciton; however, their rate equation formalism ignores the coupling in the phase space for the creation of optically active and inactive excitons, which was discussed in section 5.1.2). The model also does not include

inhomogeneous broadening of the excitonic line and the associated spectral diffusion (the possibility that excitons would scatter within the inhomogeneous line), which are evidently important in our case. Nor does the theory include the biexcitonic effects (as will be discussed in detail in the following chapter, an instantaneous rise and a long-term drop due to the biexcitonic interaction must be included in the treatment of the σ^- signal).

Meanwhile, Ferreira and Bastard have proposed an alternative model for the spin relaxation in quantum wells.[48] They have shown that spatial assymetry leads to a D'Yakonov and Perel-like mechanism for the relaxation of the hole spin. Their work suggests that the hole spin relaxation time will increase in "low quality" samples, and that this may explain the strong sample dependence of the measured spin relaxation rates (it is possible that this also applies to our square MQW sample, in which disorder may be less important, leading to a slow momentum relaxation and a fast spin relaxation). Clearly, more experimental work and theoretical analysis are required, to understand the differences between various measurements, and to establish the validity of the different models in each case.

4.6. Exciton spin relaxation in a magnetic field

The spin relaxation in GaAs quantum wells in a magnetic field was studied in cw photo-luminescence depolarization experiments, in the same manner that the zero magnetic field spin relaxation rates were measured.[27,43] An inhibition of the spin-flip of conduction electrons during thermalization was observed in a photo-luminescence excitation experiment in a quantum well sample, in magnetic fields up to 20 Tesla. Time-resolved optical experiment on heterostructures in high magnetic fields were at their infancy as we started our work. Only early results had been reported, including the pioneering work of Stark *et al.*,[49] who have studied the energy relaxation and thermalization of conduction electrons in a fsec DA experiment, in magnetic fields up to 12 Tesla. The spin relaxation in this regime was not measured yet.

We have studied the effect of moderate magnetic fields, up to 5 Tesla, on the spin flip of excitons under resonant excitation. Figure 4.5 shows typical measurements with oppositely handed circular polarizations on the stepped MQW sample. The three measurements, at zero magnetic field, 2 Tesla and 4 Tesla, were all taken with a pump intensity of 3 W/cm^2 (exciton density of 1.5×10^9 cm^{-2}). The three curves show a few

differences which will be discussed later in this section. The spin relaxation times, however, remain nearly constant: a careful analysis of the data, by subtracting the σ^- signal from the σ^+ signal, shows a modest decrease of no more than 25% in the relaxation rates between 0 to 4 Tesla. We also looked at the case of pumping with σ^- polarization and probing with σ^+ polarization, by reversing the direction of the magnetic field. In this case a *slight increase* of the relaxation rate was observed.

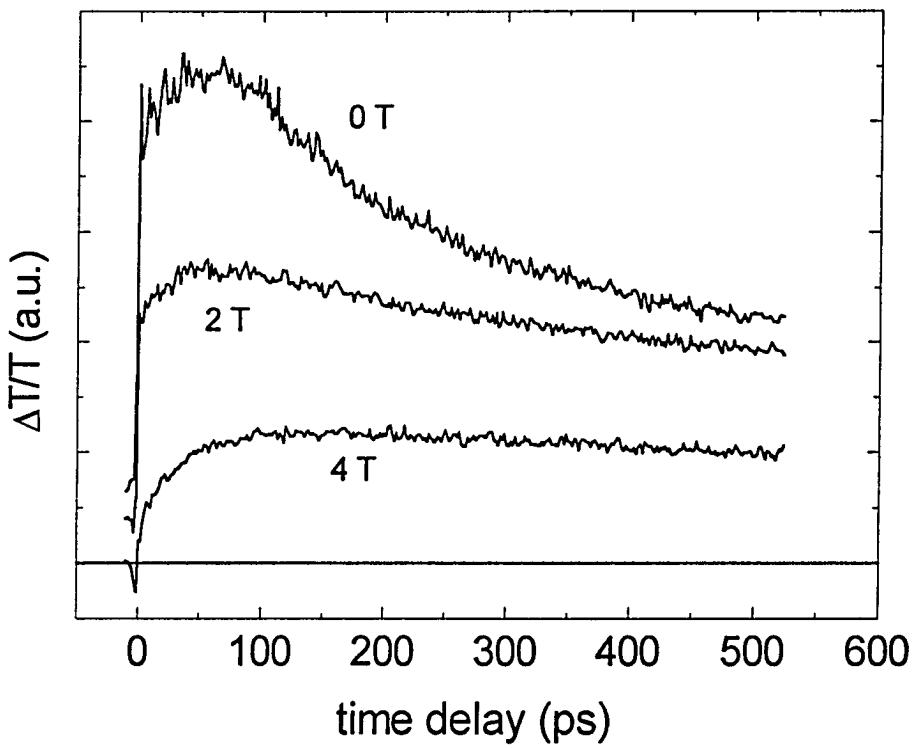

FIG. 4.5: The differential absorption signal in the stepped MQW sample, with σ^+ pump polarization, σ^- probe polarization, and intensities of 3 W/cm^2, at magnetic fields of 0T, 2T and 4T. The 0T curve is identical with Fig. 4.3.

The only theoretical work on spin-flip of excitons in a magnetic field is that of Maialle *et al.*.[47] Their calculations, which are valid only for low magnetic fields (when Landau levels are not important), predict that the effect of a magnetic field normal to the layers is to inhibit exchange-induced spin relaxation. They show that the spin relaxation rate due to exchange is proportional to $(1+\Omega^2\tau^2)^{-1}$, where Ω is the Zeeman splitting and τ is the

momentum relaxation time. Therefore any finite Ω, positive or negative, would slow the spin relaxation due to exchange. This implies that, in contrast to our observations, identical results should have been measured with σ^+ and σ^- excitation. The symmetry with respect to the magnetic field orientation in the work of Maialle *et al.* results from the fact that they do not consider the thermodynamic aspects of the problem. As the spin relaxation of σ^+ excitons in a magnetic field requires absorption of acoustic phonons, it must be slower than the spin relaxation of σ^- excitons. This was verified by Wang *et al.*, who used FWM spectral hole-burning measurements to study the effect of magnetic fields up to 6 Tesla on the spin-flip induced spectral hole.[45] However, the σ^+ to σ^- ratio in their measurements, which is related to the spin relaxation time, was found to depend *strongly* on the magnetic field: this ratio decreased by a factor of 4 when the magnetic field was increased from 2 Tesla to 6 Tesla. To explain the difference between our measurement and theirs, the effects of temperature and the Zeeman splitting should also be considered. The quantum well used in the experiment of Wang *et al.* exhibited a splitting of 0.37 meV in a field of 6 Tesla, and the experiment was carried out at 2.5 K. Based on our quantum beats measurements (which are discussed in following sections), we estimate the Zeeman splitting in our step MQW sample to be 0.4 meV in a field of 4 Tesla. Our experiments were carried out above 4.2 K. It is possible that that the lower relative temperature $k_BT/\Delta\varepsilon$ in Wang's experiment quenched inelastic scattering processes more effectively as the magnetic field was increased.

Since the publication of our data, Stark *et al.* have extended their fsec DA measurements in high magnetic fields to studies with circularly polarized light.[50] Their studies give the following spin relaxation times at 12 Tesla: 105 ps and 65 ps for the spin-flip of σ^+ and σ^- excitons, respectively, into optically inactive states, and 200 ps for complete relaxation. These relaxation times are consistent with our measurements in moderate fields. The lack of data for zero magnetic field in their report, and different well widths and sample qualities, make a direct comparison with our own data difficult.

Let us return now to the data presented in Fig. 4.5, and examine the detail differences between the three curves. The B=0 curve shows a large instantaneous rise and a pronounced drop at long delay times. When the magnetic field is applied, however, both features gradually disappear. We observe that the larger the instantaneous rise, the larger is the drop at long delays. A similar behavior is observed as the intensity of the excitation is increased: note that the 4 Tesla curve in Fig. 4.5, which was measured at 3 W/cm^2, shows a similar temporal evolution to the zero field measurement at 30 W/cm^2 which is

plotted in Fig. 4.2. We attribute both the instantaneous rise of the σ^- signal and its pronounced drop when spin relaxation is not complete to biexcitonic effects, which will be discussed in detail in chapter 6. The detail changes of the σ^- signal therefore represent a relative diminishing of the biexcitonic contribution with increasing magnetic field and excitation intensity.

5. Quantum beats of spin-polarized magnetoexcitons

The fact that spin polarization is preserved for a relatively long time in quantum wells has allowed us to observe quantum beats between spin polarized magneto-excitons as the spin degeneracy was removed by an applied magnetic field. These quantum beats appeared when linear polarizations were used to coherently drive the two nondegenerate, Zeeman-split magneto-excitonic two-level systems.

Quantum beats are usually associated with coherence-sensitive experimental methods, such as four-wave-mixing, photon echoes, coherent Raman scattering, and resonance fluorescence. When two nondegenerate states are coherently driven by an optical field, the induced polarizations in the medium interfere and give rise to a beating in the radiated wave, at a frequency given by the difference between the energies of these states (which must be smaller than the bandwidth of the driving optical field). Time-resolved DA measurements are usually considered as a coherence-insensitive method for investigating decay rate of the population in excited states (as in our study of spin relaxation with circular polarizations). However, this is not always the case, and quantum beats *can* be observed in the temporal evolution of the absorption. This is implicit in the Bloch equations, which couple the polarization and population in a two-level system. In fact, absorption quantum beats have been reported in the literature for the case of hyperfine splitting of atomic states.[51]

In semiconductors, the continuous density of states at the band-to-band transition is generally considered as a cause for rapid dephasing and loss of coherence. Bound excitons, however, form discrete transitions which make coherent phenomena observable in semiconductors. Indeed, quantum beats had been previously observed in four-wave-mixing experiments in GaAs quantum wells.[22] In that case the two split energy levels in a coupled-well structure produced the beating.

5.1. Absorption quantum beats

We have demonstrated absorption quantum beats which originate from the Zeeman splitting between spin-polarized magneto-excitons. Figure 5.1(a) shows the relative change in transmission, $\Delta T/T$, at B = 0 in our stepped MQW sample, when pumped and probed with roughly equal intensities of approximately 3 W/cm^2, slightly below the heavy-hole exciton absorption peak (1.619 eV). Since $\Delta T/T \ll 1$ ($\approx 5\%$) this signal is directly proportional to the change of exciton absorption $\Delta\alpha$. The slow decay (~20 ps) of the

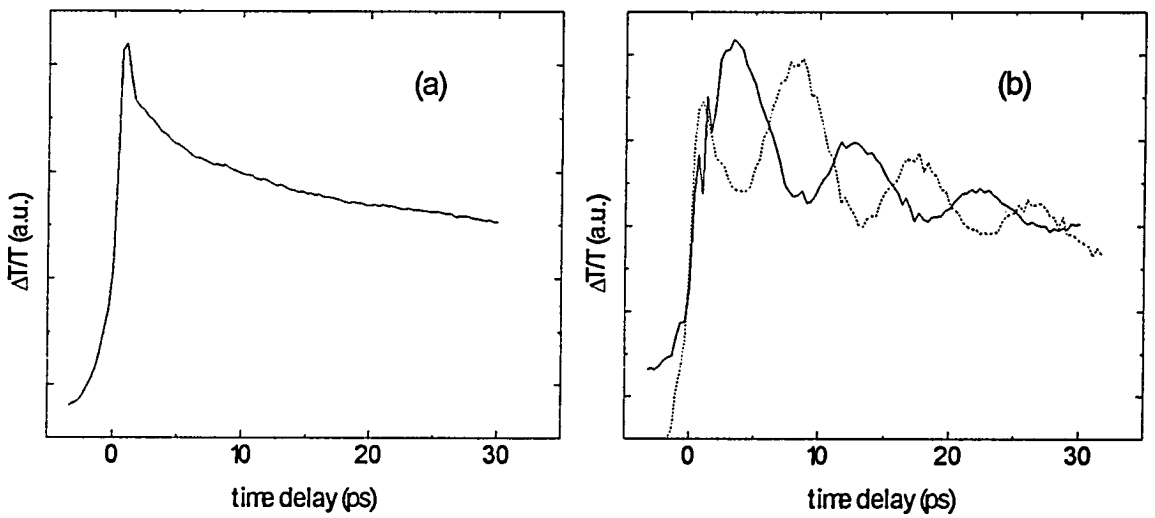

FIG. 5.1: Temporal evolution of $\Delta T/T$ at the heavy-hole exciton for (a) B=0 and (b) B=4T. The solid curves were measured with cross-linearly polarized pump and probe, and the dotted curve was measured with parallel linear polarizations.

signal is attributed[20] to spectral diffusion of low-energy localized excitons within the inhomogeneously broadened excitonic line. As a magnetic field is applied normal to the layers, oscillations appear in the time-resolved DA signal. The solid curve in Fig. 5.1(b), which was measured at B = 4 Tesla with crossed linear polarizations (CP), exhibits a slow rise (relative to the pulse width) followed by deep, damped oscillations. These oscillations have a period of 8 ps, with the first minimum occuring a full period after t = 0. A similar temporal behavior is observed in the case of parallel linear polarizations (PP), as shown by the dotted curve of Fig. 5.1(b), but in this case the oscillations have a π phase shift relative to the signal in the CP configuration. The envelope of the oscillations is identical in both cases, and is decaying with a time constant of ~20 ps, approximately the same as the decay time for the B = 0 case. Fig. 5.2 demonstrates that the period of the oscillations is

inversely proportional to the magnetic field strength. The two traces were measured at 2 Tesla (solid curve) and 4 Tesla (dotted curve), in the CP configuration. We observed less pronounced oscillations with a slightly longer period in the superlattice sample (Fig. 5.3). The square MQW sample showed no trace of coherent beating.

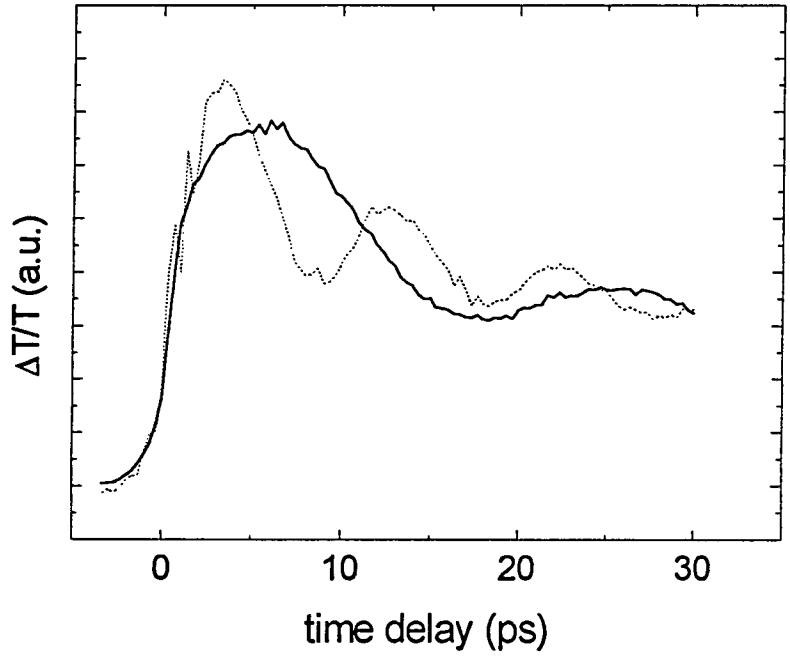

FIG. 5.2: Pump-probe signal at 2T (solid curve) and 4T (dotted curve).

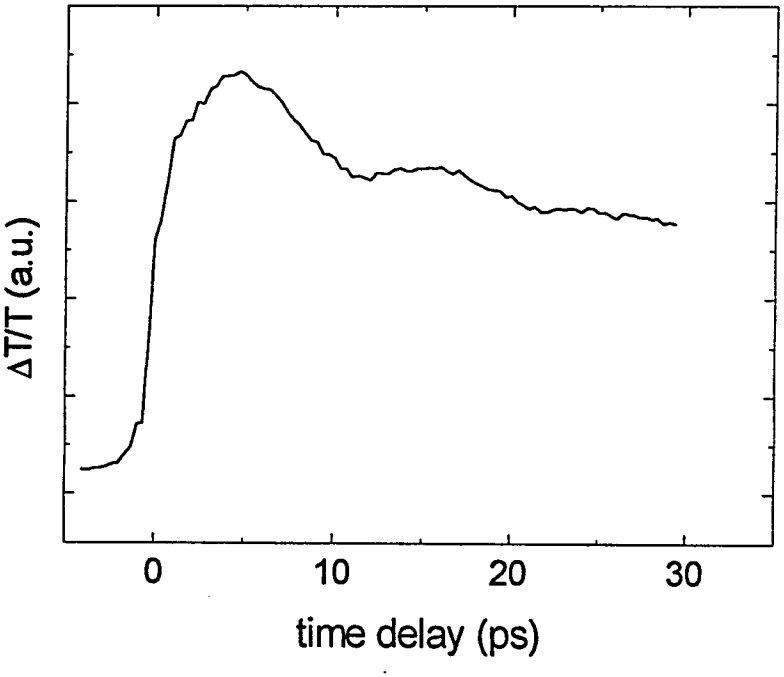

FIG. 5.3: Quantum beats in the superlattice sample in a field of 4T.

5.2. Theoretical interpretation

Consider the energy level diagram depicted in Fig. 5.4. The spin splitting between the different J_z levels in each subband is given by $2g\mu_B B\Delta J_z$, where g is the Lande g-factor in the subband. In bulk GaAs g is negative for electrons in the conduction band and positive for electrons in the vallence band.[52] Since spin-flip is not important on the time scale of this experiment, the four-level system in Fig. 5.4 may be treated as a simple superposition of two uncoupled two-level systems, which interact with either σ^+ or σ^- circularly polarized light. As the splitting between the two spin states is small compared to the bandwidth of the laser, linearly polarized pump and probe interact with both transitions. In other words, a linearly polarized pump excites the two transitions coherently, and the polarizability of the medium seen by a linearly polarized probe is a linear combination of these eigenstates. The two different transition energies result in two different time dependencies of the induced polarization, and their linear combination exhibits a beating behavior. How this comes about will be shown in the following.

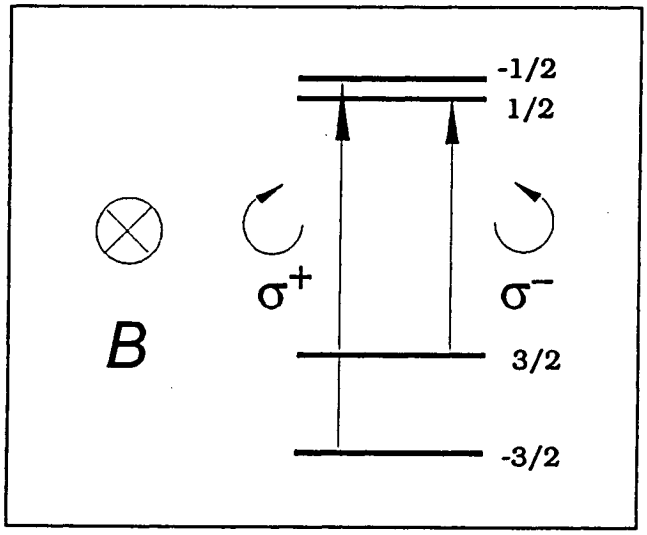

FIG. 5.4: Electron energy levels in a normal magnetic field, and allowed dipole transitions from the heavy-hole subband to the conduction band.

For any one of the two-level systems in Fig. 5.4, the total absorbed intensity in the sample can be written in general as:

$$\Delta I = \int dt\, E \cdot dP/dt \qquad (5.1)$$

where E is the time-dependent optical field and P is the induced polarization. We now derive the change in absorption resulting from excitation by the pump pulse from the Bloch equations.[30] Assuming that the relaxation times T_1 and T_2 are much longer than the duration of the pulse, and that the laser frequency is tuned to resonance, we can write the

change in the probe intensity I_t, as measured by a slow detector, as:

$$\Delta I_t \sim \int dt\, E_t \cdot dv(t)/dt \sim \int dt\, E_t^2 \cdot \Delta w(t) \tag{5.2}$$

where E_t is the amplitude of the probe field, $v(t) = -i\,[\rho_{12}(t)-\rho_{21}(t)]$, $w(t) = \rho_{22}(t)-\rho_{11}(t)$, $\Delta w(t) \equiv w(t)-w_{eq}$, w_{eq} is the steady-state value of w, and $\rho_{ij}(t)$ are density matrix elements. The effect of the pump pulse is implicit in this expression through $\Delta w(t)$, which is the change in $w(t)$ due to the excitation of the two-level system by the pump. Using the fact that $\mathrm{Tr}(\rho) = 1$, and taking $w_{eq} = -1$, i.e., the system in steady state is at its ground state, we get that $\Delta w(t) = \rho_{22}(t)$. We therefore conclude that ΔI_t which is measured in a pump-probe experiment is proportional to $\rho_{22}(t)$ induced by the pump pulse. When the short pump field is turned off, the induced population w decays exponentially with a relaxation time T_1, and the excitonic wave function can be written as:

$$\psi(t) = |\psi_{R,L}\rangle \exp\left(iw_{1,2}t - t/T_1\right), \tag{5.3}$$

where $|\psi_R\rangle$ ($|\psi_L\rangle$) is the wave function of an exciton created by a photon with σ^+ (σ^-) polarization and energy $\hbar\omega_1$ ($\hbar\omega_2$).

The same analysis holds for the case of two uncoupled two-level systems, but since a linearly polarized probe interacts with both systems we should take the *joint density matrix*. To construct this joint density matrix let us consider the case in which the pump is polarized in the x direction. The wave function of the system right after the excitation by the pump can be written as $\psi(0) = |\psi_x\rangle = \left(|\psi_R\rangle + |\psi_L\rangle\right)/\sqrt{2}$ and the temporal evolution of the system after the pump pulse has left the sample is given by:

$$\psi(t) = \frac{1}{\sqrt{2}}\left(|\psi_R\rangle e^{i\omega_1 t} + |\psi_L\rangle e^{i\omega_2 t}\right)e^{-t/T_1}. \tag{5.4}$$

We now rewrite the spin eigenfunctions in terms of x-like and y-like wave functions, $|\psi_R\rangle = \left(|\psi_x\rangle - i|\psi_y\rangle\right)/\sqrt{2}$ and $|\psi_L\rangle = \left(|\psi_x\rangle + i|\psi_y\rangle\right)/\sqrt{2}$. Inserting these expressions into

Eq. 5.4 we express $\psi(t)$ in terms of $|\psi_x\rangle$ and $|\psi_y\rangle$:

$$\begin{aligned}\psi(t) &= \tfrac{1}{2}e^{-t/T_1}\left[\left(e^{i\omega_1 t}+e^{i\omega_2 t}\right)|\psi_x\rangle - i\left(e^{i\omega_1 t}-e^{i\omega_2 t}\right)|\psi_y\rangle\right] = \\ &= a(t)|\psi_x\rangle + b(t)|\psi_y\rangle .\end{aligned} \tag{5.5}$$

As we have seen, the measured DA signal depends only on the density matrix element $\rho_{22}(t)$, which is defined in terms of the coefficients $a(t)$ and $b(t)$. A probe which is linearly polarized along the x direction would detect only the component $a(t)$, while a probe which is linearly polarized along the y direction would detect only the component $b(t)$:

$$\begin{aligned}\Delta I_x(t) &\sim |a(t)|^2 = \tfrac{1}{2}\left[1+\cos(\omega_1-\omega_2)t\right]e^{-2t/T_1} , \\ \Delta I_y(t) &\sim |b(t)|^2 = \tfrac{1}{2}\left[1-\cos(\omega_1-\omega_2)t\right]e^{-2t/T_1} .\end{aligned} \tag{5.6}$$

It follows that the DA signals for linearly polarized pump and probe exhibit interference terms which oscillate at the difference frequency $\omega_1 - \omega_2$. This frequency is linear with B, as indeed observed experimentally. Note that the oscillations in the PP case (x - polarized probe) start at a peak and are shifted by a π phase with respect to the CP case (y - polarized probe), also in agreement with the experiment [Fig. 5.1(b)].

5.3. Discussion - g factor, dephasing and spin orientation

Obviously the simple two-level system model, which is generally used in the interpreatation of optical experiments in GaAs heterostructures, is incomplete. In the interpretation of our measurements of spin relaxation rates and Zeeman quantum beats, we have used a four-level system picture, as presented in Fig. 5.4. An alternative excitonic picture is shown in Fig. 5.5. In this picture the two allowed optical transitions are between the vacuum ground state and two spin-polarized excitonic states, and the beating results from interference through the ground state. It was noted by Koch *et al.*, in a recent discussion of interference versus quantum beating effects,[53] that the common ground state is essential in defining the observed oscillations as "true" quantum beats. Our original approach, which treats the oscillations as a quantum interference phenomenon, has the advantage of being more transparent as far as an absorption experiment is considered.

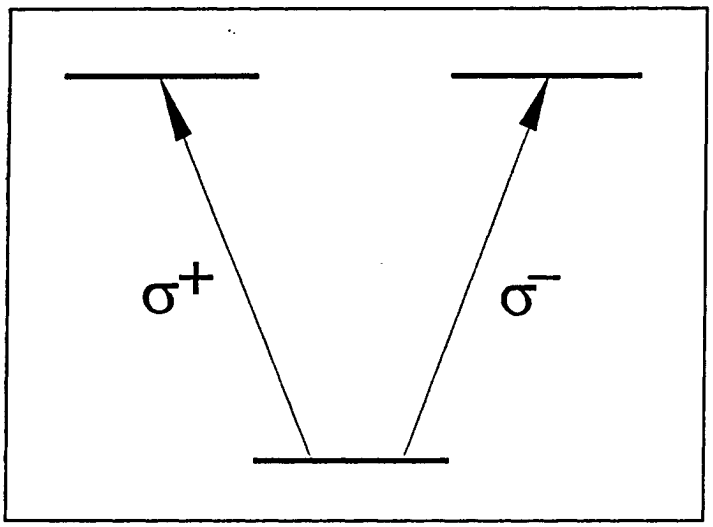

FIG. 5.5: An excitonic representation of the energy levels associated with optical transitions from the heavy-hole valence subband to the conduction band.

The previous section establishes the oscillations which were observed in our DA measurements as Zeeman quantum beats. Similar Zeeman quantum beats were also observed in FWM experiments in a magnetic field, which were performed by Carmel *et al.* on the same samples in which we have demonstrated the absorption quantum beats.[54,55] The period of the beating in the FWM signal is identical to that measured by us in the DA experiment. The characteristic π phase shift of the oscillations in the CP case relative to the oscillations in the PP case was also observed. The analysis of the results in these FWM experiments was based on the excitonic level diagram depicted in Fig. 5.5. In this representation the excitonic g-factor g_{exc} is defined in terms of the total Zeeman splitting between the two excitonic transitions: $2g_{exc}\mu_B B$.

The g-factors of electrons and holes in GaAs were intensively investigated in both bulk and heterostructures, using various techniques. Measurements show a dependence on well width,[56,57] magnetic field strength,[45,58] and orientation.[57] From our DA experiment, the effective excitonic g-factor in the stepped MQW sample is $g_{exc} \sim 0.9$ in a field of 5 Tesla. In his MSc work, Carmel applied the technique which was demonstrated by us in systematic FWM measurements of the excitonic g-factor and its variation with the quantum well width and the magnetic field strength.[54,55] He also used this technique in evaluations of the g-factors of higher heavy-hole magneto-excitons and light-hole excitons.[55] Carmel *et al.* have found that g_{exc} is magnetic field dependent, and their fit to the step MQW data gives $g_{exc} = 0.76+0.016B$, with an estimated error of 10%. A lower g-factor was measured for our superlattice sample. These values are consistent with measurements by other groups, which have used different experimental techniques, as discussed in detail by Carmel *et al.*. It should be noted that in parallel to our work on

quantum beats in GaAs, other groups demonstrated similar Zeeman quantum beats in different semiconductors - CdS[59] and AgBr.[60] A major advantage of this technique is that it makes it possible to measure very small energy splittings in cases where inhomogeneous broadening precludes direct spectroscopic measurements.

Another interesting aspect of the beating in the DA experiment is the capability to accurately and unambiguously extract *dephasing times* from the decey rate of their envelope (note that the signal in a pump-probe experiment is much stronger and easier to detect than a FWM signal). We found out in the experiment that the decaying envelope of the oscillations corresponds to the difference between the PP and CP signals in zero magnetic field. This observation is substantiated by the theoretical expression for the coherent signal (Eq. 5.6), which at zero magnetic field yields a vanishing CP signal and a non-vanishing but decaying PP signal. This justifies the association of the initial decay of the zero field signal with the dephasing of the excitons.

We find that the dephasing time of the excitons is correlated with their spin relaxation time. This is borne from a comparison between the three samples which we have studied: while in our stepped MQW and superlattice samples the spin-flip and dephasing times are long, in the square MQW sample the hole spin relaxation is instantaneous and quantum beats are not observed. O. Carmel's FWM measurements in different samples substantiate the relation between the duration of the Zeeman quantum beats and the well-width dependent spin relaxation. On the other hand, the dephasing time of approximately 20 ps in our stepped MQW and superlattice samples is comparable to spectral diffusion times of localized excitons.[20] Our data also show that the dephasing rate is energy dependent, in the sense that the oscillations appear only in the low-energy side of the exciton absorption line. Such a behavior is indeed expected in the case of localized excitons. We are thus led to believe that spin-flip leads to dephasing, and that where spin-flip is slow spectral diffusion determines the rate of dephasing.

6. The biexcitonic coupling

6.1. Evidence for a coupling between spin-polarized excitons

The slow spin relaxation in GaAs quantum wells, which was discussed in detail in chapter 4, makes it possible to excite and explore the behavior of spin-polarized excitons in the picosecond regime. One interesting subject which has recieved only limited attention is the correlation between σ^+ and σ^- excitons, or in other words - how the creation of a σ^+ exciton would affect the possibility to excite σ^- excitons.

Consider the three-level system model in Fig. 5.5. This model does not allow the creation of an exciton with a certain spin at a certain site following the creation of an exciton with the opposite spin in the same site, since there is no dipole matrix element between the two spin-polarized states. In such a system the DA signal with pump and probe with the same circular polarization would be identical to the DA signal with oppositely-handed circular polarizations. In the alternative electronic four-level system of Fig. 5.4, on the other hand, there is no coupling of σ^+ and σ^- excitons: this system can be excited independently by σ^+ and σ^- photons.

As a matter of fact, it can be recalled that the DA signal which we measured with oppositely-handed circular polarizations did exhibit coupling between the two transitions. A careful examination of Figs. 4.2 and 4.3 reveals an instantaneous (within the pulse-width) change of absorption of σ^- light which accompanies the σ^+ excitation. Our experiments, as well as theoretical calculations, ruled out the possibility that this abrupt response represented a spin relaxation phenomenon. Clearly, this observation was inconsistent with any of the above models, and further studies were required.

To resolve this issue we performed high resolution measurements of the instantaneous rise of the signal. These measurements revealed a striking phenomenon. Fig. 6.1 is a 20 ps scan of the σ^- DA signal with σ^+ pumping, which was measured in the stepped MQW sample, with pump and probe intensities of 3 W/cm^2 (corresponding to an exciton density of 1.5×10^9 cm^{-2}. It is clearly seen from Fig. 6.1 that the sudden change of absorption is accompanied by an oscillatory response. Three main features are apparent in the figure: a

negative dip at negative delays, followed by deep damped oscillations, and a final positive signal (decreased absorption) at positive delays. All three features exist throughout the low-energy side of the excitonic absorption line, and the amplitude of the oscillations scales linearly with the intensity of the probe and also linearly with the intensity of the pump, across almost three orders of magnitude. Figure 6.2 shows a few measurements at various intensities. Note that although the signal changes as function of intensity, particularly close to saturation intensity, the period of the oscillations is independent of intensity. It was also found to be independent of the excitation energy. The oscillations' period was measured to be 1.6 ps for the stepped MQW sample.

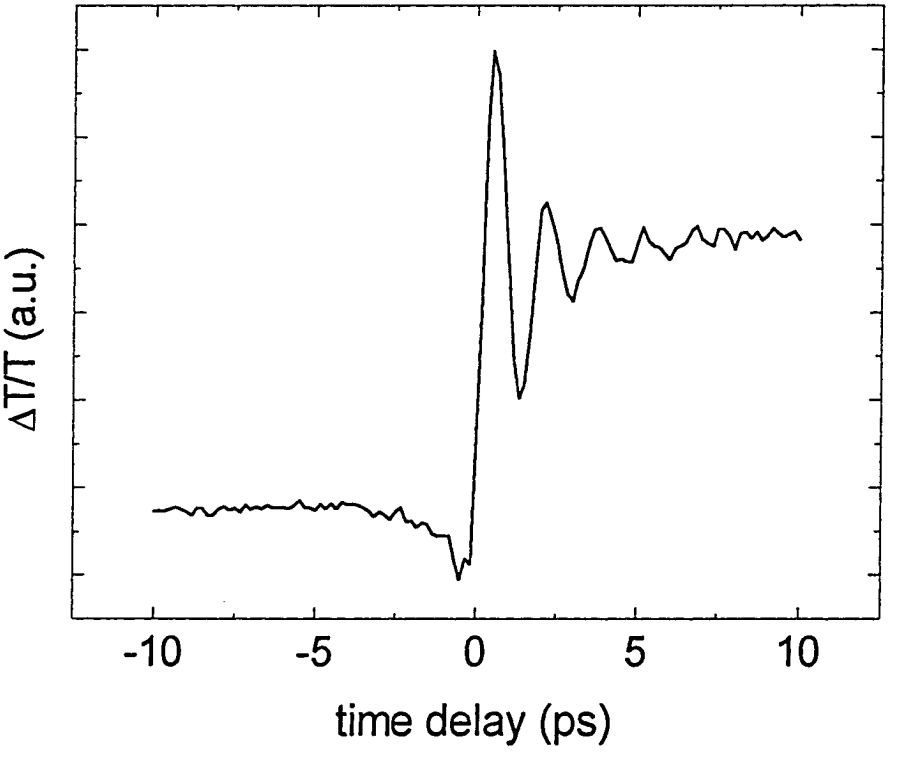

FIG. 6.1: The transient differential absorption signal in the stepped MQW sample, with σ^+ pump polarization, σ^- probe polarization, and intensities of 3 W/cm^2 (B=0).

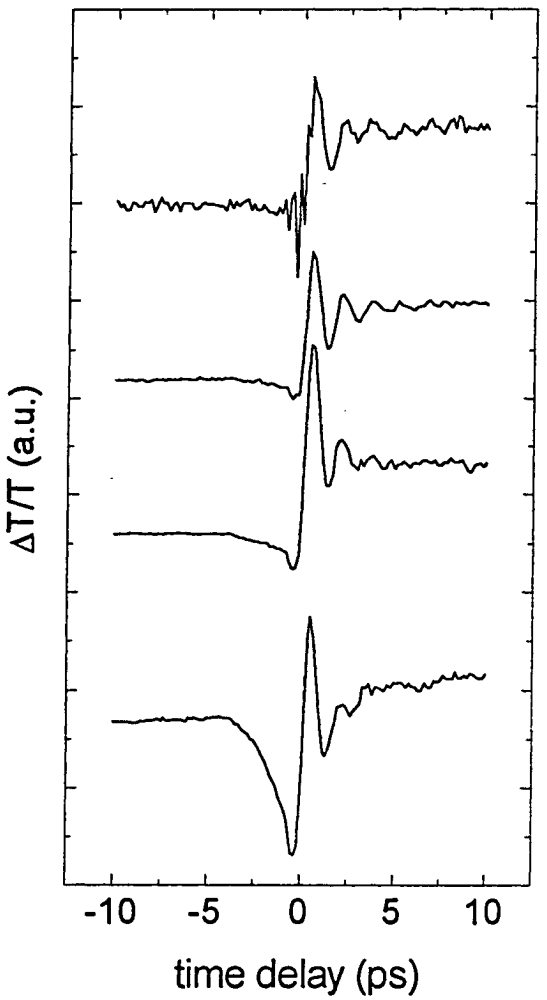

FIG. 6.2: The oscillatory differential absorption signal in the stepped MQW sample, with σ^+ pump and σ^- probe polarizations, for several intensities. From top to bottom: 0.3 W/cm^2, 3 W/cm^2, 20 W/cm^2, 100 W/cm^2 (B=0).

Similar oscillations were observed with our superlattice sample. In this case the oscillations' period was 2 ps (Figure 6.3). We used the superlattice sample to study the temperature dependence of the oscillations, and found that their amplitude decreases slightly at 30 K, while at 60 K they are completely washed out. We also verified that the oscillations' period was not dependent on the pulse width and pulse shape of the laser or on a transverse electric field. The main effect of an increase of the pulse width was a corresponding increase of the number of observable periods in the oscillatory signal.

6.2. The biexcitonic interpretation

We examined several possible mechanisms to explain the observed oscillations, whose fixed period in a given sample is indicative of the existence of a fundamental energy gap of 2 - 2.5 meV. We considered removal of spin degeneracy due to spin-orbit coupling, which can exist in principle in assymetric structures (such as the step MQW sample or the superlattice which is embedded in a *p-i-n* structure, with a built-in reverse voltage). However, the energies of the σ^+ and σ^- transitions remain degenerate in this case. In addition, this effect is too small (by orders of magnitude) to explain such a large energy gap. Other experimental observations also ruled out the possibility that assymetry is the common factor behind the oscillatory transient: the measured signal in the superlattice sample in a flat-band situation

was identical to the signal which was measured with no electrical contacts, which convinced us that the optically excited charge carriers screen the electrical field in the no-contact situation. We later also observed oscillations in a symmetrical MQW sample.

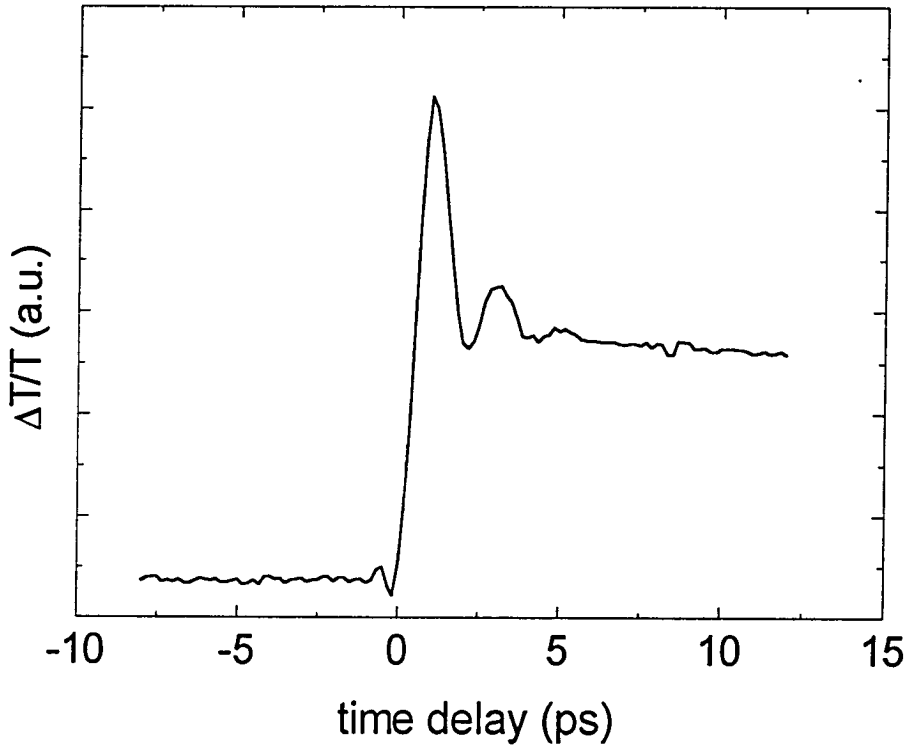

FIG. 6.3: The oscillatory differential absorption signal in the superlattice, with σ^+ pump and σ^- probe polarizations, and intensities of 3 W/cm^2 (B=0).

Another possible explanation to the oscillations was based on optical nutations,[30] but the insensitivity of the oscillations' period to the energy and intensity of the excitation tended to reject this explanation as well. The fact that the oscillations are observed only for pump and probe with oppositely handed circular polarizations led us to attribute the phenomenon to the formation of biexcitons.

This interpretation suggests that the fixed beating frequency is directly related to the biexcitonic binding energy. It also gives a plausible explanation to the instantaneous σ^- change of absorption following σ^+ excitation. The change results from the fact that the

pump-generated σ^+ excitons create a possibility to form a bound biexcitonic state *with a single* σ^- *photon*, at the expense of a reduced probability to create independent σ^- excitonic states. This corresponds to a transfer of oscillator strength from the σ^- excitonic transition to the single-photon exciton-to-biexciton transition energy, which is the exciton energy minus the biexcitonic binding energy (Figure 6.4). Such a change is seen by a probe which is tuned to the excitonic transition as an abrupt decrease of the absorption, as indeed observed experimentally.

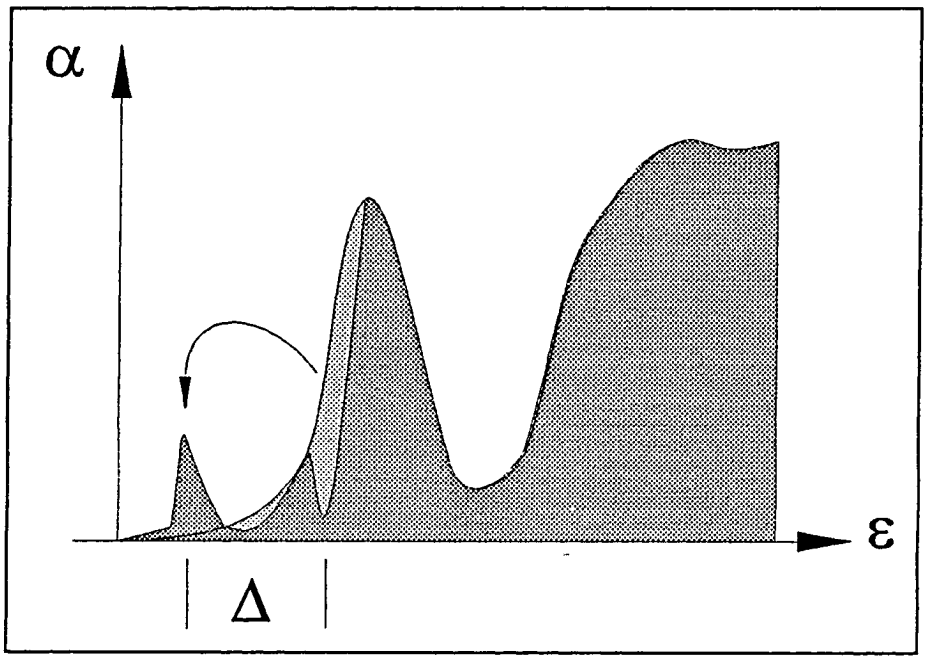

FIG. 6.4: The change of the absorption spectrum for a σ^- probe following an excitation with a σ^+ pump. The absorption curve before the arrival of the pump is shown in pale gray, and the spectrum following excitation is drawn in dark gray. Oscillator strength is removed from the exciton lineshape at energy ε and added at energy $\varepsilon - \Delta$, where Δ is the biexciton binding energy.

The intuitive picture presented above is substantiated by a calculation of the third order polarization for a four-level system model of the exciton-biexciton interaction. This model, which is described in detail in section 6.3, gives a very good agreement with our experimental results, and also confirms the appearance of oscillations with identical period in FWM measurements in the CP configuration. Such oscillations were observed by various groups,[61,62] and were also attributed to biexcitons. O. Carmel, in his FWM experiments on our samples,[54] observed similar oscillations in the CP signal (Fig. 6.5), the

period of which were *identical to the period of the oscillations in the DA experiments.* The similarity between the oscillations' period in the DA and FWM experiments clearly indicates that they originate from a common mechanism.

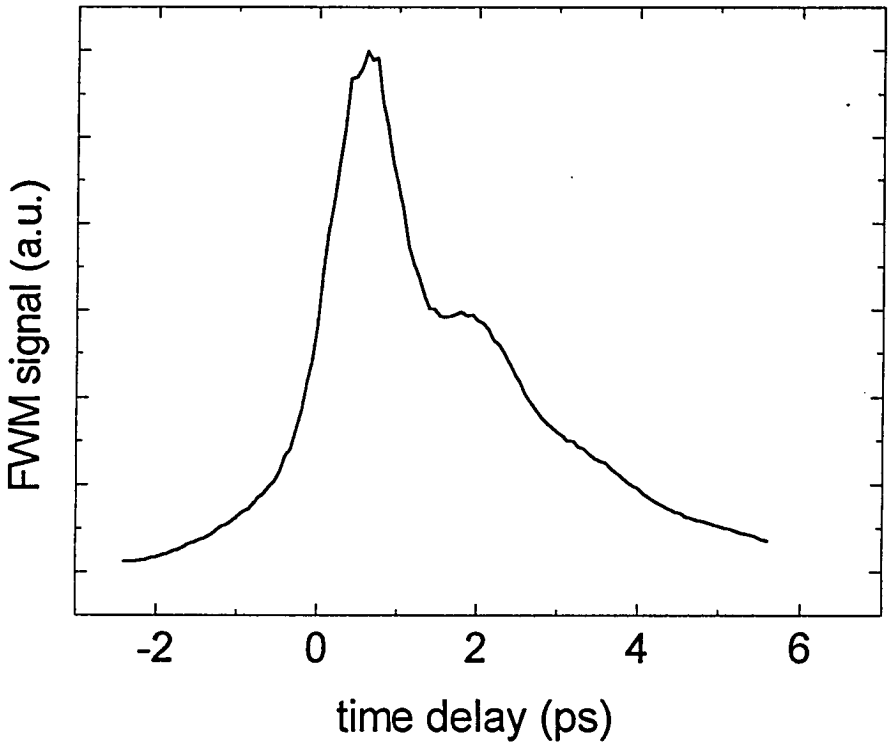

FIG. 6.5: The oscillatory signal measured by Carmel *et al.*[54] in a four-wave mixing experiment with crossed limearly-polarized exciting beams, on our stepped MQW sample.

6.3. A four-level model for the biexcitonic nonlinearities

In collaboration with Y. Levinson and G. Finkelstein we have proposed a model for the nonlinear optical response of quantum wells, which takes into account the biexcitonic state. We show that within this model, the interaction of two laser pulses, mediated by the nonlinear susceptibility, results in oscillations and in coupling between σ^+ and σ^- excitons. The frequency of the oscillations is the binding energy of the biexciton. This explains the temporal behavior which was observed in the DA and FWM experiments described above.

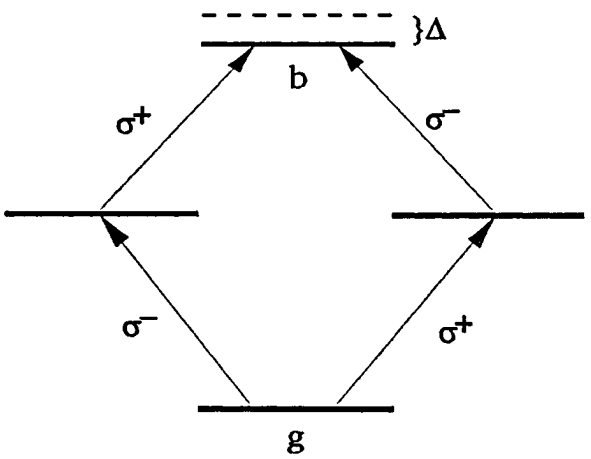

FIG. 6.6: The four-level system consisting of a ground state *g*, two exciton states $\sigma^{\pm}$, and a biexciton state *b* with a binding energy Δ.

We assume that two excitons may bind to form a biexciton only if the *z* projections *m* of their angular momenta are $m = +1$ and $m = -1$, that is, if they are created by circularly polarized light of opposite handedness. We describe the system with the four-level diagram shown in Fig. 6.6. The ground state $|g\rangle$, with $m = 0$, corresponds to the state of no excitons and no biexcitons, and the states $|\sigma^{\pm}\rangle$, with degenerate energy ε and $m = \pm 1$, correspond to one exciton with either a right or a left polarization. The state $|b\rangle$ with energy $2\varepsilon - \Delta$ and $m = 0$ corresponds to the singlet biexciton, Δ being the binding energy. The Hamiltonian of this four-level system is:

$$H_0 = \varepsilon a^+ a + \varepsilon c^+ c - \Delta a^+ a c^+ c \qquad (6.1)$$

where a^+ (a) and c^+ (c) are creation (annihilation) operators of right and left excitons, respectively. Note that this model neglects the continuous spectrum of the biexciton and is valid only at low excitation densities, where the average distance between excitons is larger than the biexciton area.

The coupling of the four-level system with light is given by:

$$V = -d_\alpha E_\alpha - d_\beta E_\beta \tag{6.2}$$

where $E_{\alpha,\beta}$ are the right and left components of the total electric field (of both pulses), defined in terms of the cartezian components:

$$E_\alpha = \left(E_x + iE_y\right)/\sqrt{2} \quad , \quad E_\beta = \left(E_x - iE_y\right)/\sqrt{2} \tag{6.3}$$

and $d_{\alpha,\beta}$ are non-Hermitian dipole moment operators, defined by:

$$d_\alpha = \left(d_x - id_y\right)/\sqrt{2} \quad , \quad d_\beta = \left(d_x + id_y\right)/\sqrt{2} \tag{6.4}$$

and given in terms of the creation and annihilation operators:

$$d_\alpha = d_{ex}a + d_{bx}c^+ \quad , \quad d_\beta = d_\alpha^+ \tag{6.5}$$

The nonvanishing matrix elements of these operators are:

$$\begin{aligned} \langle g|d_\alpha|\sigma^+\rangle &= \langle \sigma^-|d_\alpha|g\rangle = \langle g|d_\beta|\sigma^-\rangle^* = \langle \sigma^+|d_\beta|g\rangle^* = d_{ex} \\ \langle \sigma^-|d_\alpha|b\rangle &= \langle b|d_\alpha|\sigma^+\rangle = \langle \sigma^+|d_\beta|b\rangle^* = \langle b|d_\beta|\sigma^-\rangle^* = d_{bx} \end{aligned} \tag{6.6}$$

Here d_{ex} is the dipole moment of the exciton transition, while d_{bx} corresponds to the transition from an already existing exciton to the biexciton state.

In matrix form one gets:

$$H_0 = \begin{pmatrix} 0 & 0 & 0 & 0 \\ 0 & \varepsilon & 0 & 0 \\ 0 & 0 & \varepsilon & 0 \\ 0 & 0 & 0 & 2\varepsilon - \Delta \end{pmatrix}$$

$$d_\alpha = \begin{pmatrix} 0 & d_{ex} & 0 & 0 \\ 0 & 0 & 0 & 0 \\ d_{ex} & 0 & 0 & d_{bx} \\ 0 & d_{bx} & 0 & 0 \end{pmatrix} \qquad d_\beta = \begin{pmatrix} 0 & 0 & d_{ex}^* & 0 \\ d_{ex}^* & 0 & 0 & d_{bx}^* \\ 0 & 0 & 0 & 0 \\ 0 & 0 & d_{bx}^* & 0 \end{pmatrix}$$

(6.7)

To calculate the nonlinear response in a DA or FWM experiment it is necessary to evaluate the third order dipole moment, which is proportional to the third power of the

electric field. The change of absorption $Q^{(3)}$ in a DA experiment with two oppositely handed circularly polarized pulses, $E_\alpha(t)$ (pump) and $E_\beta(t)$ (probe), is given by:

$$Q^{(3)} = \int_{-\infty}^{\infty} dt\, E_\beta(t) \frac{\partial}{\partial t} d_\beta^{(3)}(t) \tag{6.8}$$

where $d_\beta^{(3)}(t)$ is the β polarization component of the third order dipole moment, proportional to $E_\beta E_\alpha^2$. Similarly, the signal in a FWM experiment with two linear cross-polarized pulses $E_x(t)$ and $E_y(t)$ (CP configuration) is:

$$P \sim \int_{-\infty}^{\infty} dt \left| d^{(3)}(t) \right|^2 \tag{6.9}$$

and $d^{(3)}(t)$ is the relevant contribution to the third order dipole moment proportional to $E_x^2 E_y$ or $E_y^2 E_x$.

To find $d^{(3)}(t)$ for either case, we solve the equation for the time evolution of the density matrix ρ iteratively, with the Hamiltonian $H_0 + V$, expanding it in powers of E and collecting terms of order E^3, which give $\rho^{(3)}$. This is most conveniently done in the interaction representation (see Appendix A), in which:

$$\rho_I^{(3)}(t) = (1/i\hbar)^3 \int_{-\infty}^{t} dt_1 \int_{-\infty}^{t_1} dt_2 \int_{-\infty}^{t_2} dt_2 \left[V_I(t_1), \left[V_I(t_2), \left[V_I(t_n), \rho^{(0)} \right] \right] \right] . \tag{6.10}$$

Next, the dipole moment is calculated from:

$$d^{(3)}(t) = \mathrm{Tr}\left\{ (d_\sigma)_I \rho_I^{(3)}(t) \right\} . \tag{6.11}$$

where σ stands for the appropriate polarization (α, β, x or y). While all the optical frequencies cancel out in the expression for $d^{(3)}(t)$, several terms involving the slowly varying pulse envelopes appear. Only the relevant terms for each case are retained, with the appropriate field dependencies, as discussed in Appendix A. Only the final expressions

for several cases are given in the following. We use the following notation in their presentation:

$$\begin{aligned}\left(A(B(C(D)))\right) &\equiv \int_{-\infty}^{\infty} dt_1 A(t_1) \int_{-\infty}^{t_1} dt_2 B(t_2) \int_{-\infty}^{t_2} dt_3 C(t_3) \int_{-\infty}^{t_3} dt_4 D(t_4) \quad , \\ (A) &= \int_{-\infty}^{\infty} dt A(t) \quad , \\ A_\omega &= A(t) e^{i\omega t} \quad ,\end{aligned} \tag{6.12}$$

and where $A(t)$ and $B(t)$ are the slowly varying envelopes of the pump and probe pulses, respectively, and are real.

6.3.1. Differential absorption

Let us consider first a DA experiment with two oppositely handed circularly polarized pulses. Calculating $Q^{(3)}$ for our system and taking the detuning $\nu = \varepsilon - \omega_0$ of the center laser frequency ω_0 from the excitonic transition as a parameter, we arrive at the following expression for $Q^{(3)}$:

$$\begin{aligned}Q^{(3)} &= Q_1^{(3)} + Q_2^{(3)} + Q_3^{(3)} + G^{-1} \cdot Q_4^{(3)} \\ Q_1^{(3)} &= \left| \left(B_{-\Delta+\nu}(A_\nu)\right) + \left(A_{-\Delta+\nu}(B_\nu)\right) \right|^2 \\ Q_2^{(3)} &= -\left\{ (B_\nu)\left(A_{-\Delta+\nu}\left(A^*_{-\Delta+\nu}(B^*_\nu)\right)\right) + \text{c.c.} \right\} \\ Q_3^{(3)} &= -\left\{ (B_\nu)\left(A_{-\Delta+\nu}\left(B^*_{-\Delta+\nu}(A^*_\nu)\right)\right) + \text{c.c.} \right\} \\ Q_4^{(3)} &= -\left\{ (B_\nu)\left(B^*_\nu\left(A_\nu(A^*_\nu)\right)\right) + \text{c.c.} \right\}\end{aligned} \tag{6.13}$$

where G is defined by $G = |d_{bx}|^2 / |d_{ex}|^2$. Figure 6.7 shows the results of a numerical calculation of Eq. 6.13 for assymetrical Lorenzian-shaped pulses (i.e. with different widths Γ for the Lorenzian function for positive and negative t). The different traces were

calculated for two values of ν/Δ. In the calculation we also assumed different dipole moments for the exciton and biexciton transitions (as will be explained in the following). In the figure $Q^{(3)}$ is plotted as function of the delay time t_D between the pump and the probe pulses, defined by $B(t) = A(t - t_D)$. We find that $Q^{(3)}$ oscillates in the delay time t_D, with a period which depends on both Δ and ν. The pattern of the calculated signal, a dip at the beginning and then damped oscillations, is in agreement with our experimental observations. One can clearly see that the oscillations persist only as long as there is overlap between the pump and probe pulses. However, the strong dependence of the oscillations' frequency in the calculated signal on the detuning of the laser is in sharp contrast to the behavior which was observed in the experiment. Similar results were obtained for different pulse shapes.

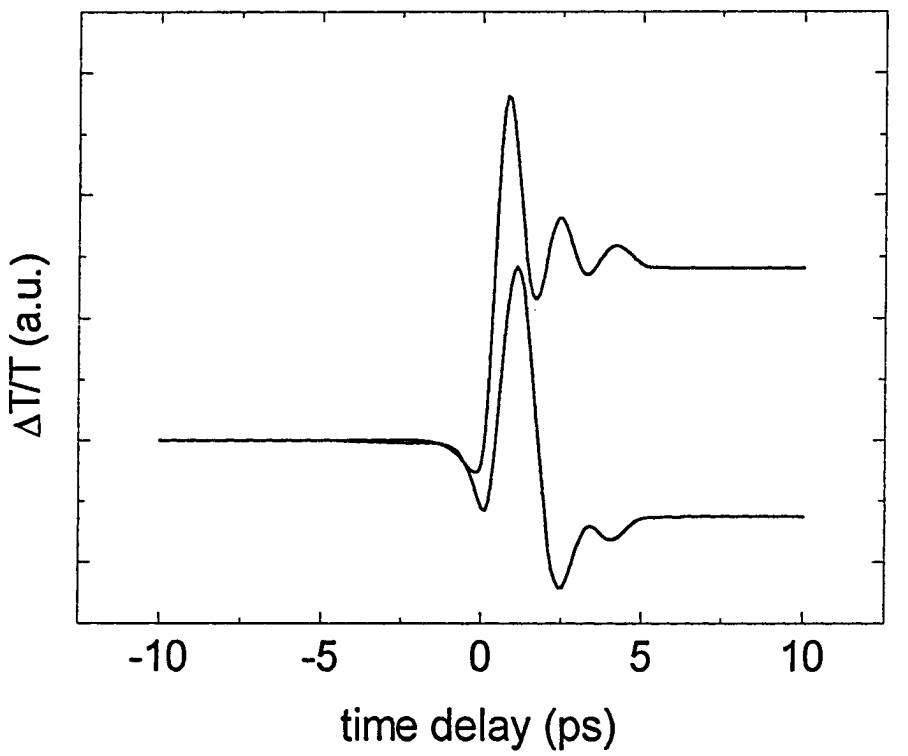

FIG. 6.7: The calculated differential absorption signal $-Q^{(3)}$ as a function of the time delay for assymetrical Lorenzian-shaped pulses with an autocorrelation width of ~1.5 ps. The solid curve was calculated for zero detuning, and the dotted curve was calculated for $\nu/\Delta = 0.25$.

6.3.2. Inhomogeneous broadening

The contradiction between the detuning-independent period in the measured signal and the results of the above calculation led us to consider the role of inhomogeneous broadening of the exciton line, which occurs in many quantum well samples, and in particular in the samples in which an oscillatory DA signal was measured. Inhomogeneous broadening implies that the laser excites an ensemble of four-level systems, each of them with a different detuning. This must lead to an averaging out of the detuning. The only parameter which determines the oscillations' period would then be the binding energy of the biexciton.

To take into account the inhomogeneous broadening of the excitonic transition we assumed that there is a distribution of four-level systems with different ε *but with the same* Δ, and averaged $d^{(3)}$ over ε. The width of the inhomogeneously broadened line W was taken to infinity, which is appropriate for $W >> \Delta$, ν , δ , where δ is the spectral width of the laser. For such an inhomogeneously broadened four-level system we get the following expression for the DA signal:

$$Q^{(3)} \sim \int_0^\infty ds\left(Ge^{-i\Delta s}-1\right)\int_{-\infty}^{\infty} dt \int_{-\infty}^{t-s} dt' \left\{\left[B(t)B^*(t-s)A^*(t')A(t'-s)+B(t)A(t-s)B^*(t')A^*(t'-s)\right]+\text{c.c.}\right\} \quad , \tag{6.14}$$

where G is defined by $G=\left|d_{bx}\right|^2/\left|d_{ex}\right|^2$, and all the omitted prefactors are positive. Note that ν does not appear in Eq. 6.14, and thus there is no dependence of the oscillations' frequency on the detuning. The result of a numerical calculation with single-sided exponential pulses [i.e. $A(t)$ = exp (t / τ) for t < 0 and $A(t)$ = 0 for t > 0] is shown in Fig. 6.8, where the value of G was taken to be 5. As will be discussed in section 6.3.4, this value agrees with theoretical estimates for the oscillator strength of the biexciton transition. One can clearly see that there is a good qualitative agreement between the calculation and the measured signal (Fig. 6.1).

It follows from our numerical calculations with different pulse shapes that the main features of $Q^{(3)}$ vs t_D, namely, zero signal for large negative delays, a dip for small negative delays (of the order of the pulse width), oscillations for positive delays within the overlap

of the pulses, and finally a constant positive value for large positive delays, are all pulse shape independent.

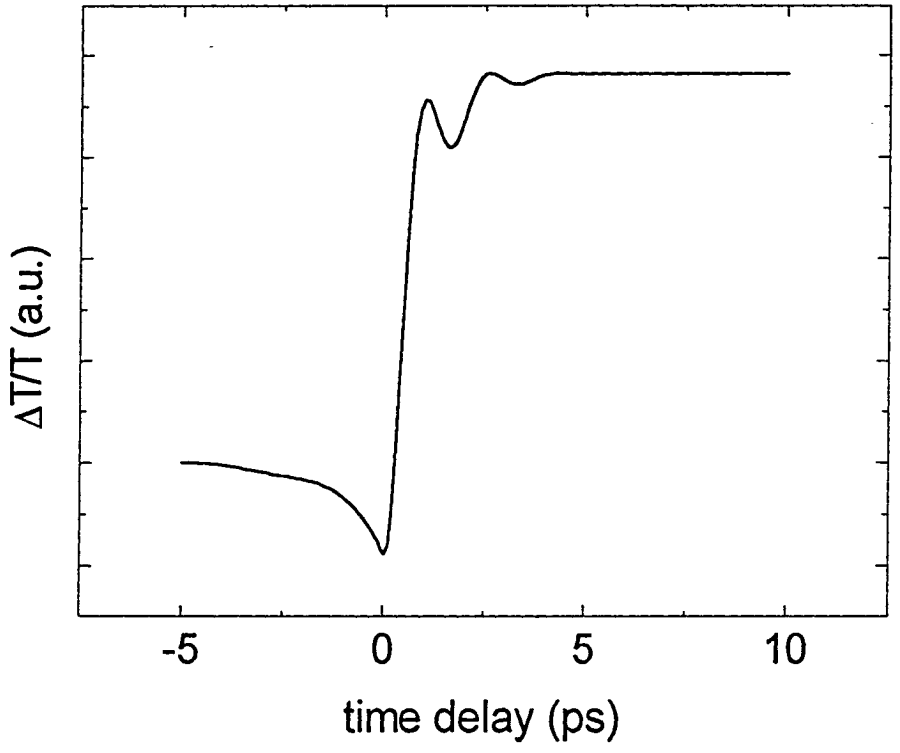

FIG. 6.8: The calculated differential absorption signal $-Q^{(3)}$ as a function of the time delay for an inhomogeneously-broadened exciton absorption line. The signal was calculated for single-sided exponential pulses with an autocorrelation width of 1.8 ps and assuming $G = 5$.

For delays which are much larger than the pulse width one can easily show that:

$$Q_{\infty}^{(3)} \sim -2\int_0^{\infty} ds(1 - G\cos\Delta s)|K(s)|^2 , \qquad (6.15)$$

where $K(s)$ is the pulse autocorrelation function. Equation 6.15 clearly shows that, due to the biexcitonic coupling, a differential absorption signal is obtained at large delays. This signal indeed reflects the transfer of oscillator strength from the excitonic transition to the biexcitonic transition due to the redistribution by the pump pulse of the population in the four-level system, as was suggested in section 6.2. It can be seen from Eq. 6.15 that

depending on the value of G and the relative size of Δ and δ, which defines the temporal spread of $K(s)$, the sign of $Q_{\infty}^{(3)}$ can be either positive or negative. In general, large G values would tend to make $Q_{\infty}^{(3)}$ positive, while a large Δ would tend to make it negative.

The main experimental observations which appear in our model when inhomogeneous broadening is introduced are the positive sign of $Q_{\infty}^{(3)}$ and frequency $\Delta/\hbar$ of the oscillations, both of which are independent of detuning. It is as if the laser was always tuned to the excitonic transition. It is interesting to note that when the original expression, without inhomogeneous broadening (Eq. 6.13), is used for calculating the DA signal for zero detuning, and G is inserted (by attenuating $Q_4^{(3)}$, which is the only term which does not involve the biexcitonic transition), a very good fit to the experiment is obtained, and the oscillations are deeper than they are in Fig. 6.8. The decrease of the oscillations amplitude in Fig. 6.8 is the result of assuming an infinite broadening in the calculation of Eq. 6.14.

6.3.3. Four-wave mixing

We now apply our model to the calculation of the signal in FWM experiments in inhomogeneously broadened systems, where two pulses with wave vectors k_1 and k_2, and envelopes $X(t)$ and $Y(t)$, are polarized along x and y, respectively. The field emitted in the direction $2k_2-k_1$ is polarized along y and is given by Eq. 6.9, where the third order dipole moment is:

$$d_y^{(3)}(t) \sim |d_{ex}|^2 d_{bx} e^{i(\varepsilon-\Delta)t} \int_{-\infty}^{t} dt' X^*(t') e^{i\Delta t'} \int_{-\infty}^{t'} dt'' X^*(t'') Y(t'+t''-t) + \text{c.c.} \qquad (6.16)$$

In the calculation of the FWM signal we must consider the decay and the dephasing of the biexciton. We describe the decay $b \rightarrow \sigma^+ + \sigma^-$ by a population relaxation Γ, while the dephasing of the nondiagonal matrix elements $\langle b|\rho^{(3)}|\sigma^{\pm}\rangle$ is described by a phase relaxation γ. If we further assume that the relaxation rates for the excitonic states are much smaller than those associated with the biexcitonic state, we get that Γ does not enter $d^{(3)}$, while the dephasing rate γ appears in Eq. 6.16 through the substitution $\Delta \rightarrow \Delta - i\gamma$.

A numerical calculation of the FWM signal with single-sided exponential pulses and $1/\gamma = 8$ ps is presented in Fig. 6.9, where we plot P as function of the delay between the two pulses. It can clearly be seen that oscillations with frequency Δ appear as long as there

is an overlap between the two pulses. The overall decay of the FWM signal is governed by biexciton dephasing rate γ. Again there is a good agreement between our calculation and the experimental data of Carmel *et al.* (Fig. 6.5).

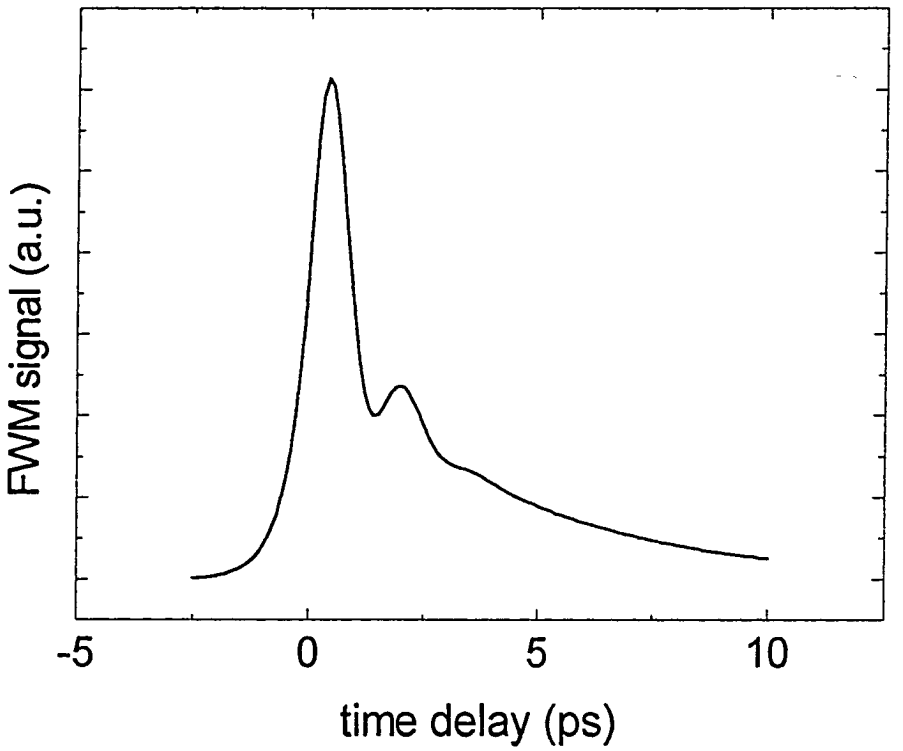

FIG 6.9: The calculated four-wave mixing signal as a function of the time delay, for single-sided exponential pulses with a width of 0.9 ps, for an inhomogeneously-broadened exciton absorption line. We assumed $1/\gamma$ = 8 ps.

6.3.4. Discussion of the model

The origin of the oscillations in the DA and FWM signals can be understood in terms of the time-dependent third order susceptibility $\chi^{(3)}$, defined by the following general expression for the third order dipole moment:[30]

$$d_{\sigma}^{(3)}(t) = \sum_{\sigma_i} \int_{-\infty}^{t} dt_1 \int_{-\infty}^{t_1} dt_2 \int_{-\infty}^{t_2} dt_3 \, \chi^{(3)}_{\sigma\sigma_1\sigma_2\sigma_3}(t,t_1,t_2,t_3) E_{\sigma_1}(t_1) E_{\sigma_2}(t_2) E_{\sigma_3}(t_3) \qquad (6.17)$$

where the polarization σ can be α,β (when the beams are circularly polarized) or x,y (in the case of linear polarizations). The nonlinear response $\chi^{(3)}$ is a function of the time intervals $t_i - t$ (i=1,2,3), oscillating with the eigenfrequencies of the four-level system, namely ε and $\varepsilon - \Delta$. An additional frequency in the system is obviously ω_o - the laser frequency. As a result, $d^{(3)}(t)$ oscillates in t with frequencies ε, $\varepsilon - \Delta$, and ω_o, as well as with sums (and differences) of these. In the special case where $E(t)$ is a superposition of two laser pulses with delay t_D, $d^{(3)}(t)$ oscillates not only in real time but also in t_D. Since in time-resolved optical experiments one measures slow time variations of the signal (relative to the laser frequency), the only frequency which survives is Δ - the binding energy of the biexciton.

The biexcitonic oscillations of $d^{(3)}(t)$ which we have observed in our two-pulse experiments are thus a result of interference of the two pulses, mediated by the oscillating susceptibility $\chi^{(3)}(t)$. These oscillations are different from known interference and quantum beat phenomena. An important characterisic of these oscillations is that, in contrast with known beating phenomena, they appear only as long as the two pulses overlap in time.

The only free parameters in our model are Δ and the enhancement factor $G = |d_{bx}|^2 / |d_{ex}|^2$ which is used in the calculation of the DA signal. For its estimation we refer to Ref. 63, according to which the ratio of the biexcitonic absorption (from an already existing exciton) to the excitonic absorption in two dimensions is $\alpha_{bx}/\alpha_{ex} \sim N_{ex}\, a_{bx}^2$, where N_{ex} is the sheet density of excitons and a_{bx} is the biexciton diameter. On the other hand, in our model we get an independent estimation $\alpha_{bx}/\alpha_{ex} \sim G\, n_e$, where n_e is the population of the excitonic levels $\sigma^{\pm}$, assuming $n_e << 1$ and a population of the ground state $n_g \approx 1$. In our model $N_{ex} = n_e N_o$, where $N_o \sim a_{bx}^{-2}$ is the density of four-level systems. From these arguments it follows that $G \sim a_{bx}^2 / a_{ex}^2 \sim E_{ex} / \Delta$, where E_{ex} is the binding energy of the exciton. Taking $\Delta \sim 2$ meV and $E_{ex} \sim 10$ meV for the binding energies, we get an estimate of $G \sim 5$ for the enhancement factor, as used in the calculation of the DA signal.

6.4. Measurements in magnetic field

Figure 6.10 shows measurements of the biexcitonic DA signal in our stepped MQW sample in a magnetic field parallel to the growth axis. Two different measurements in a

field of 7 Tesla are shown, corresponding to two different orientations of the field - parallel to and anti-parallel to the exciting laser beams (this is equivalent to a reversal of the pump and probe polarizations in a fixed magnetic field). The DA signal in zero magnetic field is shown for comparison. The data shows three main effects of the magnetic field: one is a small change in the oscillations' period, which increases for one orientation of the field and decreases for the other; another effect is a "phase shift" of the oscillations, which begin as a dip for one orientation of the field and as a peak for the other; and the last effect is a decrease of the signal at large delays, for both field orientations.

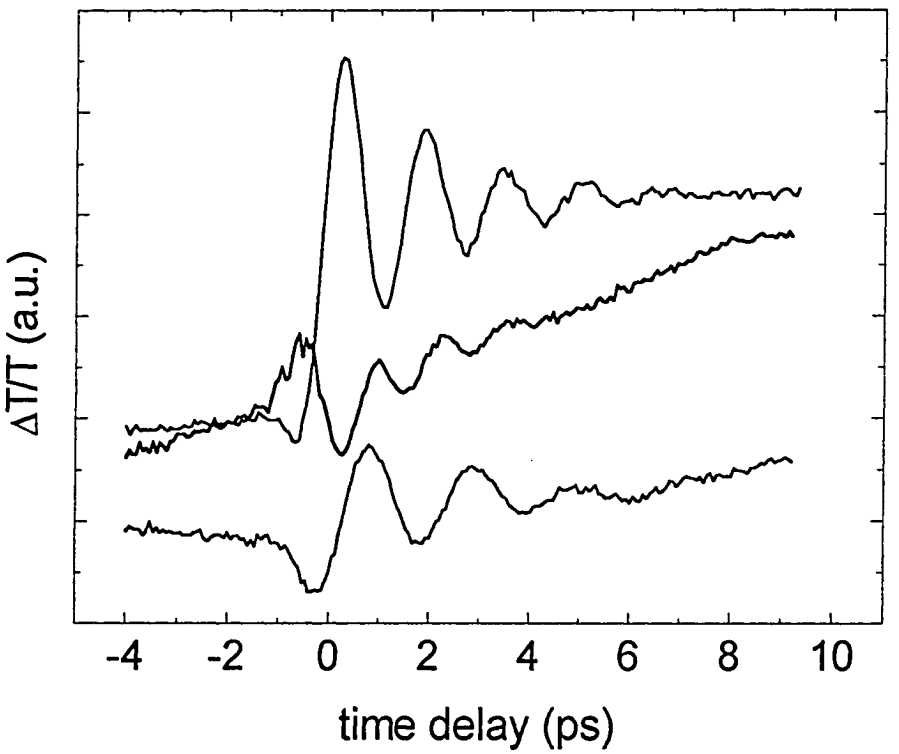

FIG. 6.10: The transient differential absorption signal in the stepped MQW sample, with oppositely-handed circular polarizations, in three magnetic fields: 0T (solid curve), and 7T in two orientations (thick curve and dotted curve).

The small changes in the period of the oscillation as function of the magnetic field are barely discernible in Fig. 6.10. However, in our measurements we were able to tune the laser for maximum pulsewidth, to allow an accurate measurement of the beating frequency. A plot of the change in frequency as function of magnetic field strength is

shown in Fig. 6.11. The data points are in very good agreement with the Zeeman splitting of the heavy-hole exciton (the curve in the figure), as deduced from Zeeman quantum beats data.[54]

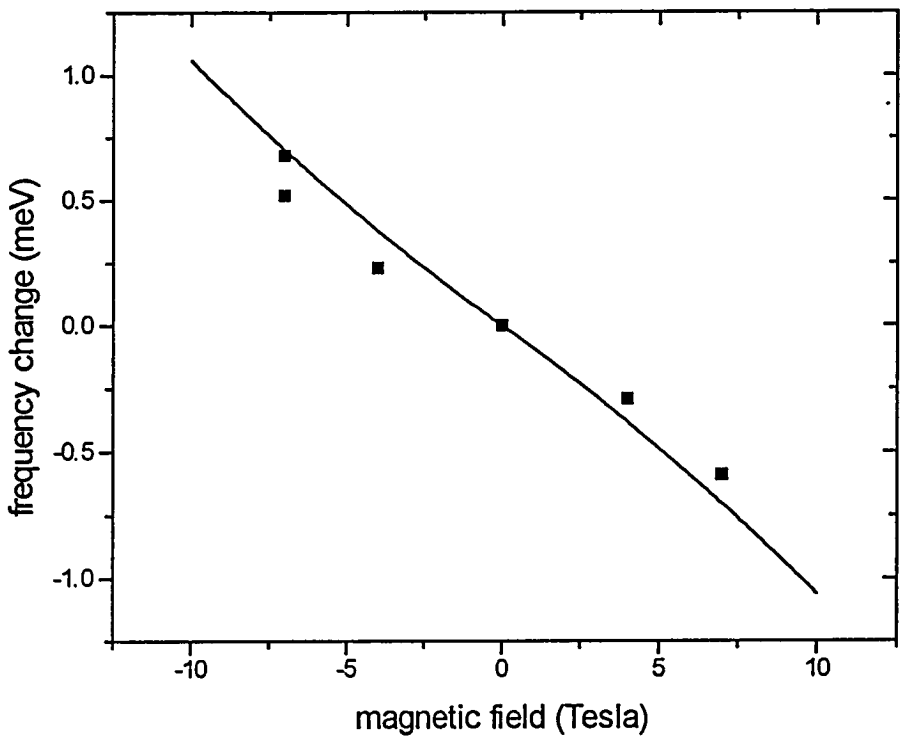

FIG. 6.11: The change of the period of the biexcitonic oscillations relative to their period in zero magnetic field (squares), compare with the Zeeman splitting in the stepped MQW sample. The curve shows a calculation of the splitting, taking the magnetic field dependent g-factor to be 0.76 + 0.016 *B*, as estimated by Carmel *et al.*[54] for the same sample.

The above effects are obviously resulting from the removal of degeneracy between the excitonic transitions due to the Zeeman energy term. To test this observation and the validity of our model, we have introduced the Zeeman splitting ω into the four-level system model. For simplicity we have used the expression for the DA signal without inhomogeneous broadening (this model has all the ingredients of the measured signal less

the dependence on detuning). Equation 6.13 now takes the form:

$$
\begin{aligned}
Q^{(3)} &= Q_1^{(3)} + Q_2^{(3)} + Q_3^{(3)} + G^{-1} \cdot Q_4^{(3)} \\
Q_1^{(3)} &= \left| \left(B_{-\Delta+\nu+\omega}\left(A_{\nu-\omega}\right) \right) + \left(A_{-\Delta+\nu-\omega}\left(B_{\nu+\omega}\right) \right) \right|^2 \\
Q_2^{(3)} &= -\left\{ \left(B_{\nu+\omega}\right)\left(A_{-\Delta+\nu-\omega}\left(A^*_{-\Delta+\nu-\omega}\left(B^*_{\nu+\omega}\right)\right)\right) + \text{c.c.} \right\} \\
Q_3^{(3)} &= -\left\{ \left(B_{\nu+\omega}\right)\left(A_{-\Delta+\nu-\omega}\left(B^*_{-\Delta+\nu+\omega}\left(A^*_{\nu-\omega}\right)\right)\right) + \text{c.c.} \right\} \\
Q_4^{(3)} &= -\left\{ \left(B_{\nu+\omega}\right)\left(B^*_{\nu+\omega}\left(A_{\nu-\omega}\left(A^*_{\nu-\omega}\right)\right)\right) + \text{c.c.} \right\}
\end{aligned}
$$

(6.18)

where we assume that the biexciton binding energy is not dependent on the magnetic field (only slight changes of the biexcitonic binding energy are expected in the moderate magnetic fields in which the experiment was performed). A numerical calculation of this expression is presented in Fig. 6.12. The three curves correspond approximately to the experimental parameters of Fig. 6.10 (we estimate the Zeeman splitting in a field of 7 Tesla to be approximately 0.8 meV, or 0.3×Δ). It is remarkable that the calculation reproduces all the features in the experiment. In particular, the opposite phase shifts for the two field orientations are reproduced, and so is the decrease of the signal at large delays, for both field orientations. The oscillations' period is somewhat ambiguous in the calculated signal, but the *average* distance between successive peaks and dips scales with the magnetic field similarly to the experiment. (In the experiment, tuning of the laser cavity for maximum pulsewidth, in order to measure as many periods as possible, results in pulses which are not transform-limited, meaning that the spectral bandwidth remains large enough to overlap with the excitonic and biexcitonic transitions at the same time. This is not the case in the model, which assumes perfect mode-locking of the laser. We are thus unable to simulate the signal for these distorted pulses).

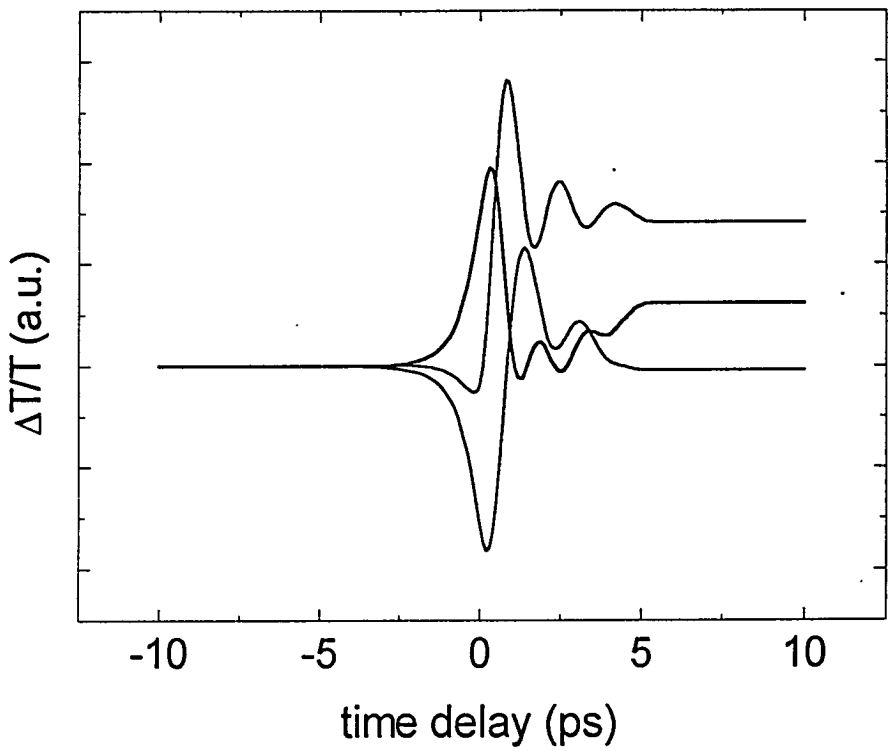

FIG. 6.12: The calculated differential absorption signal for three values of the magnetic field, which correspond to the measurements presented in Fig. 6.10.

6.5. Implications on nonlinear experiments and the biexciton binding energy

We have shown that the four-level model of the exciton-biexciton system explains very well the temporal oscillations and the coupling between σ^+ and σ^- excitons which are observed in nonlinear optical experiments in GaAs quantum well samples. An important test of the validity of the four-level model is the effect of a magnetic field on the DA signal. The predictions of the theory with regard to this effect were verified experimentally, and an excellent agreement between experiment and theory was demonstrated. Our work thus emphasizes the importance of biexcitons in nonlinear optical experiments in GaAs quantum wells.

The coupling of the two excitonic states through both the ground state and the biexcitonic state gives a possible explanation to the polarization dependence of FWM experiments in GaAs quantum wells in zero magnetic field. The model attributes the

different relaxation rates of the FWM signals which are observed in the PP and CP cases to the dephasing time of the exciton and biexciton, respectively. Cundiff *et al.* have proposed an alternative explanation,[64] in which they attribute the CP signal to extended excitons and the PP signal to localized excitons (their explanation implies the simultaneous presence of localised and extended excitons of equal energies). Other groups proposed generic couplings between the excitonic levels[65] or dephasing due to excitonic screening[66] as alternative explanations. We believe that our four-level system model provides a more consistent description of the excitonic nonlinear response.

There are plenty of data that suggest that biexcitons indeed exist in GaAs at low temperatures. High quality GaAs quantum wells, 80-Å to 300-Å wide, were reported to exhibit a biexciton-related photo-luminescence peak below the free exciton line at high intensity excitations.[67] This peak is separated by ≈1 meV from the free exciton line. When the temperature is increased to ≈10 K (k_BT ≈1 meV) the intensity of the biexcitonic peak diminishes. Another characteristic of this peak is the low polarization of the emitted photo-luminescence following an excitation with polarized light, as a result of the equal probability to emit σ^+ and σ^- photons. Recent photo-luminescence measurements in narrow quantum wells give biexciton binding energies up to 2.8 meV.[68]

Thus, photo-luminescence experiments on high quality GaAs quantum well samples give biexciton binding energies in the range between 1 and 3 meV. Kleinman has made a variational calculation of that binding energy,[69] and found that it is 3-4 times larger than the corresponding quantity in the 3D case, but still obeys the rule $E_{bx} \approx 0.1\ E_x$ which was found in the bulk case. Nevertheless, this calculation predicts a large enhancement of the binding energy for well widths below 100-Å, and for very narrow quantum wells it approaches 2 meV.

The association of the fast oscillations in the DA and FWM experiments with the biexciton phenomenon suggest binding energies of 2-3 meV. From the biexcitonic oscillations in the FWM measurements of Oberhauser *et al.* a binding energy of 1.75 meV is deduced for a 116-Å quantum well.[62] Lovering *et al.* report a lower biexciton binding energy of 1.15 meV for a 102-Å quantum well,[61] but it is possible that an unexplained second harmonic in their data should be considered, leading to a larger estimation, by a factor of 2, of the binding energy. These values are in agreement with the afforementioned photo-luminescence experiments, but are higher than the 1-2 meV which are predicted by the variational calculations. It should be noted, though, that photo-luminescence

experiments on bulk GaAs have indicated a biexcitonic binding energy of up to 0.7 meV,[70] high above the 0.13 meV value which was estimated by variational calculations.[67] It is possible that localization effects give rise to a significant enhancement of the biexciton binding energy.

Finally, biexcitonic effects must be considered when analysing the slow spin dynamics of the excitons which were discussed in chapter 5. Our four-level system model has shown that due to the biexcitonic coupling, a differential absorption signal is obtained at time delays which are large compared to the pulsewidth. It follows that the instantaneous (within the pulsewidth) rise of the σ^- signal which was reported in our spin relaxation studies represents a contribution of biexcitonic origin. Such a contribution is not included in any of the attempts to give a comprehensive explanation to spin relaxation measurements.

As noted in section 5.1.3, in our spin-flip studies we have observed a correlation between the instantaneous rise of the σ^- signal and a pronounced drop of that signal along with the slow spin relaxation of the conduction band electrons: the larger the instantaneous rise was, the larger was the drop at long delays. Another finding was that both the rise and the drop were suppressed as the magnetic field strength or the excitation intensity were increased (see section 5.1.3). We believe that this behavior can be understood as resulting from the interplay between spin relaxation and biexciton pairing. According to this interpretation, the pure biexcitonic contribution, which is responsible for the signal at $t = 0$, must be suppressed for a probe pulse which arrives after a long delay, when the system is not spin-polarized any more. The observed intensity and magnetic field dependencies then suggest a relative diminishing of the biexcitonic contribution with increasing magnetic field and excitation intensity. While the decrease of the long-delay biexcitonic contribution at high magnetic fields is explicitly contained in our biexcitonic model (Fig. 6.12), the intensity dependence might be related to the low density limit for which our model is valid. Further investigations are required to fully resolve the issue.

7. The 2DEG in high magnetic fields

7.1. Optical properties of degenerate semiconductors

In the previous chapters we have considered the optical response in intrinsic quantum well samples. In these semiconductor structures the Coulomb interaction between the optically excited electron and hole pairs results in the formation of excitons. The relatively large binding energy of these excitons implies that when the laser is tuned to the exciton line, one may ignore the higher-energy continuum states, and treat the dynamics of the exciton independently. As previously discussed, it is possible to describe these dynamics in the framework of a four-level system, and in many cases even a simpler two-level model suffices.

The relatively simple excitonic picture is substantially modified in doped semiconductor structures, in which a degenerate electron (hole) gas is formed in the conduction (valence) band. An obvious modification is the shift of the optical absorption edge to higher energies, known as the Moss-Burstein shift,[71] as a result of the inhibition of transitions into filled states. One also expects that the screening of the Coulomb interaction by free carriers would result in the absence of excitonic effects. However, it turns out that the Coulomb interaction between the electrons and the hole in the final state still drastically affects the optical spectra. Using many-body techniques, Mahan had shown[8] that the main effect of the sharp Fermi edge is to make the Coulomb interaction nonlocal, and to restrict the electron's scattering. Were it not for lifetime broadening, a real electron-hole bound state would exist. Mahan also demonstrated that the scattering of a noninteracting electron gas by a photo-excited hole leads to a logarithmic divergence of the absorption at the band edge. This is the well-known Fermi-edge singularity. It was subsequently shown by Mahan and other workers[72] that a similar singularity exists for an infinite hole mass.

The Fermi-edge singularity was first investigated in the X-ray absorption and emission of metals (in which the infinite mass approximation applies to the deep localized holes).[73] Its experimental observation in doped bulk semiconductors is, however, practically impossible because of the strong impurity scattering. The spatial separation between the

ionized donors and the carriers in MD structures makes possible the observation of the Fermi-edge resonance in semiconductors. Indeed, this resonance was recently observed in the low-temperature absorption[74] and photo-luminescence[75] spectra of such structures. Ruckenstein *et al.* adapted the Mahan formalism to semiconductors.[76] Recent calculations for semiconductor quantum wells[77] have treated the evolution from bound excitons to the Fermi-edge singularity as function of the two-dimensional carrier density. It was shown that the effect of the finite hole mass is to wash out the singularity in absorption.

The presence of a sharp Fermi edge also modifies other carrier-carrier scattering processes, most importantly electron-electron (e-e) scattering in n-type MD quantum wells. In a recent FWM experiment on n-type MD quantum wells,[78] Kim *et al.* have shown a strong inhibition of e-e scattering rates near the Fermi energy. Their measurements show that the dephasing of the induced polarization varies with excess energy as predicted by the Fermi liquid theory for e-e scattering, i.e., the scattering times are inversely proportional to the square of the excess energy above the Fermi level. While hole dephasing times were claimed to be much longer than those of the electrons, the role of the electron-hole scattering in the dephasing of the nonlinear signal was not treated in this work. The afforementioned Fermi-edge singularity, however, implies that this scattering mechanism must be quite important.

Various experimental and theoretical works in high magnetic fields have shown that the many-body interactions which are manifested in transport measurements, such as the integer and fractional quantum Hall effect, are also evident in optical experiments. Among the many-body effects which were studied in optical experiments were the enhanced exchange interaction,[79] and resonances in photo-luminescence and inelastic light scattering experiments which were correlated with fractional collective states.[80] The clear footprint of the Fermi surface is also evident in these measurements, and the Fermi-edge singularity in the photo-luminescence spectra of the 2DEG has proved to be a crucial aspect of optical studies of many-body interactions in the integer and fractional quantum Hall effect regimes.[29] These works motivated us to study the behavior of the 2DEG in the time domain. The purpose of our research was to perform time-resolved measurements in MD samples in high magnetic fields, and to investigate possible modifications to the relatively simple dynamics of magneto-excitons, which we had observed in intrinsic samples and discussed in detail in the previous chapters.

Of particular interest to us was to extend the zero-field measurements of Kim *et al.*[78] to the high magnetic field regime. The magnetic field changes the electronic density of states, from the zero field continuous density of states to a discrete spectrum of degenerate Landau levels, whose occupation varies with the magnetic field strength. Thus the available phase space for scattering is modified by the magnetic field. At the same time the change of the electronic wave functions, from plane waves to localized (gauge dependent) functions, is reflected in changes of the scattering matrix elements. We had expected these effects to modify the simple excess-energy dependence of e-e scattering which Kim *et al.* had observed in their time-resolved experiment.

7.2. FWM on a 2DEG in high magnetic field

We have studied two MD samples, consisting of 30 periods of 100 Å GaAs wells between 500 Å $Al_{0.3}Ga_{0.7}As$ Barriers, the center 100 Å of which were doped with silicon. The carrier concentrations in the wells at 4 K, 1.8×10^{11} cm^{-2} in one sample and 1.0×10^{11} cm^{-2} in the other, were deduced from V.d.P. measurements, which also gave a low temperature mobility of $4\text{-}5\times10^{4}$ for both samples (implying a Drude relaxation time of ≈ 2 psec). The excitation power densities were kept below $\approx 10^{10}$ cm^{-2}, or about 5% of the electron densities in the wells.

Fig. 7.1 shows the evolution of the absorption spectrum in the two samples with increasing magnetic field. The gradual change from a continuous two dimensional density of states to a discrete Landau level spectrum is clearly observed. At low magnetic fields a step like absorption spectrum with two peaks, associated with the heavy and light hole transitions, is observed. As the magnetic field is increased the higher Landau Levels are emptied from electrons and absorption to these levels becomes possible. Consequently, we observe the appearance of a new peak at the absorption edge each time the Fermi level shifts to a lower Landau level. It can be seen that at the high magnetic field regime, above 5 Tesla, the electrons in both samples reside at the lowest Landau level and the absorption spectrum consists of broad but well separated peaks.[14]

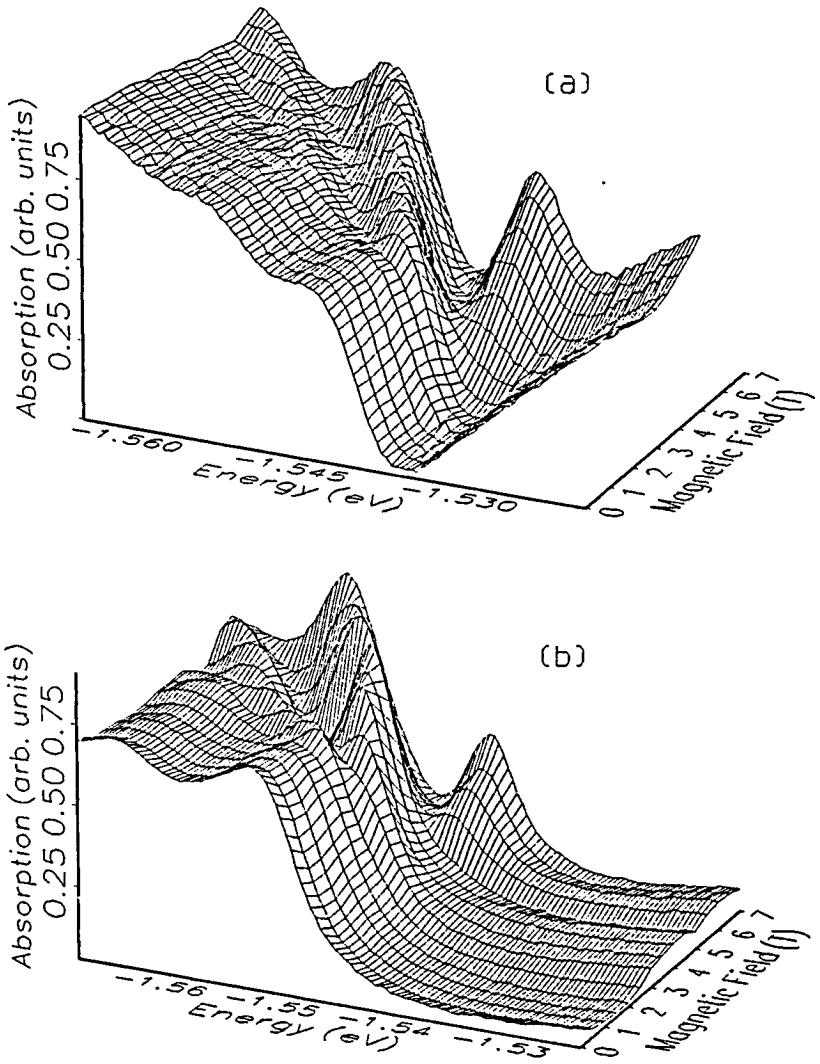

FIG. 7.1: Absorption spectra for increasing magnetic field, for the low (a) and high (b) density MD samples (1.0×10^{11} cm^{-2} and 1.8×10^{11} cm^{-2}, respectively.

7.2.1. Dephasing rates

The FWM signal from both samples shows an identical behavior, up to a scaling with the carrier concentration of the magnetic field dependencies. The peak intensity at 7 Tesla is weaker by about 3 orders of magnitude than that measured in intrinsic samples. This

reflects the absence of excitonic effects in the MD samples due to screening of the electron-hole Coulomb interaction by the Fermi sea.

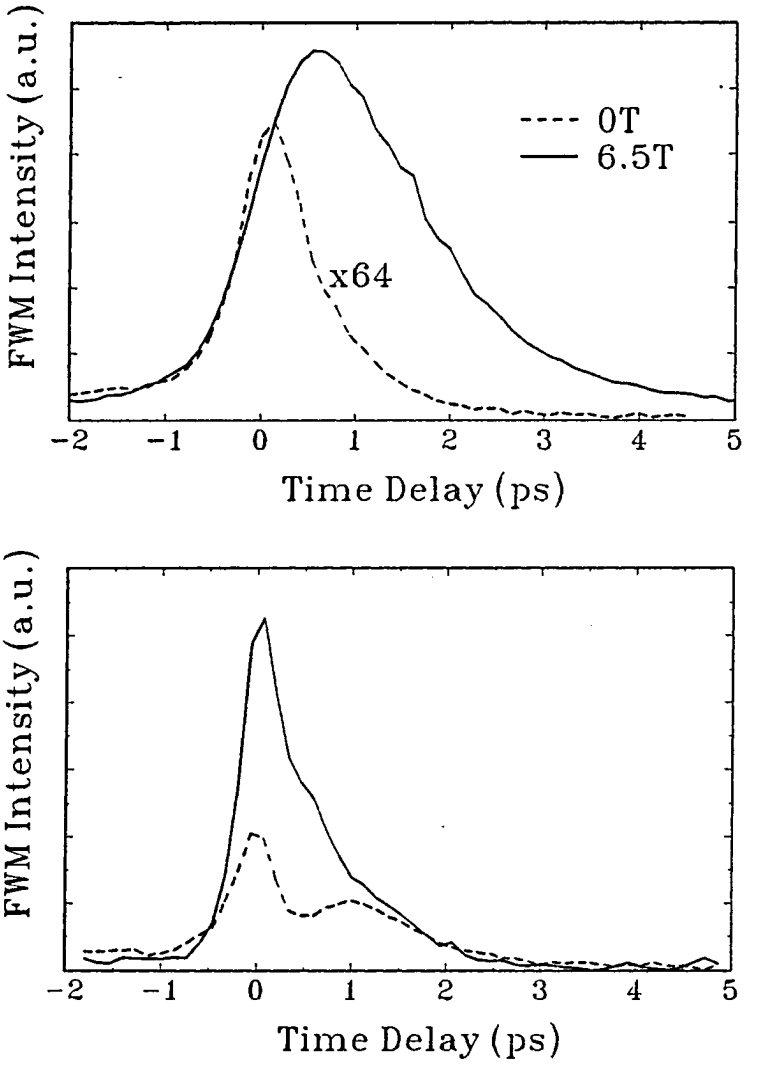

FIG 7.2: The temporal evolution of the FWM signal in the MD samples: (a) close to the Fermi energy at 0T and in the first Landau level at 6.5T (high density sample), and (b) at two excitations energies within the second Landau level at 6T (low density sample).

Figure 7.2(a) compares the time dependence of the FWM signal, which is measured close to the Fermi energy at B = 0, to that measured at a high magnetic field. It can be seen that both the rise and the fall times of the signals are different. The B = 0 signal is slightly asymmetric but roughly follows the autocorrelation of the laser pulse, peaking at

zero time delay. Such a behavior indicates a very fast dephasing time, comparable with the pulse autocorrelation width (0.7 ps). This is in agreement with Ref. 78, where dephasing times of less than 1 ps were measured close to the Fermi energy at similar excitation densities. The high field signal rises more slowly, with a rise time which is the pulse autocorrelation width, and decays exponentially with a time constant of 1.5 ps. The same temporal behavior is measured *throughout* the lowest Landau level. Clearly, there is a drastic change in the e-e scattering rate as well as in its dependence on excess energy above the Fermi level.

The slow dephasing time observed at the first Landau level implies that e-e scattering rate is lower in high magnetic fields than at B = 0. Our measurements can only set an upper limit for the e-e scattering rate. It is possible that impurity scattering is the limiting process which determines the dephasing time. In fact, the measured dephasing time of 1.5 ps is very similar to the Drude scattering time determined from the mobility measurements.

In Fig. 7.2(b) we show two temporal scans taken at different spectral positions at the second Landau level. Two temporal components can be identified in both scans: a fast component, which follows the pulse autocorrelation, and a *slow component*, which has the same decay time (1.5 ps) as the signal in the first Landau level. The relative weights of the two components depend on the polarizations of the exciting pulses and on the spectral position, but they both peak approximately at the center of the second Landau level and gradually fall at the high and low energy sides. The FWM signal at the second Landau level is much weaker than that measured at the first Landau level.

7.2.2. Enhancement at the Fermi edge

We now turn to the spectral behavior of the FWM signal. Figure 7.3(a) illustrates the evolution of the FWM spectrum as the magnetic field is increased. These spectra were measured at zero time delay with cross polarized exciting pulses. Similar results were obtained at later time delays and with exciting pulses with parallel polarizations. It can be seen that the FWM spectra are dominated by a single peak, which at 3 Tesla shifts to lower energy and significantly increases in intensity. This behavior is markedly different from that of the linear absorption, where multiple peaks of comparable height are observed. The substantial spectral changes in the FWM signal which occur above 3 Tesla are correlated with the jump of the Fermi level from the second to first Landau level.

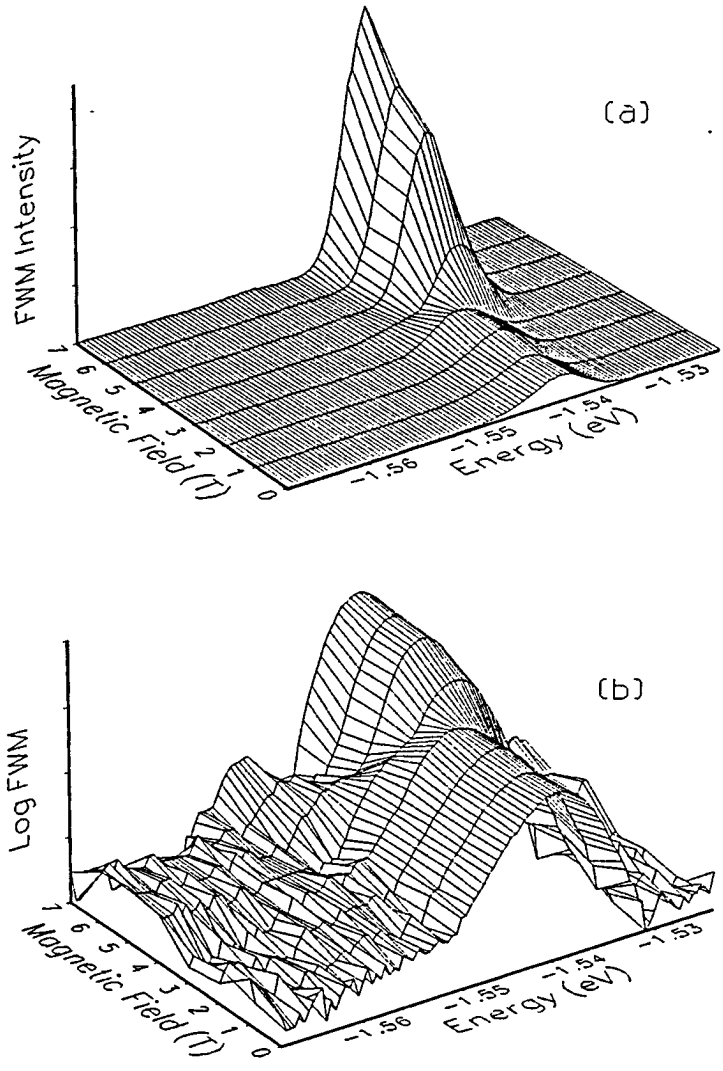

FIG 7.3: FWM spectra for increasing magnetic field for the low density sample, plotted on (a) linear and (b) logarithmic scales.

Replotting the FWM spectra on a logarithmic scale [(Fig. 7.3(b)] it is possible to identify the signal from the second Landau level, which is weaker by more than two orders of magnitude than the signal from the first Landau level in high magnetic fields. The peak which dominates the spectra at low fields evolves into the second Landau level transition, but *decreasing* its strength with increasing magnetic field. This anomalous behavior is demonstrated in Fig. 7.4(a), where we show the FWM signal at the second Landau level

as function of magnetic field, in the two samples. In these measurements the laser was tuned to follow the second Landau level peak energy, as determined from the absorption spectra, and the magnetic field was ramped. A sharp decrease in the signal is observed in both samples at the magnetic field at which the Fermi level drops into the first Landau level. (The increase of the signal between 3 Tesla to 4 Tesla in the high-density sample reflects the emptying of the second Landau level.)

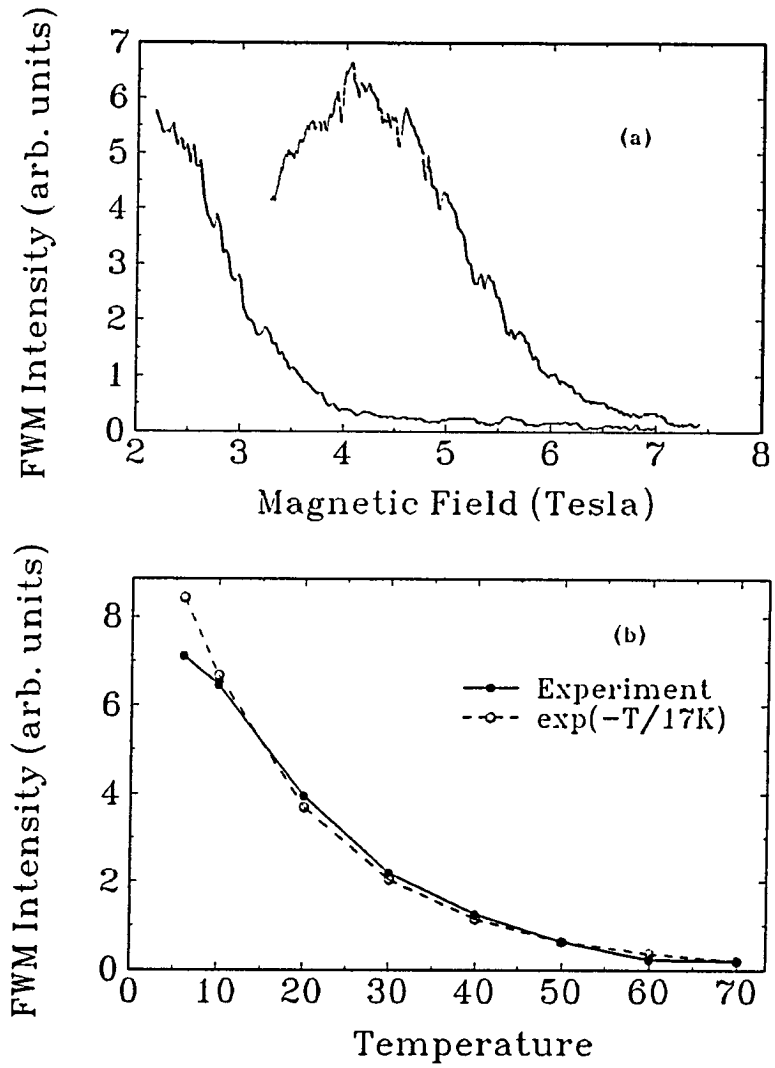

FIG. 7.4: (a) FWM intensity at the peak of the second Landau level as a function of magnetic field at zero time delay. The solid and dashed lines describe the low and high density samples, respectively. (b) FWM intensity as a function of temperature for the low density sample at zero time delay and 7T, and a fit to an exponential decay.

It is evident from our results that the proximity of the Fermi energy to the excitation energy strongly affects the observed FWM signal in the MD samples. A strong dependence of the FWM intensity on the excess energy above the Fermi level was also observed in zero field.[78] In that case it was attributed to the decrease of dephasing time as function of excess energy (a short dephasing time leads to a weak integrated signal). However, tuning the laser across the first Landau level did not produce any noticeable change in the dephasing time. The strong enhancement at the Fermi level suggests that the observed signal is related to a singularity at the Fermi level. An insight into the origin of this singularity is obtained by examining the temperature dependence of the signal. Figure 7.4(b) shows the measured FWM signal at the first Landau level in a field of 7 Tesla as a function of temperature. The rapid decrease of the signal can be very well fitted to an exponential decay, with a decay constant of 17 K or $\approx$ 1.4 meV. The dephasing time changes much more slowly as a function of temperature, and no significant change is observed up to 30 K. Therefore, the fast drop of the signal with temperature can not be attributed to a fast dephasing. On the other hand, these temperature and energy scales are characteristic of the decay of the Fermi-edge singularity in absorption and photo-luminescence measurements.[74] We thus arrive at the conclusion that the measured signal in our FWM experiments is the nonlinear response of the Fermi-edge singularity.

7.3. Electron-electron scattering in a magnetic field

In order to understand the effect of the high magnetic field on the interaction between the photo-excited carriers and the 2DEG in the sample, we have carried out a formal study of the problem, concentrating on its dynamical aspect. We analyse the e-e scattering of the optically-excited electrons with the conduction band electrons and, following Kim *et al.*,[78] neglect the effect of holes.

We are not aware of any detailed calculation of e-e scattering rate in two dimensional structures in a magnetic field. However, some simple considerations can provide an insight into the origin of the observed behavior. Generally, scattering rates depend on the scattering matrix elements and on the density of final states. In the following we will show that at high magnetic fields the matrix element for inter-Landau level e-e scattering, in which a test electron in the second Landau level is scattered by the Fermi sea into the first Landau level (and an electron from the Fermi sea is scattered into the second Landau

level), is suppressed. Therefore, the dominant e-e scattering mechanism at high magnetic field is intra-Landau level processes, the rate of which increases with magnetic field.

The e-e scattering rate is calculated using the Fermi golden rule. For this approach to be valid one must assume that the degeneracy of the Landau levels is removed by some kind of perturbation. Otherwise degenerate perturbation theory must be applied. We therefore assume that the Landau levels are inhomogeneously broadened due to disorder. We first calculate the scattering matrix elements for the homogeneously (lifetime) broadened case, and then consider the modifications which result from the inhomogeneous broadening.

7.3.1. The degenerate problem

Consider an electron in the lowest conduction subband of a heterostructure in a magnetic field.[81] In the Landau gauge, the eigenstates of that electron are characterized by two quantum numbers: the Landau quantum number l and the wavevector component k_x. The transition rate of two electrons from the states l_1k_1 and l_2k_2 to the states $l_1'k_1'$ and $l_2'k_2'$ as a result of e-e scattering can be written in the following form:

$$W_{1,2\to 1',2'} = \frac{2\pi}{\hbar}\left|M_{1,2\to 1',2'}\right|^2 \delta(\varepsilon_1+\varepsilon_2-\varepsilon_{1'}-\varepsilon_{2'}) f_2(1-f_{1'})(1-f_{2'}) \tag{7.1}$$

where we have used the abbreviated notation: $l_1k_1 \equiv 1$, $l_1'k_1' \equiv 1'$, etc.. $M_{1,2\to 1'2'}$ is the transition matrix element from the state $|1,2\rangle$ to the state $|1',2'\rangle$. This matrix element is defined as:

$$M_{1,2\to 1',2'} \equiv \langle 1,2|U^{ee}(r_1,r_2)|1',2'\rangle, \tag{7.2}$$

where $U^{ee}(r_1,r_2) = e^2/\kappa|r_1-r_2|$ is the Coulomb interaction potential for two electrons and κ is the dielectric constant. U^{ee} depends only on the difference $r = r_1 - r_2$ and may be written in terms of its Fourier components U_q^{ee}:

$$U^{ee}(r) = \int \frac{d^3q}{(2\pi)^3} e^{iqr} U_q^{ee}. \tag{7.3}$$

In the calculation the Fourier components of the screened Coulomb interaction are inserted into Eq. 7.3, which is in turn used in the calculation of the matrix elements defined by Eq. 7.2. Care should be taken with regard to screening, since in quantum wells the Coulomb potential is three-dimensional, but the 2DEG screens only in two dimensions.[82] The details of the calculation are given in Appendix B. It turns out that for both 3d and 2d screening the dependence of the e-e scattering rates on the magnetic field strength turn out to be the same. Furthermore, in our samples the screening length is comparable to the width of the quantum well, so the results for the two screening models also turn out to be comparable. Thus in the following only 3d screening is discussed. We get the scattering rate *for a given set of Landau indices* $l_1 l_2 \rightarrow l_1' l_2'$ in the degenerate problem:

$$\left.\frac{1}{\tau}\right|_{l_1 l_2 \rightarrow l_1' l_2'} \approx \frac{4e^4}{\hbar d^2 \kappa^2} F(l_1, l_2, l_1', l_2', \alpha)\, \delta(\varepsilon_1 + \varepsilon_2 - \varepsilon_{1'} - \varepsilon_{2'}) f_2 (1 - f_{1'})(1 - f_{2'}) \qquad (7.4)$$

where d is the width of the quantum well, κ is the dielectric constant of the intrinsic semiconductor, and α is defined by $\alpha \equiv a_H^2 / \lambda^2$, where a_H is the magnetic length and λ is the screening length. The dimensionless parameter α is inversely proportional to the magnetic field strength, and the dimensionless function F is given in terms of exponential integrals $E_n(\alpha)$.[83] The function F is plotted in Fig. 7.5 for three different cases: the first, denoted by F_1, describes the process in which a photo-excited test electron is scattered within the second Landau level by the 2DEG in the partially-filled first Landau level: $F_1 \equiv F(2,1,2,1,\alpha)$. The second case, denoted by F_2, again involves the scattering of a photo-excited test electron in the second Landau level by the 2DEG in the first Landau level, but this time the test electron is scattered to the first Landau level, while an electron from the 2DEG is scattered into the second Landau level to conserve energy: $F_2 \equiv (2,1,1,2,\alpha)$. By F_3 we denote the process in which the test electron is photo-excited into the first , partially-filled Landau level: $F_3 \equiv F(1,1,1,1,\alpha)$. It can be seen from Fig. 7.5 that in the high magnetic field limit F_1 and F_3 increase like $1/\alpha$, while F_2 decreases slightly. In a field of 7 Tesla, where $a_H \approx 100\,\text{Å}$, α is expected to be of order unity. In this field regime the matrix elements F_i of all three processes are also of order unity.

Although Eq. 7.4 provides insight to the dependence of the various e-e scattering matrix elements on the magnetic field strength, it is impossible to use it for the calculation of the scattering rates. This is because the delta function in Eq. 7.4 diverges for the degenerate problem. As already noted, this is in turn a consequence of using the Fermi

golden rule instead of degenerate perturbation theory. In the following section we discuss how inhomogeneous broadening due to a disorder potential modifies the above calculation, leading to a suppression of the divergence. Such broadening is always present in quantum well samples, including our samples (see Fig. 7.1), and was reported[15] and discussed[14] in the literature.

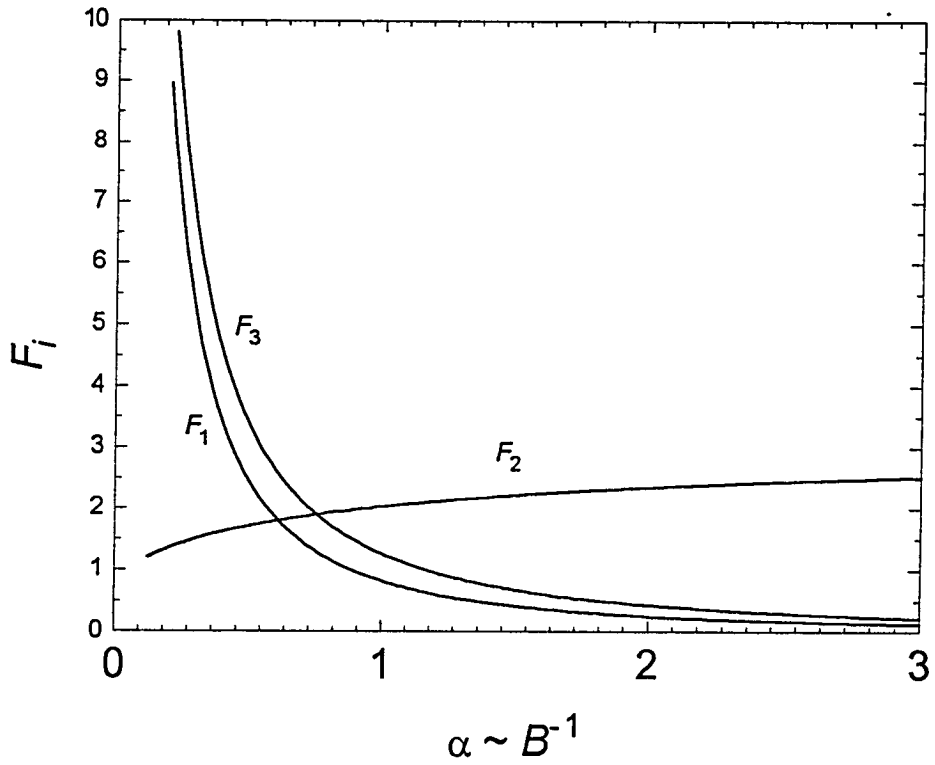

FIG. 7.5: The functions $F_i(\alpha)$, describing the different inter-level and intra-level electron-electron scattering matrix elements in the first and second Landau levels. The three different processes are defined in the text.

7.3.2. Disorder and inhomogeneous broadening

In the calculation of the e-e scattering rates for the degenerate case we assumed an ideal sample with no disorder. Therefore, in the calculation of the scattering matrix elements (Eq. B.7 in Appendix B) we could simply sum over all possible degenerate initial and final states. When disorder is introduced the degeneracy is removed and care should be taken in summing over the scattering states. Such a procedure is complicated for an

arbitrary disorder potential. For simplicity we consider a special type of disorder potential, in which the energy ε is dependent on the coordinate of the guiding center. In the Landau gauge, in which we formulated our problem (Appendix B), this means that the disorder potential is dependent on only one coordinate, the y coordinate for which a_H is defined. (In the general case a different gauge should be used ; We believe that the result would remain the same, up to a geometrical factor of order unity).

Let us characterize the disorder potential by its correlation length Λ, and consider the scattering process depicted in Fig. 7.6. The magnetic length a_H defines a length scale within which the initial and final states of each particle should reside. λ defines the length scale over which two initial states can interact. Moreover, in a scattering event both energy and momentum (i.e. the mean y coordinate in the Landau gauge) must be conserved. Clearly, the fluctuations of the disorder potential inhibits the scattering by those states for which energy and momentum would not be both conserved. This effectively reduces the phase space for scattering and the scattering rate.

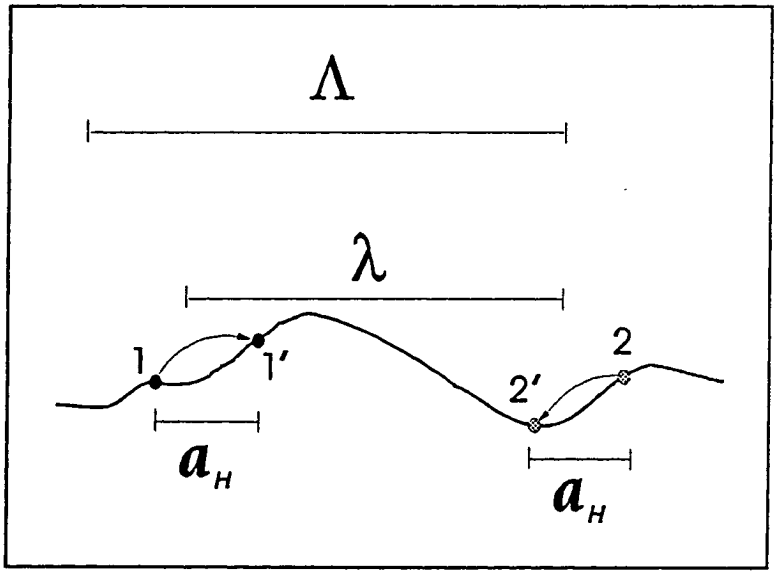

FIG. 7.6: Length scales for e-e scattering in presence of a disorder potential: the correlation length Λ, the magnetic length a_H, and the screening length λ.

One can define several regimes depending on the relative magnitude of a_H, λ and Λ. a_H is dependent only on the magnetic field. It is large for low fields and small in the high field limit. The magnitude of λ is less clear: in the ideal 2d case it is independent of the electron sheet density, while in three dimensions it decreases as the density of electrons is increased. Λ is sample-dependent. In the following we discuss two of these regimes: a short range disorder potential and a long range disorder potential.

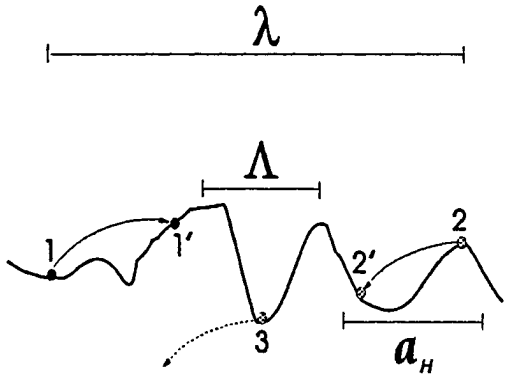

FIG. 7.7: A short range disorder potential. Electron 3 can only gain energy, so it cannot scatter electron 1.

a. short range disorder potential:

A short range disorder potential is defined by $\Lambda << a_H, \lambda$, and is schematically shown in Fig. 7.7. Conservation of energy and momentum implies that an electron in a state $|1\rangle$ can be scattered to the state $|1'\rangle$ by the electron in state $|2\rangle$ (which is scattered to state $|2'\rangle$), but cannot be scattered by the electron in state $|3\rangle$. For a short range potential one can take the density of states $g(\varepsilon)$ (the inhomogeneous line shape) to represent the probability that *any given change of momentum* would be accompanied by *a corresponding change of energy*. The summation in Eq. B.7 (Appendix B) should therefore be modified to a triple integration over energy of such probabilities, multiplied by the delta-function representing energy conservation. For a short range potential the probabilities are independent, and one should therefore integrate over $g(\varepsilon_2)g(\varepsilon_{1'})g(\varepsilon_{2'})$. In formal writing this "statistical approach" gives the following averaging expression:

$$f_2(1-f_{1'})(1-f_{2'})\,\delta(\varepsilon_1+\varepsilon_2-\varepsilon_{1'}-\varepsilon_{2'}) \;\rightarrow$$

$$\rightarrow \iiint d\varepsilon_2\, d\varepsilon_{1'}\, d\varepsilon_{2'}\, g(\varepsilon_2)g(\varepsilon_{1'})g(\varepsilon_{2'})f(\varepsilon_2) \;\times$$
$$\times\; [1-f(\varepsilon_{1'})][1-f(\varepsilon_{2'})]\,\delta(\varepsilon_1+\varepsilon_2-\varepsilon_{1'}-\varepsilon_{2'}) =$$

$$= \iint d\varepsilon_2\, d\varepsilon_{2'}\, g(\varepsilon_2)g(\varepsilon_{1'})g(\varepsilon_1+\varepsilon_2-\varepsilon_{2'})f(\varepsilon_2) \;\times$$
$$\times\; [1-f(\varepsilon_1+\varepsilon_2-\varepsilon_{2'})][1-f(\varepsilon_{2'})]$$

(7.5)

We now define Δ as the excess energy of the photo-excited electron. We differentiate between two different cases: When the test electron is excited into the first broadened Landau level (F_3 in Eq. 7.4) Δ is defined relative to the Fermi energy ; When the test electron is excited into the second broadened Landau level (F_1 and F_2 in Eq. 7.4) Δ is defined relative to the bottom of this level. It can be shown that for a small Δ and zero temperature this approach leads to a factor Δ^2/W^3 in the expression for the scattering rate, where W is the inhomogeneous width of the Landau levels. Such a quadratic dependence on excess energy is similar to the behavior in zero magnetic field.

b. long range disorder potential:

In the high magnetic field regime the long range disorder approximation, defined by $\Lambda >> \lambda > a_H$ and depicted in Fig. 7.8, is more appropriate. Since the shift of the center of the electron orbit in the scattering event is limited by a_H, the energy transfer is restricted by $\Delta\varepsilon < a_H \cdot \nabla V(\mathrm{r}) \approx a_H \cdot W/\Lambda \equiv \overline{W}$. It follows that for a large excess energy Δ the available phase space for scattering is determined by $\overline{W}$ and not by Δ. For $\Delta > \overline{W}$ the density of states factor in strong magnetic field is $\overline{W}^2/W^3 = a_H^2/(W \cdot \Lambda^2)$. Consequently, the scattering rate and its energy dependence are suppressed.

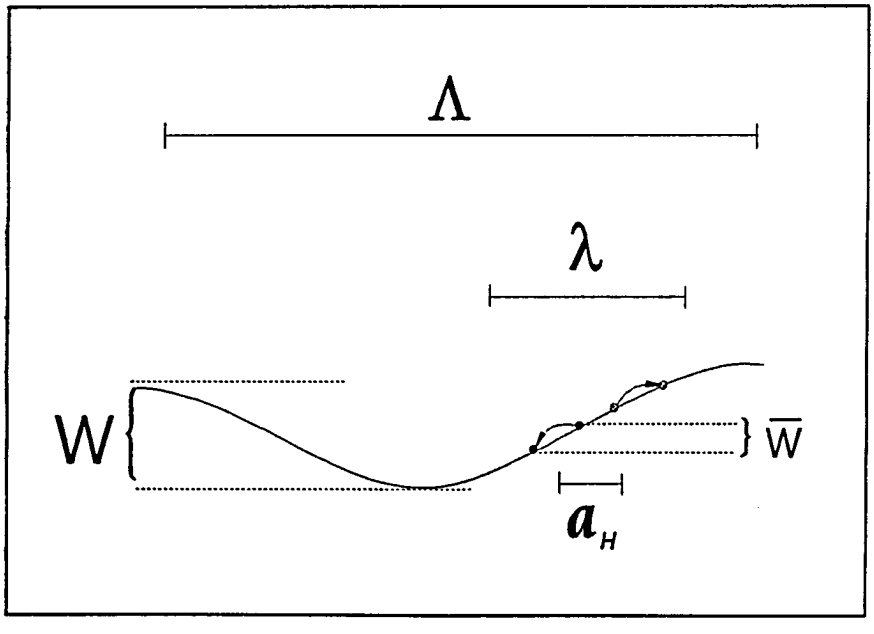

FIG. 7.8: A long range disorder potential - the change of energy in a scattering event is limited to $\overline{W}$, determined by a_H. W is the width of the broadened level.

The final expression for e-e scattering rate in high magnetic field, in the presence of a long-range disorder potential is (assuming 3d screening):

$$\left.\frac{1}{\tau}\right|_j \approx \frac{4e^4}{\hbar d^2 \kappa^2} F_j(\alpha) \frac{a_H^2}{\Lambda^2 W} \quad , \qquad (7.6)$$

where the index j = 1,2,3 was defined above for the three scattering processes which we consider. For a 100Å -wide quantum well the pre-factor $4e^4/(\hbar d^2\kappa^2)$ equals 1.2 erg/sec, or approximately 7.5×10^{14} meV/sec. Taking $F_j \approx 1$, $W \approx 5$ meV and $a_H \approx 100$Å, the 1.5 ps phase relaxation time which was measured in our experiments is consistent with a correlation length $\Lambda \approx 14 \times a_H \approx 1400$Å. We can use the mobility measurements on our samples to get an independent estimate for the length scale of the potential fluctuations. Taking the Fermi velocity to be ~ 10^7 cm/sec and a 2 ps Drude relaxation time, we get a mean free path of 2000Å, in reasonable agreement with the above estimate.

7.4. Discussion

To explain the temporal and spectral aspects of our FWM measurements on the two MD samples, we have calculated the e-e scattering rates in high magnetic fields, and found that they exhibit important changes relative to the e-e scattering in zero magnetic field. Our calculation suggests that the relatively low, energy independent dephasing rates which we measure in the first Landau level can be explained by these changes. The calculation also predict a suppression of the e-e scattering rates at the second Landau level, but in this case the dephasing rates which we measure in the experiment are very close to the laser pulse width, preventing a reliable quantitative analysis.

The analysis of our data in terms of e-e scattering exclusively is clearly incomplete. It is important to realize that we neglected electron-hole scattering completely. This scattering mechanism in particular may explain the spectral dependence of the signal intensity, since it is known to bring about the Fermi-edge singularity. Undoubtfully there is a need for a more complete theory, that will include these effects. An initial step in this

direction was done by Hawrylak,[84] who has applied the theory of the Fermi-edge singularity to give an alternative explanation to the experimental results of Kim *et al.*. To the best of our knowledge there is no comparable calculation for high magnetic fields. It was pointed out by Hawrylak that the Fermi-edge singularity in linear absorption is expected to disappear in the limit of discrete Landau level,[85] but the effects of Landau level broadening were not investigated.

Assuming that the continuous density of states in the broadened level does give rise to a Fermi-edge singularity, we believe that in the nonlinear signal it would be more pronounced than in linear absorption. This is borne out of the following argument: one can attempt to assign a phenomenological transition dipole moment d which characterizes the transition from the valence band to the partially filled conduction band ; In this phenomenological approach the absorption would be proportional to $|d|^2$ and the FWM signal would be proportional to $|d|^8$, and it is obvious that a much stronger enhancement is expected in the latter case.

It is surprising to note the apparent lack of any contribution to the FWM signal from light hole related transitions. This absence of light hole FWM signal is in contrast to their appearance in the absorption spectra (Fig. 7.1). A possible explanation for the absence of the light hole signal could be the strong dependence of the Fermi-edge singularity on the hole mass: the lighter the hole mass, the weaker is the enhancement.[77]

The experimental results leaves some puzzling questions, especially with regard to the polarization dependence of the signal. The behavior described above is generally true for both the parallel and crossed polarizations cases. We find, however, different ratios of the parallel polarizations to the crossed polarizations signals (CP/PP) at the first and second Landau levels. While in the first Landau level this ratio is approximately unity, in the second Landau level the parallel polarizations signal is much stronger. Although the polarization dependence of the FWM signal in the first Landau level is apparently similar to that of a four-level system with no biexcitonic coupling, there is no trace of the Zeeman quantum beats which dominate the high magnetic field FWM signal in intrinsic samples. It is possible that a large spin splitting due to exchange[79] effectively transforms the doped sample into a two-level system close to a filling factor of unity. It is equally possible that the many-body interactions result in a fundamental change of the selection rules, and of the simplified two-level model which generally applies in intrinsic quantum wells.

A more rigorous theory is clearly required to fully explain the experimental results, as are experiments with circular polarizations and an extension of the experimental work to higher quality single quantum well samples. A detailed study of the gradual change from an excitonic behavior to a Fermi-edge singularity, as function of carrier density, is also required.

8. Summary

In this research work we have implemented time-resolved spectroscopy in a study of the time-dependent optical response of GaAs heterostructures. Our experimental results demonstrate the power of time resolved spectroscopy as a tool in the research of dynamical processes and many-body interactions in solid state, especially in the high magnetic field regime. Apart from the capability to measure directly scattering processes, this coherent technique allows the measurement of minute energy splittings, as demonstrated in the various quantum beating phenomena which we have observed. As we have shown for the case of the biexcitonic interaction and in our experiments on modulation-doped samples, the nonlinear nature of this technique makes it very sensitive to interactions which are beyond the single particle theory.

Through the study of the time-dependent optical response we have proposed various modifications to the simple two-level system model which is generally used in the interpretation of optical experiments in GaAs heterostructures. The application of a magnetic field has allowed us to separate the two degenerate two-level systems. Following the study of spin relaxation - the long term scattering between the four levels, we were able to identify a biexcitonic coupling between the spin-polarized systems, and to propose it as an explanation to the anomalous polarization dependence of FWM measurements in zero magnetic field. Finally, we have studied how the interaction with the two-dimensional electron gas in doped samples modifies that behavior. We have shown that many-body interactions significantly modify the optical response of modulation-doped samples in the high magnetic field regime. A further charactrerization is still needed, and this may eventually lead to a better understanding of the many-body interactions in such systems.

9. References

[1] *Physics and Applications of Quantum Wells and Superlattices*, ed. E.E. Mendez and K. von Klitzing, NATO ASI Series B, Vol. 170, Plenum Press (1987).

[2] *The Physics of the Two-Dimensional Electron Gas*, ed. J.T. Devreese and F.M. Peeters, NATO ASI Series B, Vol. 157, Plenum Press (1987).

[3] *Ultrafast Phenomena* VIII, Proceedings of the 8th International Conference, Antibes 1992, ed. J.L. Martin, A. Migus, G.A. Mourou and A.H. Zewail, Springer-Verlag Series in Chemical Physics 55 (1993).

[4] M.I. Dyakonov and V.I. Perel, *Theory of Optical Spin Orientation of Electrons and Nuclei in Semiconductors*, in *Optical Orientation*, ed. F. Meier and B.P. Zakharchenya, *Modern Problems in Condensed Matter Sciences* Vol. 8, Seris ed. V.M. Agranovich and A.A. Maradudin, North-Holland (1984).

[5] Gerald Bastard, *Wave mechanics applied to semiconductor heterostructures*, les editions de physique (1988), p. 101.

[6] R. Ferreira and G. Bastard, *"Spin"-flip scattering of holes in semiconductor quantum wells*, Phys. Rev. **B43**, 9687 (1991).

[7] R.S. Knox, *Theory of Excitons*, Solid State Physics, Suppl. 5, ed. F. Seitz and D. Turnbull, Academic Press (1963).

[8] G.D. Mahan, *Excitons in Degenerate Semiconductors*, Phys. Rev. **153**, 882 (1967).

[9] L.M. Roth, B. Lax and S. Zwerdling, Theory of Optical Magneto-Absorption Effects in Semiconductors, Phys. Rev. **114**, 91 (1959).

[10] C. Hermann and C. Weisbuch, *Optical Detection of Conduction Electron Spin Resonance in Semiconductors and its Application to $k \cdot p$ Perturbation Theory*, in *Optical Orientation*, ed. F. Meier and B.P. Zakharchenya, *Modern Problems in Condensed Matter Sciences* Vol. 8, Seris ed. V.M. Agranovich and A.A. Maradudin, North-Holland (1984).

[11] e.g. Ref. 5, p. 317.

[12] e.g. Ref. 1, p. 357.

[13] S.R. Eric Yang and L.J. Sham, *Theory of Magnetoexcitons in Quantum Wells*, Phys. Rev. Lett. **58**, 2598 (1987).

[14] S. Das Sarma and X.C. Xie, *Strong-Field Density of States in Weakly Disordered Two-Dimensional Electron Systems*, Phys. Rev. Lett. **61**, 738 (1988).

[15] B.B. Goldberg, D. Heiman, M.J. Graf, D.A. Broido, A. Pinczuk, C.W. Tu, J.E. English and A.C. Gossard, *Optical transmission spectroscopy of the two-dimensional electron gas in GaAs in the quantum Hall regime*, Phys. Rev. **B38**, 10131 (1988).

[16] K. von Klitzing, G. Dorda and M. Pepper, *New Method for High-Accuracy Determination of the Fine-Structure Constant Based on Quantized Hall Resistance*, Phys. Rev. Lett. **45**, 494 (1980).

[17] W.H. Knox, D.S. Chemla, G. Livescu, J.E. Cunningham and J.E. Henry, *Femtosecond Carrier Thermalization in Dense Fermi Seas*, Phys. Rev. Lett. **61**, 1290 (1988).

[18] S. Schmitt-Rink, D.S. Chemla and D.A.B. Miller, *Linear and nonlinear optical properties of semiconductor quantum wells*, Adv. Phys. **38**, 89 (1989).

[19] L. Schultheis, J. Kuhl, A. Honold and C.W. Tu, *Ultrafast Phase Relaxation of Excitons via Exciton-Exciton and Exciton-Electron Collisions*, Phys. Rev. Lett. **57**, 1635 (1986); *Picosecond Phase Coherence and Orientational Relaxation in Excitons in GaAs*, Phys. Rev. Lett. **57**, 1797 (1986).

[20] J. Hegarty and M.D. Sturge, *Studies of exciton localization in quantum-well structures by nonlinear-optical techniques*, J. Opt. Soc. Am. B2, 1143 (1985); H. Wang, M. Jiang and D.G. Steel, *Measurement of Phonon-Assisted Migration of Localized Excitons in GaAs/AlGaAs Multiple-Quantum-Well Structures*, Phys. Rev. Lett. **65**, 1255 (1990).

[21] T. Takagahara, *Excitonic relaxation processes in quantum well structures*, J. Lumin. 44, 347 (1989).

[22] E.O. Gobel, K. Leo, T.C. Damen, J. Shah, S. Schmitt-Rink, W. Schafer, J.F. Muller and K. Kohler, *Quantum Beats of Excitons in Quantum Wells*, Phys. Rev. Lett. **64**, 1801 (1990).

[23] T. Uenoyama and L.J. Sham, *Hole relaxation and Luminescence Polarization in Doped and Undoped Quantum Wells*, Phys. Rev. Lett. **64**, 3070 (1990).

[24] M.R. Freeman, D.D. Awschalom, J.M. Hong, L.L. Chang and K. Ploog, *Ultrafast Spin-Polarization Spectroscopy in GaAs/AlGaAs Quantum Wells*, in *Proc. Twentieth Int. Conf. on Physics of Semiconductors*, ed. E. Anastassakis and J.D. Joannopoulos, World Scientific, Singapore (1990).

[25] A. Takeuchi, S. Muto, T. Inata and T. Fujii, *Direct observation of picosecond spin relaxation of excitons in GaAs/AlGaAs quantum wells using spin-dependent optical nonlinearity*, Appl. Phys. Lett. **56**, 2213 (1990).

[26] T.C. Damen, K. Leo, J. Shah and J.E. Cunningham, *Spin relaxation and thermalization of excitons in GaAs quantum wells*, Appl. Phys. Lett. **58**, 1902 (1991).

[27] M. Potemski, J.C. Maan, A. Fasolino, K. Ploog and G. Weimann, *Spin Conservation of Photocreated Carriers in Quantum Wells in High Magnetic Fields: A New Spectroscopic Tool*, Phys. Rev. Lett. **63**, 2409 (1989).

[28] e.g. A. Pinczuk, J.P. Valladares, D. Heiman, A.C. Gossard, J.H. English, C.W. Tu, L. Pfeiffer and K. West, *Observation of Roton Density of States in Two-Dimensional Landau-Level Excitations*, Phys. Rev. Lett. **61**, 2701 (1988).

[29] e.g. D. Heiman, B.B. Goldberg, A. Pinczuk, C.W. Tu, A.C. Gossard and J.H. English, *Optical Anomalies of the Two-Dimensional Electron Gas in the Extreme Magnetic Quantum Limit*, Phys. Rev. Lett. **61**, 605 (1988); W. Chen, M. Fritze, A.V. Nurmikko, D. Ackley, C. Colvard and H. Lee, *Interaction of Magnetoexcitons and Two-Dimensional Electron Gas in the Quantum Hall Regime*, Phys. Rev. Lett. **64**, 2434 (1990).

[30] Y.R. Shen, *The Principles of Nonlinear Optics*, Wiley (1984); L. Allen and J.H. Eberly, *Optical Resonance and Two Level Atoms*, Wiley, New York (1975).

[31] Christos Flytzanis, *Theory of Nonlinear Optical Susceptibilities*, in *Quantum Electronics*, Vol. I (Nonlinear Optics, Part A), ed. H. Rabin and C.L. Tang, Academic Press (1975).

[32] T. Yajima and Y. Taira, *Spatial Optical Parametric Coupling of Picosecond Light Pulses and Transverse Relaxation Effect in Resonant Media*, J. Phys. Soc. Japan, **47**, 1620 (1979).

[33] G.E. Pikus and A.N. Titkov, *Spin Relaxation under Optical Orientation in Semiconductors*, in *Optical Orientation*, ed. F. Meier and B.P. Zakharchenya, *Modern Problems in Condensed Matter Sciences* Vol. 8, Seris ed. V.M. Agranovich and A.A. Maradudin, North-Holland (1984).

[34] Y. Yafet, *g-Factor and Spin-Lattice Relaxation of Conduction Electrons*, in *Solid State Physics: Advances in Research and Applications*, ed. F. Seitz and D. Turnbull, Vol. 14, Academic, New York (1963).

[35] R.C. Miller, D.A. Kleinman, W.A. Nordland, Jr. and A.C. Gossard, *Luminescence studies of optically pumped quantum wells in GaAs-$Al_xGa_{1-x}As$ multilayer structures*, Phys. Rev. **B22**, 863 (1980).

[36] R.J. Elliott, *Theory of the Effect of Spin-Orbit Coupling on Magnetic Resonance in Some Semiconductors*, Phys. Rev. **96**, 266 (1954).

[37] M.I. D'yakonov and V.I. Perel', *Spin Orientation of Electrons Associated with the Interband Absorption of Light in Semiconductors*, Sov. Phys. JETP **33**, 1053 (1971) [original paper in Zh. Eksp. Teor. Fiz. **60**, 1954 (1971)]; M.I. D'yakonov and V.I. Perel', *Spin Relaxation of Conduction Electrons in Noncentrosymmetric Semiconductors*, Sov. Phys. Solid State **13**, 3023 (1972) [original paper in Fizika Tverdogo Tela **13**, 3581 (1971)].

[38] A.H. Clark, R.D. Burnham, D.J. Chadi and R.M. White, *Spin relaxation of conduction electrons in $Al_xGa_{1-x}As$*, Phys. Rev. **B12**, 5758 (1975); *Spin relaxation of conduction electrons in GaAs*, Solid State Commun. **20**, 385 (1976).

[39] G.E. Pikus and G.L. Bir, *Exchange Interaction in Excitons in Semiconductors*, Sov. Phys. JETP **33**, 108 (1971) [original paper in Zh. Eksp. Teor. Fiz. **60**, 195 (1971)]; G.L. Bir, A.G. Aronov and G.E. Pikus, *Spin relaxation of electrons due to scattering by holes*, Sov. Phys. JETP **42**, 705 (1976) [original paper in Zh. Eksp. Teor. Fiz. **69**, 1382 (1975)].

[40] G. Fishman and G. Lampel, *Spin relaxation of photoelectrons in p-type gallium arsenide*, Phys. Rev. **B16**, 820 (1977); K. Zerrouati, F. Fabre, G. Bacquet, J. Bandet, J. Frandon, G. Lampel and D. Paget, Phys. Rev. **B37**, 1334 (1988).

[41] T.C. Damen, L. Vina, J.E. Cunningham, J. Shah and L.J. Sham, *Subpicosecond Spin Relaxation Dynamics of Excitons and Free Carriers in GaAs Quantum wells*, Phys. Rev. Lett. **67**, 3432 (1991).

[42] L. Schultheis, M.D. Sturge and J. Hegarty, *Photon echoes from two-dimensional excitons in GaAs-AlGaAs quantum wells*, Appl. Phys. Lett. **47**, 995 (1985).

[43] E.C.F. Quivy-da Silva, V. Chitta, D. Toet, M. Potemski, J.C. Maan and K. Ploog, *Relaxation of magnetic moments in GaAs/GaAlAs quantum wells*, Semicond. Sci. Technol. **7**, 1369 (1992).

[44] Ph. Roussignol, P. Rolland, R. Ferreira, C. Delalande, G. Bastard, A. Vinattieri, J. Martinez-Pastor, L. Carraresi, M. Colocci, J.E Palmier and B. Etienne, *Hole polarization and slow hole-spin relaxation in an n-doped quantum-well structure*, Phys. Rev. **B46**, 7292 (1992).

[45] H. Wang, M. Jiang, R. Merlin and D.G. Steel, *Spin-Flip-Induced Hole Burning in GaAs Quantum Wells: Determination of the Exciton Zeeman Splitting*, Phys. Rev. Lett. **69**, 804 (1992).

[46] I. Brener, W.H. Knox, K.W. Goossen and J.E. Cunningham, *Shallow Quantum Well Excitons: 2D or 3D?*, Phys. Rev. Lett. **70**, 319 (1993).

[47] M.Z. Maialle, E.A. de Andrada e Silva and L.J. Sham, *Exciton spin dynamics in quantum wells*, Phys. Rev. **B47**, 15776 (1993).

[48] R. Ferreira and G. Basterd, *Hole "Spin" Relaxation in Semiconductor Quantum Wells*, Europhys. Lett. **23**, 439 (1993).

[49] J.B. Stark, W.H. Knox, D.S. Chemla, W. Schafer, S. Schmitt-Rink and C. Stafford, *Femtosecond Dynamics of Excitons under Extreme Magnetic Confinement*, Phys. Rev. Lett. **65**, 3033 (1990).

[50] J.B. Stark, W.H. Knox and D.S. Chemla, *Femtosecond Circular Dichroism Study of Nonthermal Carrier Distributions in Two- and Zero-Dimensional Semiconductors*, Phys. Rev. Lett. **68**, 3080 (1992); J.B. Stark, W.H. Knox and D.S. Chemla, *Spin-resolved femtosecond magnetoexciton interactions in GaAs quantum wells*, Phys. Rev. **B46**, 7919 (1992).

[51] T.W. Ducas, M.G. Littman and M.L. Zimmerman, *Observation of Oscillations in Resonance Absorption from a Coherent Superposition of Atomic States*, Phys. Rev. Lett. **35**, 1752 (1975); R. Zygan-Maus and H.H. Wolter, *Quantum Beats in Absorption*, Phys. Lett. **64A**, 351 (1978).

[52] A.M. White, I. Hinchliffe, P.J. Dean and P.D. Greene, *Zeeman Spectra of the Principal Bound Exciton in Sn-Doped Gallium Arsenide*, Solid State Commun. **10**, 497 (1972).

[53] M. Koch, J. Feldmann, G. von Plessen, E.O. Gobel, P. Thomas and K. Kohler, *Quantum Beats versus Polarization Interference: An Experimental Distinction*, Phys. Rev. Lett. **69**, 3631 (1992).

[54] O. Carmel and I. Bar-Joseph, *Four-wave-mixing studies of quantum-well excitons in a magnetic field*, Phys. Rev. **B47**, 7606 (1993).

[55] O. Carmel, H. Shtrikman and I. Bar-Joseph, *Quantum-beat spectroscopy of the Zeeman splitting of heavy- and light-hole excitons in GaAs/$Al_xGa_{1-x}As$ quantum wells*, Phys. Rev. **B48**, 1955 (1993).

[56] G.E.W. Bauer, *Mixing of Magnetoexcitons in Quantum Wells*, in *High Magnetic Fields in Semiconductor Physics II*, Proc. Int. Conf. Wurzburg, 1988, ed. G. Landwehr, Springer-Verlag (1989).

[57] D.C. Reynolds, K.K. Bajaj, C.W. Litton, R.L. Greene, P.W. Yu, C.K. Peng and H. Morok, *Magneto-optical studies of GaAs-$Al_xGa_{1-x}As$ multi-quantum-well structures grown by molecular-beam epitaxy*, Phys. Rev. **B35**, 4515 (1987).

[58] G. Lommer, F. Malcher and U. Rossler, *Reduced g factor of subband Landau levels in AlGaAs/GaAs heterostructures*, Phys. Rev. **B32**, 6965 (1985); M. Dobers, K. von Klitzing and G. Weimann, *Electron-spin resonance in the two-dimensional electron gas of GaAs-$Al_xGa_{1-x}As$ heterostructures*, Phys. Rev. **B38**, 5453 (1988).

[59] H. Stolz, V. Langer, E. Schreiber, S. Permogorov and W. von der Osten, *Picosecond Quantum-Beat Spectroscopy of Bound Excitons in CdS*, Phys. Rev. Lett. **67**, 679 (1991).

[60] V. Langer, H. Stolz and W. von der Osten, *Observation of Quantum Beats in the Resonance Fluorescence of Free Excitons*, Phys. Rev. Lett. **64**, 854 (1990).

[61] D.J. Lovering, R.T. Phillips, G.J. Denton and G.W. Smith, *Resonant Generation of Biexcitons in a GaAs Quantum Well*, Phys. Rev. Lett. **68**, 1880 (1992).

[62] D. Oberhauser, K.H. Pantke, W. Langbein, V.G. Lyssenko, H. Kalt, J.M. Hvam, G. Weimann and C. Klingshirn, *Coherent and Incoherent Exciton Dynamics in* $Al_{1-y}Ga_yAs$ */ GaAs Multiple Quantum Wells*, phys. stat. sol. (b) **173**, 53 (1992).

[63] E. Rashba, Sov. Phys. Semicond. **8**, 807 (1975) [original paper in Fiz. Tekh. Poluprovodn. Fiz. **8**, 1241 (1974)].

[64] S.T. Cundiff, H. Wang and D.G. Steel, *Polarization-dependent picosecond excitonic nonlinearities and the complexities of disorder*, Phys. Rev. **B46**, 7248 (1992).

[65] D. Bennhardt, P. Thomas, R. Eccleston, E.J. Mayer and J. Kuhl, *Polarization dependence of four-wave-mixing signals in quantum wells*, Phys. Rev. **B47**, 13485 (1993).

[66] H. Wang, K. Ferrio, D.G. Steel, Y.Z. Hu, R. Binder and S.W. Koch, *Transient Nonlinear Optical Response from Excitation Induced Dephasing in GaAs*, Phys. Rev. Lett. **71**, 1261 (1993).

[67] R.C. Miller and D.A. Kleinman, *Excitons in GaAs Quantum Wells*, J. Lumin. **30**, 520 (1985).

[68] B. Deveaud (private communication).

[69] D.A. Kleinman, *Binding energy of biexcitons and bound excitons in quantum wells*, Phys. Rev. **B28**, 871 (1983).

[70] T.W. Steiner, A.G. Steele, S. Charbonneau, M.L.W. Thewalt, E.S. Koteles and B. Elman, *Time-Resolved Studies of Biexcitons in GaAs*, Solid State Commun. **69**, 1139 (1989).

[71] E. Burstein, *Anomalous optical absorption limit in InSb*, Phys. Rev. **93**, 632 (1954).

[72] B. Roulet, J. Gavoret and P. Nozieres, *Singularities in the X-Ray Absorption and Emission of Metals. I. First-Order Parquet Calculations*, Phys. Rev. **178**, 1072 (1969); P. Nozieres, J. Gavoret and B. Roulet, *Singularities in the X-Ray Absorption and Emission of Metals. II. Self-Consistent Treatment of Divergencies*, Phys. Rev. **178**, 1084 (1969); P. Nozieres and C.T. de Dominicis, *Singularities in the X-Ray Absorption and Emission of Metals. III. One-Body Theory Exact Solution*, Phys. Rev. **178**, 1097 (1969).

[73] T.A. Callcot, E.T. Arakawa and D.L. Ederer, *L_{23} soft-x-ray emission and absorption spectra of Na*, Phys. Rev. **B18**, 6622 (1978).

[74] G. Livescu, D.A.B. Miller, D.S. Chemla, M. Ramaswamy, T.Y. Chang, N. Sauer, A.C. Gossard and J.H. English, *Free Carrier and Many-Body Effects in Absorption Spectra of Modulation-Doped Quantum Wells*, IEEE J. Quant. Electron. **QE24**, 1677 (1988).

[75] M.S. Skolnick, J.M. Rorison, K.J. Nash, D.J. Mowbray, P.R. Tapster, S.J. Bass and A.D. Pitt, *Observation of a many-body edge singularity in quantum well luminescence spectra*, Phys. Rev. Lett. **58**, 2130 (1987).

[76] A.E. Ruckenstein and S. Schmitt-Rink, *Many-body aspects of the optical spectra of bulk and low-dimensional doped semiconductors*, Phys. Rev. **B35**, 7551 (1987).

[77] P. Hawrylak, *Optical properties of a two-dimensional electron gas: Evolution of spectra from excitons to Fermi-edge singularities*, Phys. Rev. **B44**, 3821 (1991).

[78] D.S. Kim, J. Shah, J.E. Cunningham, T.C. Damen, S. Schmitt-Rink and W. Schafer, *Carrier-Carrier Scattering in a Degenerate Electron System: Strong Inhibition of Scattering near the Fermi Edge*, Phys. Rev. Lett. **68**, 2838 (1992).

[79] A. Pinczuk, B.S. Dennis, D. Heiman, C. Kallin, L. Brey, C. Tejedor, S. Schmitt-Rink, L.N. Pfeiffer and K.W. West, *Spectroscopic Measurement of Large Exchange Enhancement of a Spin-Polarized 2D Electron Gas*, Phys. Rev. Lett. **68**, 3623 (1992).

[80] B.B. Goldberg, D. Heiman, A. Pinczuk, L. Pfeiffer and K. West, *Optical Investigations of the Integer and Fractional Quantum Hall Effects: Energy Plateaus, Intensity Minima, and Line Splitting in Band-Gap Emission*, Phys. Rev. Lett. **65**, 641 (1990); A.J. Turberfield, S.R. Haynes, P.A. Wright, R.A. Ford, R.G. Clark, J.F. Ryan, J.J. Harris and C.T. Foxon, *Optical Detection of the Integer and Fractional Quantum Hall Effects in GaAs*, Phys. Rev. Lett. **65**, 637 (1990); A. Pinczuk, B.S. Dennis, L.N. Pfeiffer and K. West, *Observation of Collective Excitations in the Fractional Quantum Hall Effect*, Phys. Rev. Lett. **70**, 3983 (1993).

[81] V.F. Gantmacher and Y.B. Levinson, *Carrier scattering in metals and semiconductors*, North-Holland (1987).

[82] T. Ando, A.B. Fowler and F. Stern, *Electronic properties of two-dimensional systems*, Rev. Mod. Phys. **54**, 437 (1982).

[83] M. Abramowitz., *Handbook of Mathematical Functions with Formulas, Graphs, and Mathematical Tables*, ed. M. Abramowitz and I.A. Stegun, Dover (1965), p.228.

[84] P. Hawrylak, J.F. Young and P. Brockmann, *Dephasing Times of Photo-excited Electron-Valence Hole Pairs Near the Fermi Edge of a Degenerate Electron Gas in Quantum Wells*, submitted to Phys. Rev. B.

[85] P. Hawrylak, *Resonant magnetoexcitons and the Fermi-edge singularity in a magnetic field*, Phys. Rev. **B44**, 11236 (1991).

Publications related to this work

1. S. Bar-Ad and I. Bar-Joseph, *Absorption Quantum Beats of Magnetoexcitons in GaAs Heterostructures*, Phys. Rev. Lett. **66**, 2491 (1991).
2. S. Bar-Ad and I. Bar-Joseph, *Exciton Spin Dynamics in GaAs Heterostructures*, Phys. Rev. Lett. **68**, 349 (1992).
3. G. Finkelstein, S. Bar-Ad, O. Carmel, I. Bar-Joseph and Y. Levinson, *Biexcitonic effects in transient nonlinear optical experiments in quantum wells*, Phys. Rev. **B47**, 12964 (1993).
4. S. Bar-Ad and I. Bar-Joseph, *Quantum Beats Spectroscopy of Exciton Spin Dynamics in GaAs Heterostructures*, in *Ultrafast Phenomena* VIII, Proceedings of the 8th International Conference, Antibes 1992, ed. J.L. Martin, A. Migus, G.A. Mourou and A.H. Zewail, Springer-Verlag Series in Chemical Physics 55 (1993).
5. I. Bar-Joseph, S. Bar-Ad, O. Carmel and Y. Levinson, *Coherent Optical Phenomena of Quantum Well Excitons in a Magnetic Field*, in *Optical Phenomena in Semiconductor Structures of Reduced Dimensions*, ed. D.J. Lockwood and A. Pinczuk, Kluwer Academic (1993).
6. S. Bar-Ad, I. Bar-Joseph, Y. Levinson and H. Shtrikman, *Time-Resolved Four Wave Mixing Studies of a Two-Dimensional Electron Gas in a Magnetic Field*, Surface Science **305** (1994) 234-7 (special issue on EP2DS, the 10th Int. Conf. on Electronic Properties of Two Dimensional Systems, Newport, RI, USA, May-June 1993).
7. S. Bar-Ad, I. Bar-Joseph, Y. Levinson and H. Shtrikman, *Coherent Optical Spectroscopy of Electron Scattering in a Two Dimensional Electron Gas in High Magnetic Fields*, Phys. Rev. Lett. **72**, 776 (1994).
8. S. Bar-Ad, I. Bar-Joseph, *A Four Wave Mixing Study of Electron Scattering in Modulation Doped GaAs Quantum Wells in High Magnetic Field*, to be published in

Ultrafast Phenomena IX, Proc. of 9th Int. Conf., Dana Point 1994, Springer-Verlag Series in Chemical Physics.

9. S.Bar-Ad, I Bar-Joseph, G. Finkelstein and Y. Levinson, Biexcitons in short-pulse optical experiments in strong magnetic field in GaAs quantum wells, to be published in Phys. Rev. B.

Certificate of originality

This thesis describes my original work. Parts of the work were performed in cooperation and with the assistance of other researchers and research students in the Physics department of the Weizmann Institute, as follows:

- The modelling of the biexcitonic nonlinear response, presented in chapter 6, was done in cooperation with G. Finkelstein, an MSc. student, and under the supervision of Prof. Y. Levinson.

- FWM measurements on intrinsic samples, such as the one depicted in Fig. 6.5, were taken by O. Carmel, an MSc. student.

- The electron-electron scattering rates discussed in chapter 7 were calculated with the help of Prof. Y. Levinson.

Appendix A: Calculation of the third order dipole moment

In this section we bring the standard density matrix formalism for the calculation of the time-dependent dipole moment [1]. This formalism is most appropriate for short-pulse experiments, and is well-known in the analysis of two-level systems. In this work we have applied it to the calculation of the DA and FWM signals in the four-level exciton-biexciton system. This procedure is inevitable if the response of the system is to be explained in detail for overlapping pulses. In simpler cases simpler approaches can be used, such as the coupled Bloch equations [2].

Consider $\rho(t)$, the density matrix describing the measured system. We suppose that in the remote past, $t=-\infty$, all perturbations vanish and the system is at its ground state, i.e.: $H'(-\infty)=0$ and $\rho(-\infty)=\rho^{(0)}$. The subsequent development of $\rho(t)$ in the presence of the electromagnetic field is governed by the Liouville equation of motion:

$$d\rho(t)/dt=(1/i\hbar)[H(t),\rho(t)]-\{d\rho/dt\}_R\,, \tag{A.1}$$

where $H(t)=H_0(t)+H'(t)$, $H'(t)$ being the off-diagonal interaction between the electric dipole and the radiation field, and the last term has been introduced to account phenomenologically for the relaxation of the system. Equation A.1 can be solved most conveniently by transforming to the interaction representation. In this representation we denote all the physical quantities with the subscript I, and Eq. A.1 has the form:

$$d\rho_I(t)/dt=(1/i\hbar)[H_I'(t),\rho_I(t)]-\{d\rho_I/dt\}_R\,. \tag{A.2}$$

The solution can be obtained by expressing $\rho(t)$ in the form of a perturbation series [power series in $H'(t)$]:

$$\rho_I(t)=\rho_I^{(0)}(t)+\rho_I^{(1)}(t)+\rho_I^{(2)}(t)+\rho_I^{(3)}(t)+\cdots \tag{A.3}$$

and then integrating by iteration. Substituting $\rho_I(t)$ in Eq. A.2 and equating terms of the same power in $H'(t)$ one obtains the chain of equations:

$$d\rho_I^{(n)}(t)\;dt=(1/i\hbar)\;H_I'(t),\rho_I^{(n-1)}(t)\;-\{d\rho_I^{(n)}\;dt\}_R\,, \tag{A.4}$$

which can be solved by step-by-step integration:

$$\rho_I^{(n)}(t)=(1/i\hbar)^n\int_{-\infty}^{t}dt_1\int_{-\infty}^{t_1}dt_2\cdots\int_{-\infty}^{t_{n-1}}dt_n\;H_I'(t_1),\;H_I'(t_2),\;\cdots H_I'(t_n),\rho^{(0)}\;\cdots\;. \tag{A.5}$$

Once the density matrix is known, the mean value of the dipole moment operator is calculated from:

$$\langle d \rangle = \mathrm{Tr}\{\rho d\} = \mathrm{Tr}\{\rho_I d_I\} . \qquad \text{(A.6)}$$

When the dipole moment is calculated in this way, all the optical frequencies cancel out, and only the sum of the slowly varying pulse envelopes $A(t)+B(t)$ remain from $H'(t)$. As already mentioned above, only the third ofder dipole moment appears in the DA and FWM experiments. The expression for it would thus consist of terms cubic in $A(t)$, $B(t)$ and their complex conjugates. In calculating the DA signal only the terms which have momentum along the direction of the probe are taken, provided that they are dependent on both the pump and probe envelopes (other terms are filtered out by the chopper and lock-in amplifier). In the FWM experiment only the terms which have momentum along the direction $2k_1$-k_2 or $2k_2$-k_1 are taken.

[1] Christos Flytzanis, *Theory of Nonlinear Optical Susceptibilities*, in *Quantum Electronics*, Vol. I (Nonlinear Optics, Part A), ed. H. Rabin and C.L. Tang, Academic Press (1975).

[2] L. Allen and J.H. Eberly, *Optical Resonance and Two Level Atoms*, Wiley, New York (1975).

Appendix B: e-e scattering in a magnetic field

In the calculation of the Coulomb interaction we take account of the screening by the electron gas. In a quantum well the Coulomb potential is three-dimensional, but the 2DEG screens only in two dimensions [1]. However, in order to simplify the calculation we consider only two limiting cases: three-dimensional Thomas-Fermi screening, which is appropriate for wide quantum wells, and an ideal two-dimensional case. In both cases the dependence on magnetic field strength turn out to be the same.

B.1 Three-dimensional screening

We assume that the screening length is independent of the magnetic field strength. For three-dimensional screening the Fourier components U_q^{ee} is:

$$U_q^{ee} = \frac{4\pi e^2}{\kappa} \frac{\lambda^2}{1+q^2\lambda^2}, \tag{B.1}$$

Rewriting the Fourier decomposition as a sum, the square of the matrix element can be expressed in terms of single-particle matrix elements in the form:

$$\left|M_{1,2\to 1',2'}\right|^2 = \frac{1}{L^6}\sum_{q,q'} U_q^{ee} U_{q'}^{ee*} \langle 1'|e^{iqr}|1\rangle\langle 1'|e^{iq'r}|1\rangle^* \langle 2'|e^{-iqr}|2\rangle\langle 2'|e^{-iq'r}|2\rangle^*. \tag{B.2}$$

In the Landau gauge the wave functions are:

$$\begin{aligned} |1\rangle &= \frac{1}{\sqrt{L}} e^{ik_x x}\Phi_{lk_x}(y)\chi(z), \\ \Phi_{lk_x}(y) &= \left[\pi^{1/2} a_H 2^l l!\right]^{-1/2} exp\left[-\frac{(y-y_o)^2}{2a_H^2}\right] \mathrm{H}_l\left(\frac{y-y_0}{a_H}\right), \end{aligned} \tag{B.3}$$

where $y_0 = -a_H^2 k_x$, a_H is the magnetic length $a_H = (\hbar c / eH)^{1/2}$, H_l is a Hermite polinomial, and $\chi(z)$ is the envelope function for the first quantum well subband.

Substituting these explicit expressions, it can be shown [2] that the single-particle matrix elements in Eq. B.2 have the form:

$$\begin{aligned}\langle 1'|e^{iqr}|1\rangle &= \langle \chi(z)|e^{iqr}|\chi(z)\rangle\, \delta_{k'_{1x},k_{1x}+q_x}\, Q_{ll'}(q_\perp) \quad \times \\ \times \quad & exp\left[-i\varphi_q(l-l')+\frac{1}{2}ia_H^2 q_y(k_x+k'_x)\right]\end{aligned} \tag{B.4}$$

where $q_\perp$ is the magnitude of the component q perpendicular to H, and φ_q is the angle it makes with the x-axis. The functions $Q_{ll'}$ are expressed in terms of the Laguerre polynomials L_l^m; for $l \geq l'$

$$Q_{ll'}(q_\perp) = \left(\frac{l'!}{l!}\right)^{1/2} e^{-\hat{\kappa}^2/2}\hat{\kappa}^{l-l'}L_{l'}^{l-l'}(\hat{\kappa}^2), \quad \hat{\kappa}^2 \equiv \frac{1}{2}a_H^2 q_\perp^2, \tag{B.5}$$

whereas for $l \leq l'$ the symmetry relation $Q_{ll'} = (-1)^{l-l'}Q_{l'l}$ can be used.

The scattering matrix element can now be written in the form:

$$\begin{aligned}\left|M_{1,2\to 1',2'}\right|^2 = \frac{1}{L^6}\sum_{q,q'} U_q^{ee}U_{q'}^{ee*}Q_{l_1l'_1}(q_\perp)Q_{l_1l'_1}(q'_\perp)Q_{l_2l'_2}(q_\perp)Q_{l_2l'_2}(q'_\perp)\left|\xi(q_z)\right|^2\left|\xi(q'_z)\right|^2 \quad \times \\ \times \quad \Theta(k,q,q')\,\delta_{k'_{1x},k_{1x}+q_x}\,\delta_{k'_{1x},k_{1x}+q'_x}\,\delta_{k'_{2x},k_{2x}-q_x}\,\delta_{k'_{2x},k_{2x}-q'_x}\end{aligned}, \tag{B.6}$$

where we have denoted $\langle \chi(z)|e^{iqr}|\chi(z)\rangle$ by $\xi(q_z)$, and where Θ is a phase factor (see Eq. B.4). When calculating the scattering rate *for a given set of Landau indices* $l_1l_2 \to l'_1l'_2$ in the degenerate problem, the energy is independent of k_x, so one can simply sum-up over k_{2x}, k'_{1x} and k'_{2x}. Summation over k_{x_2} brings out a factor $L^2/(2\pi a_H^2)$, while Θ vanishes (averages at zero) unless $q_x = q'_x$ and $q_y = q'_y$. k'_{1x} and k'_{2x} are uniquely determined by k_{1x}, k_{2x}, q and q' (equivalent to momentum conservation, where q and q' define the

momentum transfer). We get:

$$\sum_{k_{2x},k'_{1x},k'_{2x}}\left|M_{1,2\to 1',2'}\right|^2=\frac{1}{2\pi a_H^2L^4}\sum_q\sum_{q'}U_q^{ee}U_{q'}^{ee*}Q_{l_1l'_1}(q_\perp)Q_{l_1l'_1}(q'_\perp)Q_{l_2l'_2}(q_\perp)Q_{l_2l'_2}(q'_\perp)\quad\times$$
$$\times\quad\left|\xi(q_z)\right|^2\left|\xi(q'_z)\right|^2\delta_{k'_{1x},k_{1x}+q_x}\delta_{k'_{2x},k_{2x}+q_x}\delta_{q_x,q'_x}\delta_{q_y,q'_y}\quad=\qquad\text{(B.7)}$$
$$=\frac{1}{2\pi a_H^2L^4}\sum_{q_\perp}\sum_{q_z}\sum_{q'_z}U_{q_\perp+q_z}^{ee}U_{q_\perp+q'_z}^{ee*}Q_{l_1l'_1}^2(q_\perp)Q_{l_2l'_2}^2(q_\perp)\left|\xi(q_z)\right|^2\left|\xi(q'_z)\right|^2$$

Replacing the sums with integrals, and substituting Eq. B.1 and Eq. B.7 into Eq. 7.1, we get the scattering rate *for a given set of Landau indices* $l_1l_2\to l'_1l'_2$ in the degenerate problem:

$$\left.\frac{1}{\tau}\right|_{l_1l_2\to l'_1l'_2}=\frac{2\pi}{\hbar}\cdot\frac{(4\pi)^2e^4}{\kappa^2}\cdot\frac{1}{(2\pi)^5a_H^2}\int d^2q_\perp\int dq_z\int dq'_z\quad\times$$
$$\times\quad\frac{\lambda^2}{\left(1+\lambda^2q_\perp^2+\lambda^2q_z^2\right)}\cdot\frac{\lambda^2}{\left(1+\lambda^2q_\perp^2+\lambda^2q_z'^2\right)}\quad Q_{l_1l'_1}^2(q_\perp)Q_{l_2l'_2}^2(q_\perp)\quad\times\qquad\text{(B.8)}$$
$$\times\quad\left|\xi(q_z)\right|^2\left|\xi(q'_z)\right|^2\delta(\varepsilon_1+\varepsilon_2-\varepsilon_{1'}-\varepsilon_{2'})\cdot f_2(1-f_{1'})(1-f_{2'})$$

Let us now take the limit of a wide quantum well. For $q_z,q'_z>>d^{-1}$, where d is the quantum well width, $\xi(q_z)$ and $\xi(q'_z)$ are falling to zero. Assuming that $d>>\lambda$ (i.e. the quantum well width is much larger than the screening length), we may neglect q_z and q'_z in the denominator of the integrand, and replace the integration over q_z and q'_z with a factor of the order $(2\pi/d)^2$. In fact it can be shown that this approximation is good for $d\geq\lambda$. This approximation leads to the following expression fot the scattering rate:

$$\left.\frac{1}{\tau}\right|_{l_1l_2\to l'_1l'_2}\approx\frac{4e^4}{\hbar d^2\kappa^2}F(l_1,l_2,l'_1,l'_2,\alpha)\,\delta(\varepsilon_1+\varepsilon_2-\varepsilon_{1'}-\varepsilon_{2'})f_2(1-f_{1'})(1-f_{2'})\qquad\text{(B.9)}$$

where the parameter $\alpha\equiv a_H^2/\lambda^2$ is inversely proportional to the magnetic field strength, and the dimensionless function F is given in terms of exponential integrals $E_n(\alpha)$ [3]. The behavior of the functions $F(l_1,l_2,l'_1,l'_2,\alpha)$ as function of the magnetic field is discussed in the text (chapter 7).

B.2 Ideal two-dimensional screening

In the ideal two-dimensional case the calculation is repeated along the same lines, but this time the Fourier components U_q^{ee} of the two-dimensional screening is:

$$U_q^{ee} = \frac{2\pi e^2}{\kappa} \frac{\lambda}{1+\lambda q} . \qquad \text{(B.10)}$$

Inserting Eq. B.10 instead of Eq. A.1, we get an expression which is similar to Eq. B.9: d^2 in the pre-factor is replaced by λ^2, and the dimensionless functions $F(l_1,l_2,l_1',l_2',\alpha)$ are replaced by different ones $\tilde{F}(l_1,l_2,l_1',l_2',\alpha)$. The functions $\tilde{F}(l_1,l_2,l_1',l_2',\alpha)$ behave similarly to the respective $F(l_1,l_2,l_1',l_2',\alpha)$ as function of the magnetic field. Furthermore, in our samples the screening length is comparable to the width of the quantum well, so the results for the two screening models are also comparable. In chapter 7 only the 3d case is discussed in detail.

[1] T. Ando, A.B. Fowler and F. Stern, *Electronic properties of two-dimensional systems*, Rev. Mod. Phys. **54**, 437 (1982).

[2] V.F. Gantmacher and Y.B. Levinson, *Carrier scattering in metals and semiconductors*, North-Holland (1987).

[3] M. Abramowitz, *Handbook of Mathematical Functions with Formulas, Graphs, and Mathematical Tables*, ed. M. Abramowitz and I.A. Stegun, Dover (1965), p. 228.

תקציר

שיטות מתקדמות לגידול גבישי מוליכים למחצה אשר פותחו במהלך השנים האחרונות, הביאו להתקדמות עצומה בשטח המחקר של מערכות בעלות מימד נמוך, כדוגמת בורות קוונטיים. אחד מכלי המחקר החשובים המשמשים במחקר זה הם לייזרים של פולסים קצרים, המאפשרים חקירת תהליכים דינמיים שעוברים נושאי המטען בגביש. חיבור זה מתאר עבודת מחקר על בורות קוונטיים של גליום־ארסניד, שבה נלמדה דינמיקת נושאי המטען בשדות מגנטיים גבוהים. בעבודה זו נעשה שימוש בשיטות שונות למחקר בפולסים קצרים, כדוגמת בליעה דיפרנציאלית וערוב ארבעה גלים. התגובה הלא־לינארית לערור האופטי נבדקה בניסוי ברזולוציה טובה מפיקו־שניה.

בתחילה עוסק המחקר בתהליכי הרלקסציה של הספין בערורים אקסיטוניים בדגמים אינטרינסיים. התוצאות הנסיוניות המוצגות בעבודה מאששות חישובים תיאורטיים, המנבאים האטה של רלקסצית הספין של חורים בבורות קוונטיים. בעבודה זו נמדדה האטה זו לראשונה באופן מובהק. שמירת ספין מוגדר למשכי זמן ארוכים יחסית איפשרה לנו להדגים פעימות קוונטיות כתוצאה מפיצול זימן. פעימות אלו איפשרו לנו למדוד בדייקנות את היחס הגירו־מגנטי של האקסיטון, ולהסיק את זמן רלקסצית הפאזה שלו מתוך דעיכתן. בשלב הבא נחקר ביסודיות הצימוד הבי־אקסיטוני בין אקסיטונים בעלי מומנטים מגנטיים הפוכים. הצימוד התבטא בזן חדש של אוסילציות, המתקיים כל עוד קיימת חפיפה בזמן בין שני פולסי העירור. מודל מפורט של האינטראקציה הלא־לינארית התלויה בזמן נתן התאמה מצויינת לתוצאות הנסיוניות. מלבד הבנת הצימוד בין האקסיטונים, האוסילציות הבי־אקסיטוניות שמדדנו איפשרו לנו למדוד את אנרגית הקשר הבי־אקסיטונית ואת זמן רלקסצית הפאזה של מצב קשור זה.

חלקה האחרון של עבודת המחקר הוקדש לחקירת השינויים בתגובה האופטית הלא־לינארית כתוצאה מקיום גז אלקטרונים דו־מימדי בדגמים מאולחים. מדידותינו מלמדות על האטה של קצב הפיזור באינטראקציות אלקטרון־אלקטרון בשדות מגנטיים גבוהים. כמו־כן הן מצביעות על חשיבותם של תהליכים רב־גופיים כדוגמת ה־ Fermi edge singularity. אנו דנים בפירוט בהשפעה של השדה המגנטי על הפיזור באינטראקציות אלקטרון־אלקטרון.

עבודה זו נעשתה בהנחייתו של דרי ישראל בר־יוסף

מחקר בשיטות אופטיות מהירות של דינמיקת נושאי מטען בבורות קונטיים בשדה מגנטי

חיבור לשם קבלת התואר "דוקטור לפילוסופיה"

מאת

שמשון ברעד

המחלקה לפיזיקה
מכון ויצמן למדע

מוגש למועצה המדעית של מכון ויצמן למדע

כסלו תשנ"ד